## Solids stabilized emulsions with interfacial mass transfer and aggregate formation

by

Andreas Pappas

Master's Thesis

Submitted in partial fulfilment of the requirements

of the award of

Master of Philosophy of Loughborough University

June 2020

To my wife, Stella

#### Acknowledgements

I would like to thank the following people for helping with this research project. My supervisors Professor Richard Holdich, Professor Chris Rielly and Dr Marijana Dragosavac who gave me guidance and support during the project. The industrial partners, mainly Christian Briard and Linda Godkin for our communication and their support, and other ExxonMobil members for their technical input, as well as ExxonMobil for the financial support. All the technicians from the Chemical Engineering department who helped me with my experiments and everything else that I had requested. Also, my family for their support and for keeping me going. And my biggest thank you to my wife for her patience and encouragement especially during the difficult times.

#### **Abstract**

This study was conducted in order to address two main problems of the halobutyl rubber production process of ExxonMobil at Fawley refinery plant: a) the interfacial mass transfer of acids (by-products) from the organic to the aqueous phase in order to be neutralised by alkaline environment and b) the understanding of the formation of the final rubber particles through rapid emulsion evaporation in a flash drum.

The first aim of this research was to investigate the effect of parameters, such as organic phase viscosity and presence of calcium stearate solids, that could affect the interfacial mass transfer of a solute, which is hydrogen bromine or hydrogen chloride in the industrial process. In addition, the size and stability of the emulsion in the presence calcium stearate as an emulsifier was investigated. In the lab, initially the interfacial mass transfer was investigated using metals (copper and chromium) as the solute species. There were interactions of each system with the calcium stearate, which is added in the industrial process as stabiliser, and so a weak acid was chosen as a more appropriate solute. The investigation of the above parameters effect on the interfacial mass transfer took place in a Lewis-cell device.

The viscosity of the organic phase was modified by the addition of butyl rubber and it was increased exponentially with the increase of the butyl rubber content, especially above 100 g/L. In the Lewis-cell, the slightest increase of the organic phase viscosity (50 g/L BR) resulted in sharp decrease of the overall mass transfer coefficient. Further increase of the butyl rubber content had negligible effect. The effect of calcium stearate on the interfacial mass transfer rate of the acetic acid was also investigated in the Lewis-cell. A slight addition of calcium stearate (5 g/L) increased the interfacial mass transfer rate. However, further addition of calcium stearate resulted in reduction of the rate due to the formation of stearic acid, which acted as a barrier to the interfacial transfer.

Furthermore, the effects of the organic phase viscosity and the calcium stearate concentration on the stability of the emulsion were examined. Calcium stearate is a common industrial emulsifier which is added in the halobutyl rubber production process as a stabiliser. The solid emulsifier, calcium stearate, formed Pickering water-in-oil emulsions. Concentration of butyl rubber above 100 g/L resulted in relatively

stable emulsion, under gentle stirring, with emulsion size of approximately 20  $\mu$ m. Also, concentration of calcium stearate above 5 g/L resulted in the same result when 100 g/L of butyl rubber was present in the organic phase. Lack of calcium stearate had as a result unstable emulsion after the  $10^{th}$  minute of gentle mixing, even the butyl rubber concertation was 100 g/L.

In addition to the above, the effect of acids (hydrogen chloride or acetic acid) on the calcium stearate was investigated. Both acids were used in excess resulting in a maximum amount of calcium stearate able to react, due to the barrier that formed on the calcium stearate particle from the stearic acid. Also, the morphology of the calcium stearate was tested in the SEM and its shape was plate-like. As calcium stearate encounters alkaline environment and high temperature in the industrial scale, their effects on the calcium stearate were tested in the lab. No reaction took place between the calcium stearate and the sodium hydroxide and the temperature had no effect on the calcium stearate up to 70 °C.

The second aim was to understand how the rubber particles were formed inside the industrial flash drum. An initial experiment took place to understand the effect of the temperature on the emulsion evaporation. A W/O emulsion drop, containing butyl rubber in the continuous phase, was exposed at high temperatures, up to 130 °C, in a controlled environment. It was shown that the higher the temperature, the faster the evaporation. Due to the presence of butyl rubber in the continuous phase, the external organic solvent was initially evaporated, and vapours were trapped inside, resulting in expansion of the drop. Also, it was concluded that calcium stearate solids did not have any effect on the evaporation mechanism.

In addition, an experimental configuration was built in the lab to mimic the industrial flash drum in order to investigate the rubber particles formation. The emulsion was formed in an emulsification vessel at 50 °C and, with the use of a peristaltic pump, it was discharged inside the "flash drum", where there was boiling water. Limited experiments took place and it was concluded that, in this configuration, the emulsion was partially evaporated before hitting the water surface. For better heat transfer rate and full emulsion evaporation, modifications were required in lab scale. On the other hand, in the industrial scale, where the volume of the emulsion stream entering the flash drum is higher (lower surface to volume ratio), it would be required very high

amount of heat transfer and it is considered possible fraction of the organic solvent to evaporate inside the boiling water.

## **Table of Contents**

List of	f Figures	ix
List of	f Tables	xiii
List of	f Abbreviations	.xv
List of	f Roman symbols	χvi
List of	f Greek Symbols	χvi
List of	f Subscriptsx	(Vii
Chapt	ter 1	1
1.	Introduction	1
Chapt	ter 2	3
2.	Literature review	3
2.1.	Halobutyl rubber	3
2.1.1.	Introduction - History	3
2.1.2.	Applications	4
2.1.3.	Halobutyl rubber production process	5
2.1.4.	Halogenation	6
2.1.5.	Neutralisation	7
2.1.6.	Rubber particles formation	7
2.2.	Emulsions	9
2.2.1.	Introduction to emulsion types	10
2.2.2.	Emulsification techniques	11
2.2.3.	The role of surfactants/emulsifiers in the emulsions	12
2.2.4.	Emulsion breaking	12
2.2.5.	The role of viscosity of the continuous phase in the emulsions	13
2.2.6.	Pickering emulsions	14
2.2.7.	Calcium stearate as a solid stabilised particle	18
2.3.	Interfacial mass transfer	19
2.3.1.	Two-film theory	20
2.3.2.	Lewis-cell technique	23
2.3.3.	Solvent extraction of metals	25
2.4.	Emulsion evaporation and aggregate formation	29
Chapt	ter 3	31
3.	Materials and Methods	31

3.1	Lewis – cell experimental configuration	. 32
3.2.	Copper solvent extraction	34
3.3.	Chromium solvent extraction	. 38
3.4.	Calcium stearate	41
	Effect of acetic acid, hydrogen chloride, alkaline environment and high erature on the calcium stearate	. 42
3.4.2.	Size and morphology of the calcium stearate	44
3.5.	Acetic acid solvent extraction	. 44
3.5.1.	Distribution coefficient of AcOH between water and heptane	44
3.5.2.	Viscosity of the organic phase – Lewis-cell	45
3.5.3.	Calcium stearate in the aqueous phase – Lewis-cell	47
3.6.	Butyl rubber water-in-oil emulsion	47
3.7.	Rubber particles formation	50
3.7.1.	Evaporation of a W/O emulsion pendant drop	51
3.7.2.	Flash evaporation of the water-in-oil emulsion	53
Chap	ter 4	57
4.	Experimental results and discussion	57
4.1.	Copper solvent extraction – Lewis-cell	57
4.2.	Chromium solvent extraction – Lewis-cell	62
4.3.	Calcium stearate	65
4.3.1.	Calcium stearate at acidic/alkaline environment and high temperature	65
4.3.2.	Calcium stearate morphology	69
4.4.	Acetic acid solvent extraction	.71
4.4.1.	Distribution coefficient of acetic acid	71
4.4.2.	Effect of butyl rubber concentration on the interfacial mass transfer coefficie 72	nt
4.4.3.	Effect of calcium stearate on the interfacial mass transfer rate of AcOH	. 77
4.5.	Size and stability of the W/O Pickering emulsion	. 80
4.6.	Rubber particles formation	. 86
4.6.1.	W/O emulsion pendant drop evaporation	86
4.6.2.	W/O emulsion flash drum evaporation	89
Chap	ter 5	93
5.	Conclusions and future work	. 93
6.	References	98

Appe	ndices	
A 1.	UV-Vis spectrophotometer	
A 1.1	. Calibration of UV-Vis spectrophotometer for copper 109	
A 2.	Flame Atomic Absorption Spectroscopy (FAAS)	
A 2.1	. Calibration of FAAS for chromium112	
A 2.2	. Calibration of FAAS for calcium114	
A 3.	High Performance Liquid Chromatography (HPLC) 115	
A 3.1	. Calibration of HPLC for AcOH in water116	
A 4.	Mathematical equations for calculating the error	
A 5.	Viscosity measurement	
A 6.	Interfacial tension measurement	
A 7.	Image analysis	
A 8. F	Particle size distribution analysis124	
	of Figures oter 2	
Figure	e 2.1. Molecular structure of BR4	
Figure	e 2.2. Tire cross-section5	
Figure	e 2.3. Simplified halobutyl rubber production process6	
Figure	e 2.4. Schematic drawing of the industrial flash drum vessel9	
Figure	e 2.5. Halobutyl rubber dried particles9	
Figure	e 2.6. Types of emulsions 10	
Figure	e 2.7. Emulsion breaking processes	
Figure	e 2.8. A. Contact angle between the solid particle (purple sphere) and the	
	ace, B. Arrangement of the solid particles at the interface on an O/W emulsion.	
	e 2.9. Network structure of the solids particles around the dispersed phase 16	
Figure	e 2.10. Two different shapes of solid particles used in Pickering emulsions 17	
Figure 2.11. Chemical modification of a hydroxylated surface (hydrophilic surface)		
with a	alkylchlorosilane to form a hydrophobic surface	
	e 2.12. Calcium stearate molecule	

Figure 2.13. The function of the CaSt <sub>2</sub> molecule around the water drops in a W/O
emulsion (example on the right) and comparison to a single hydrocarbon chain
emulsifier (example on the left)19
Figure 2.14. The transfer of the solute (A) in a ternary system between organic and
aqueous phase20
Figure 2.15. Lewis–cell schematic apparatus24
Figure 2.16. The effect of stirring speed on the extraction rate in the Lewis-cell 25
Figure 2.17. Effect of pH on the extraction of copper from the organic to aqueous
phase with 0.02 mol/L Aliquat 336 and Cyanex 272 (0.005 mol/L Cu(II), 0.05 mol/L
Na <sub>2</sub> SO <sub>4</sub> )27
Chapter 3
Figure 3.1. Schematic drawing of the Lewis-cell with single stirring shaft (not to
scale)33
Figure 3.2. Schematic drawing of the updated Lewis-cell (not to scale)34
Figure 3.3. The two phases in the Lewis-cell at the start of the experiment 37
Figure 3.4. Third phase formed after the separation of the two phases
Figure 3.5. Schematic of the Jorin ViPa image analysis technique working
configuration49
Figure 3.6. Photo taken from the Jorin ViPa analyser in the lab
Figure 3.7. Experimental configuration of the pendant emulsion drop evaporation
(not to scale)
Figure 3.8. Schematic drawing of the initial rubber particles formation experimental
configuration (not to scale).
Figure 3.9. Schematic drawing of the updated rubber particles formation
experimental configuration (not to scale)56
Chapter 4
Figure 4.1. % of extracted copper from the aqueous to the organic phase at various
pH values (error bars show the spread of results from 3 repeats)57
Figure 4.2. Effect of stirring speed on the extraction rate of Cu from the organic to
the aqueous phase in the Lewis-cell (0 g/L BR) (error bars show the spread of
results from 3 repeats)

Figure 4.3. Effect of stirring speed on the extraction rate of Cu from the organic to
the aqueous phase in the Lewis-cell (50 g/L BR) (error bars show the spread of
results from 3 repeats)
Figure 4.4. Extraction efficiency at 330 <sup>th</sup> min of Cu from the organic to the aqueous
phase at various stirring speeds for 0 and 50 g/L BR at the end of Lewis-cell
experiments60
Figure 4.5. Effect of BR concentration in the organic phase on the extraction rate of
copper from the organic to the aqueous phase in the Lewis-cell at the highest
impeller speeds 60
Figure 4.6. Visual observation of the effect of acidic and alkaline environment in the
CaSt <sub>2</sub> suspension61
Figure 4.7. Effect of ionic strength on the extraction efficiency of Cr from the organic
to the aqueous phase63
Figure 4.8. Cr solid particles formulation at high concentration of NaCl experiment. 63
Figure 4.9. (A) Cr-CaSt <sub>2</sub> solids during and (B) at the end of the Lewis-cell experiment
64
Figure 4.10. Effect of molar ratio (AcOH/CaSt <sub>2</sub> ) on the % of CaSt <sub>2</sub> that reacted with
the AcOH65
Figure 4.11. The % CaSt <sub>2</sub> that reacted with excess of AcOH or HCI
Figure 4.12. Final pH solution (acid and CaSt <sub>2</sub> ) is comparison with the % of CaSt <sub>2</sub>
that reacted with each acid67
Figure 4.13. Effect of alkaline environment (various concentrations of NaOH) on the
dissociation of CaSt <sub>2</sub> 68
Figure 4.14. Effect of temperature on CaSt <sub>2</sub> dissociation
Figure 4.15. Morphology of the CaSt <sub>2</sub> dried particles (SEM image)70
Figure 4.16. Particle size distribution of CaSt <sub>2</sub> at various pH values70
Figure 4.17. Extraction efficiency of AcOH and % of reacted CaSt <sub>2</sub> after the organic
to aqueous phase mass transfer of AcOH by mixing72
Figure 4.18. Viscosity of the organic phase at various concentrations of BR (0 – 200
g/L in n-heptane) (Logarithmic scale)73
Figure 4.19. AcOH profile organic concentration with time at various concentrations
of BR in the organic phase and without CaSt <sub>2</sub> in the aqueous phase

Figure 4.20. $-lnKOorgAVorg$ as a function of time during the Lewis-cell
experiments at various concentration of BR in the organic phase and without CaSt <sub>2</sub>
in the aqueous phase75
Figure 4.21. Experimental mass transfer coefficient of AcOH at various viscosities of
the organic phase77
Figure 4.22. Effect of $CaSt_2$ on the AcOH extraction rate in the Lewis-cell without the
presence of NaOH78
Figure 4.23. Formation of stearic acid during the Lewis-cell experiment. (A) The
aqueous phase with 10 g/L CaSt <sub>2</sub> at the start (time: 0 sec) and (B) the end of the
Lewis-cell experiment (time: 3600 sec)
Figure 4.24. Effect of $CaSt_2$ on the AcOH extraction rate with the presence of NaOH
in the Lewis-cell80
Figure 4.25. Effect of BR content on the emulsion size and stability - with 5 g/L $CaSt_2$
in the aqueous phase (Experiment: 1 to 3)
Figure 4.26. Effect of BR content on the interfacial tension between the organic and
the aqueous phase without the presence of CaSt <sub>2</sub>
Figure 4.27. Effect of $CaSt_2$ content on the emulsion size and stabilization – with 100
g/L BR in the organic phase (Experiments: A to D)
Figure 4.28. Example of the arrangement of fine $CaSt_2$ particles on the interface 85
Figure 4.29. Effect of CaSt <sub>2</sub> on the interfacial tension between the aqueous and
organic phases without the presence of BR85
Figure 4.30. Photos taken by the KRUSS DSA 100 instrument showing the W/O
emulsion (organic phase: 100 g/L BR in hexane, aqueous phase: 0 g/L CaSt <sub>2</sub> ) drop
changing through time until the final collapse at 130 °C
Figure 4.31. Emulsion drop evaporation at various temperature with (black) and
without (red) CaSt <sub>2</sub>
Figure 4.32. (A) Emulsion inlet pipe in the "flash drum", (B) Partially dried BR in the
"flash drum" (W/O emulsion: organic phase: 50 g/L BR, aqueous phase: 0.1 M NaOH
and 15 g/L CaSt <sub>2</sub> )90
Figure 4.33. BR particles after their formation in the "flash drum" (W/O emulsion:
organic phase: 50 g/L BR, aqueous phase: 0.1 M NaOH and 15 g/L CaSt <sub>2</sub> ) 91
Figure 4.34. Dried BR particles formulated in the lab

## Appendices

Figure A.1. Calibration curve of UV-Vis spectrophotometer for copper	111
Figure A.2. Main parts of the FAAS	112
Figure A.3. Calibration curve of FAAS for chromium	113
Figure A.4. Calibration curve of FAAS for calcium.	115
Figure A.5. Main parts of the HPLC.	116
Figure A.6. Calibration curve of HPLC for AcOH	117
Figure A.7. Shear stress as a function of shear rate for 50 g/L BR in heptane	119
Figure A.8. Shear stress as a function of shear rate for 100 g/L BR in heptane.	119
Figure A.9. Shear stress as a function of shear rate for 200 g/L BR in heptane.	120
Figure A.10. Instrumental configuration for the measurement of the interfacial t	tension
with the technique of the pendant drop in the KRUSS DSA 100 instrument	121
Figure A.11. W/O emulsion (100 g/L BR, 5 g/L $CaSt_2$ , volume phase ratio 4:1 $CaSt_2$ )	D:W).
	123
Figure A.12. Conversion to black and white of the W/O emulsion photo (100 g/	L BR,
5 g/L CaSt <sub>2</sub> , volume phase ratio 4:1 O:W).	123
Figure A.13. Detection of aqueous drops from the software (100 g/L BR, 5 g/L $$	CaSt <sub>2</sub> ,
volume phase ratio 4:1 O:W)	124
Figure A.14. Schematic diagram of the Malvern Mastersizer 2000	124
List of Tables	
Chapter 3	
Table 3.1. Initial concentrations of the two phases for the investigation of the e	ffect of
pH on the extraction efficiency of Cu.	35
Table 3.2. Stirring speeds tested on Lewis-cell according to BR concentration	in the
organic phase	37
Table 3.3. Initial composition of the aqueous and organic phases at the aqueou	us to
organic phase extraction of Cr.	39
Table 3.4. Concentrations of the aqueous phase aiming to achieve high organi	ic to
aqueous phase extraction efficiency.	40
Table 3.5. Concentrations of AcOH and CaSt <sub>2</sub> in solution	42

Table 3.6. Concentrations of CaSt <sub>2</sub> , ACOH and HCI in each solution with their
respective pH
Table 3.7. Concentrations of CaSt <sub>2</sub> and NaOH in each solution with their respective
pH43
Table 3.8. Initial concentrations of the organic and aqueous phases for the
calculation of the distribution coefficient45
Table 3.9. BR and AcOH concentrations in the organic phase on Lewis-cell
experiments examine the effect of the organic phase viscosity on the extraction rate
of AcOH
Table 3.10. Stirring speed of the organic phase in the Lewis-cell at various
concentration of BR
Table 3.11. The concentrations of each species in each phase in the Lewis-cell
experiment for the investigation of the effect of $CaSt_2$ on the interfacial mass transfer
rate
Table 3.12. Concentration of CaSt <sub>2</sub> and BR in each phase for the formation of the
W/O emulsions
Table 3.13. Combination of aqueous and organic phases that used to measure the
interfacial tension
Table 3.14. Concentration of each species in each phase and their volumes that
used in the emulsion pendant drop experiment
Table 3.15. Concentration and volume of each phase used in the rubber particles
formation experiment54
Chapter 4
Table 4.1. Concertation of the NaOH and NaCl in the aqueous phases and the
respective ionic strength and Cr extraction efficiency
Table 4.2. Concentrations of CaSt <sub>2</sub> , AcOH and HCl in each solution with their
respective pH
Table 4.3. Concentrations of CaSt <sub>2</sub> and NaOH in each solution with their respective
pH values68
Table 4.4. The average diameter (D[3,2]) of CaSt <sub>2</sub> measured by the Malvern
instrument at various pH values71

l able 4.5.	Effect of BR concentration in the organic phase (organic phase viscosity)	)
on the ove	rall mass transfer coefficient (KOorg)7	76
Table 4.6.	Concentration of CaSt <sub>2</sub> and BR in each phase for the formation of the	
W/O emuls	sions8	31
Appendi	ces	
Table A.1.	Copper calibration solution' preparation11	10
Table A.2.	Absorbances measured for every calibration solution by the UV-Vis	
spectropho	otometer11	10
	Chromium calibration solutions' preparation11	
	Absorbances measured for every calibration solution of Cr by the FAAS.	
	Coloium colibration colutions' proparation	
	Calcium calibration solutions' preparation	
	11	
	AcOH calibration solutions' preparation for HPLC11	
	Area measured for every calibration solution of AcOH by the HPLC 11	
Table A.9.	Solutions' viscosities, containing various BR concentrations, at 20 and	
50 °C	12	20
List of A	bbreviations	
BR	Butyl rubber	
CaSt <sub>2</sub>	Calcium stearate	
FAAS	Flame Atomic Absorption Spectroscopy	
HPLC	High Performance Liquid Chromatography	
O/W	Oil-in-water emulsion	
$\Omega/W/\Omega$	Oil-in-water-in-oil emulsion	

W/O

Water-in-oil emulsion

#### W/O/W Water-in-oil-in-water emulsion

## List of Roman symbols

A Area

Abs Absorbance

C Concentration

*G* Adhesion energy

I Intensity of light

IS lonic strength

K Overall mass transfer coefficient

k Mass transfer coefficient

MW Molecular weight

m Distribution coefficient

N Mass transfer flux

P Pressure

R Radius

s Standard deviation

t Time

V Volume

X Number of values

Z Charge of an ion

## List of Greek Symbols

 $\delta$  Film thickness

 $\theta$  Contact angle

 $\mu$  Viscosity

ho Density

 $\sigma$  Interfacial tension

## List of Subscripts

aq Aqueous phase

act Actual value

*i* Interface

O Overall coefficient

org Organic phase

ow Oil-water interface

pred Predicted value

so Solid-oil interface

sw solid-water interface

#### Chapter 1

#### 1. Introduction

This research is focused on the halobutyl rubber production process of ExxonMobil at Fawley refinery plant. The conditions for the ExxonMobil process are commercially sensitive and are not revealed in this thesis for reasons of confidentiality. Instead, typical ranges of process conditions are discussed, based on knowledge that is available in the public domain. Halobutyl rubber is a halogenated synthetic co-polymer mainly used in the tire manufacturing industry (Evans, 2001). The research is focused on two main problems that contribute to low quality and productivity.

In the first step of the halobutyl rubber production process, the butyl rubber, dissolved in hexane, is halogenated and acids are formed as by-products. The acids need to be neutralised with an alkaline aqueous phase (Happ et al., 2012). Due to mixing of the two phases an emulsion is formed, and hence improved interfacial mass transfer of the acids is achieved. The first part of the research is focused on understanding the parameters that affect the interfacial mass transfer of the acids during the neutralisation step with the alkaline aqueous phase (ExxonMobil, 2017; Xie et al., 2018). Due to the hazardous acids produced during the halogenation reaction, the interfacial mass transfer was replicated using metal solvent extraction method in the lab. Initially, copper and chromium were used as an alternative to the acids in order to mimic the industrial process in the lab. However, calcium stearate, which is added as stabiliser and cure modifier of the final product in the industrial process (ExxonMobil, 2017; McDonald et al., 2000; NIIR Board of Consultants and Engineers, 2016), proved to be incompatible with the metal solvent extraction processes. Calcium stearate could be potentially used as solid emulsifier in the neutralisation step. Hence, a weak acid (acetic acid) was used in the lab as a more appropriate solute to mimic the solutes being transferred between the organic and the aqueous phase in the industrial process. Two parameters affecting the interfacial mass transfer of a solute were examined in a Lewis-cell apparatus: the organic phase viscosity, controlled by the rubber mass fraction, and the calcium stearate concentration.

The study also investigated the effects of (1) the rubber concentration in the organic phase, and (2) the concentration of calcium stearate (used as stabiliser in the halobutyl

rubber production process), on the size and stability of the halobutyl rubber emulsion formed (ExxonMobil, 2017; McDonald et al., 2000).

In the final step of the industrial process, the halogenated rubber (product) is extracted from the emulsion produced in the previous stages. In order to extract the product, the emulsion is continuously discharged into a flash drum, where it encounters boiling water and steam to achieve full evaporation of the hexane and form solid rubber particles (Kresge and Wang, 2000; McDonald et al., 2000). In the industrial process, a wide range of particles' size are formed, which could potentially cause issues, such as: fouling in pipelines, due to large agglomerated particles, and low productivity, as small rubber particles are drained when the water is removed. These are the reasons why it is important to understand the fundamentals of the rubber particles formation through the evaporation of the emulsion and at which area inside the industrial flash drum it is taking place.

An experimental apparatus was built in the lab to mimic the industrial flash drum and understand how this evaporation process affects the formation of the rubber particles. This apparatus could be used also in the examination of parameters that could affect the size of the particles, such as the concentration of calcium stearate, emulsion discharge speed, etc. Finally, it is crucial to understand the evaporation mechanism of the emulsion containing a dissolved polymer in the continuous phase and, as next step for further investigation, how it could be controlled.

In this thesis, a literature review is presented in Chapter 2, including an outline description of the halobutyl rubber industrial production. The literature review is also focused on the emulsions and their properties and especially Pickering emulsion, as the calcium stearate could be potentially used as an emulsifier in the halobutyl rubber production process. Furthermore, fundamental theory of interfacial mass transfer and solvent extraction of metals are presented. At the end of Chapter 2, a literature review on emulsion evaporation techniques is presented. Chapter 3 presents the two experimental configurations that were developed in the lab and used in the research: the Lewis-cell and the laboratory scale flash drum, as well as the respective experiments, while Chapter 4 is focused on the results and discussion of this research. Chapter 5 presents the overall conclusions and makes recommendations for future work.

#### Chapter 2

#### 2. Literature review

As this study is focused on the halobutyl rubber production process, in the first part of the literature review, the industrial process is presented, as well as the issues that are encountered, which are addressed and analysed later in this study. The review covers the production stages between the halogenation of the butyl rubber and the formation of the final product. Furthermore, an interfacial mass transfer is taking place in an emulsion during the production process and that is why literature reviews both on emulsions and interfacial mass transfer are presented. Finally, a review on the emulsion evaporation techniques is presented, as the final product, halobutyl rubber, is retrieved through an evaporation of the emulsion in which it is dissolved.

#### 2.1. Halobutyl rubber

In this section, the halobutyl rubber production process is presented, as well as information about the product and applications. In addition, the two main problems of the industrial production process are addressed.

## 2.1.1. Introduction - History

Butyl rubber (BR, poly(isobutylene-co-isoprene) is a copolymer which consists of typically 98% of isobutylene and 2% of isoprene, and its molecular structure is shown in Figure 2.1 (Vitiello et al., 2017). Michael Faraday was the first scientist who discovered isobutylene in 1825 and then, BASF was the first company which commercially produced it (BASF SE, 2015; Hsu and Robinson, 2019). The first BR was developed by William J. Sparks and Robert M. Thomas, researchers of the Standard Oil company (Reese, 1988). BR started its commercialised production in USA in 1943 during the World War 2, when there was high demand of tires and USA lost access to their rubber plantations in Malaysia (Roberts, 1952). BR was used in car tires, as it has low permeability and good flexible properties. In 1950s, halogenated butyl rubber was developed by the introduction of a halogen into the BR chain. This modification enhanced various properties of the copolymer, such as permeability, ageing resistance, flexibility, thermal stability and easier vulcanization (Evans, 2001;

Parent et al., 2001; Rodgers, 2015). In addition, one of the most important advantages is the easier blending of the halobutyl rubber combined with other types of elastomers in order to be vulcanised. There are two halobutyl variants: the chlorinated BR (chlorobutyl rubber) and the brominated BR (bromobutyl rubber) (Parent et al., 2001).

Figure 2.1. Molecular structure of BR. (Vitiello et al., 2017)

#### 2.1.2. Applications

The synthetic rubber market is growing every year. In 2018 the value of the halobutyl rubber market was \$3.60 billion and it is predicted to increase to \$5.62 billion by 2025, due to extensive applications and global demand (Research Adroit Market, 2019). One the most important applications of halobutyl rubber is its use as a thin layer of rubber on the inside of a tubeless tire, the inner liner, due to its low permeability, in order to achieve air retention. Figure 2.2 shows a commercial tire' cross-section and all the parts that constitute it (Evans, 2001). Also, other applications of halogenated BR are in automotive hoses, pharmaceutical closures, insulators for electric cables, shock absorbers and mechanical goods (Fusco et al., 1990; Monakov and Zaikov, 2006; Xie et al., 2018).

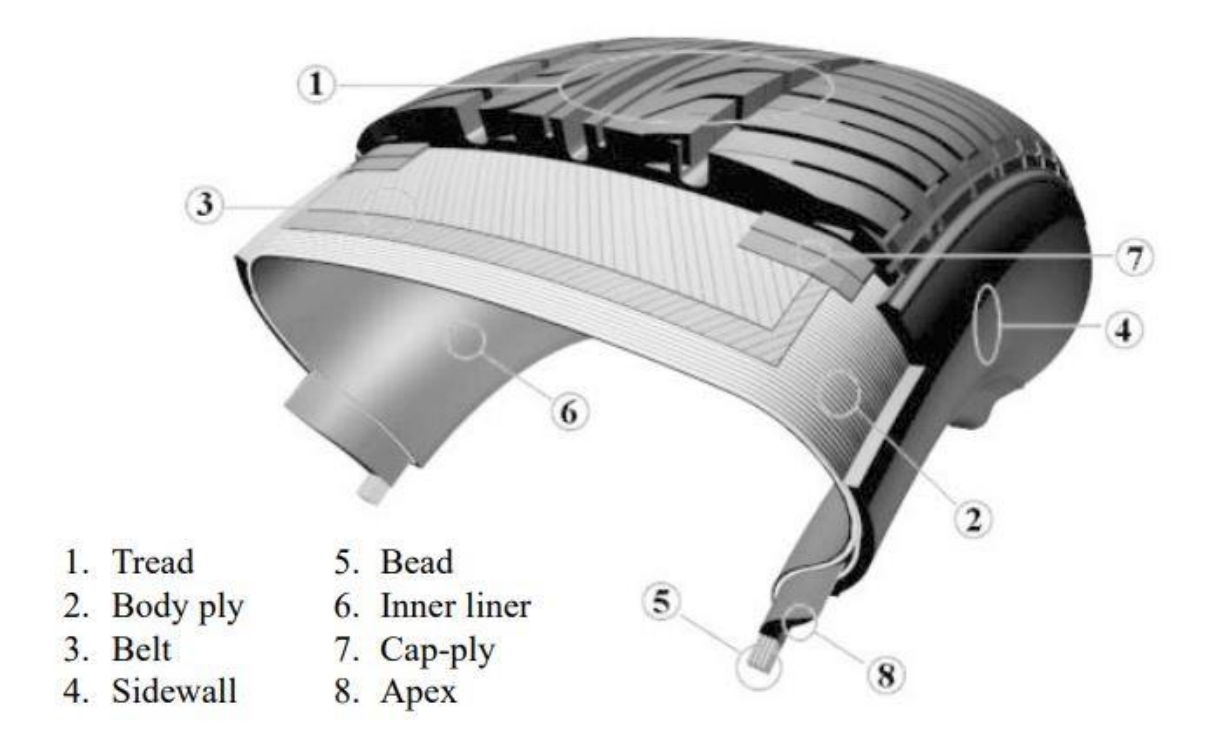


Figure 2.2. Tire cross-section. (Evans, 2001)

## 2.1.3. Halobutyl rubber production process

The manufacturing process for halobutyl rubber has two main stages, the halogenation of the BR and the rubber particles formation process, as shown in Figure 2.3. In the first stage, there are two main operations: the halogenation and the neutralisation and each step takes place in a continuous high shear rate reactor (Happ et al., 2012). The second part of the process, where the product, halogenated BR, is formulated, takes place in a flash drum (ExxonMobil, 2017; Kowalski et al., 1986; McDonald et al., 2000). The halobutyl rubber production process steps are analysed in detail in the following sections. The operating conditions are described as typical ranges used in the halobutyl rubber production process.

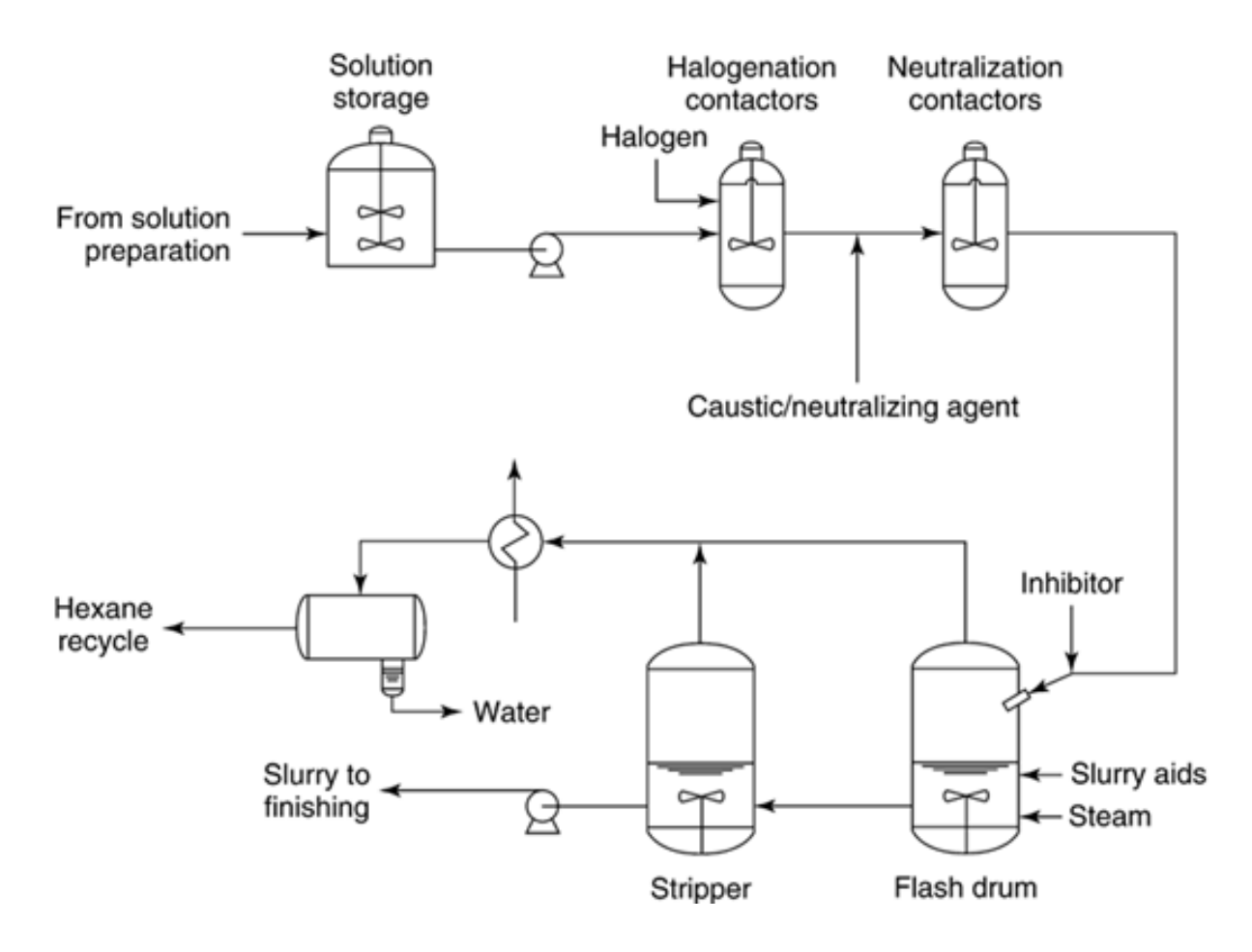


Figure 2.3. Simplified halobutyl rubber production process.

(Kresge and Wang, 2000)

## 2.1.4. Halogenation

The first step is the halogenation of the BR with either liquid bromine (Br<sub>2</sub>) or gaseous chlorine (Cl<sub>2</sub>) through ionic substitution reaction in a high shear rate mixer (Kresge and Wang, 2000). Typically, the BR is introduced into the reactor dissolved in hexane at concentration between 200 g/L and 250 g/L between 20 and 65 °C (ExxonMobil, 2017; Happ et al., 2012). High temperature is used to reduce the organic phase viscosity in the reactors and to facilitate the solvent evaporation at the final step. Every mole of chlorine or bromine reacts with one mole of the copolymer and hydrobromic acid (HBr) or hydrochloric acid (HCl) are formed as by-products, as shown in the Chemical Reactions 2.1 and 2.2 (Mark et al., 2013; Rodgers, 2015). The produced acids need to be neutralised in the next step of the process, as high concentration of acids results in slower halogenation and higher energy consumption (Xie et al., 2018).

Bromination reaction:

$$\sim \sim Polymer \sim \sim + Br_2 \rightarrow \sim \sim Polymer Br \sim \sim + HBr$$
 (2.1)

Chlorination reaction:

$$\sim \sim Polymer \sim \sim + Cl_2 \rightarrow \sim \sim Polymer Cl \sim \sim + HCl$$
 (2.2)

#### 2.1.5. Neutralisation

The acids, which were the by-products of the previous step, need to be neutralised with sodium hydroxide in an aqueous phase (see Figure 2.3). To achieve that, alkaline aqueous phase is introduced into the reactor and the two phases create an emulsion. During this stage, the emulsion is formed as a result of mixing (Kresge and Wang, 2000). Interfacial mass transfer of the acids takes place in the emulsion. Due to the high viscosity of the emulsion, high shear rate is applied to increase the contact area between the two phases, by creating smaller droplet size of the dispersed phase, the aqueous, in the emulsion (Kresge and Wang, 2000; McDonald et al., 2000; Rodgers, 2015). The high contact area helps the interfacial mass transfer and, as a result, the acids are transferred to the aqueous phase and react with the NaOH. The phase ratio is approximately between 1 and 5 for the organic to aqueous phase by volume. The reactions between the NaOH and the acids are shown in the Chemical Reactions 2.3 and 2.4.

Neutralisation reaction of HBr:

$$HBr + NaOH \rightarrow NaBr + H_2O$$
 (2.3)

Neutralisation reaction of HCI:

$$HCl + NaOH \rightarrow NaCl + H_2O$$
 (2.4)

## 2.1.6. Rubber particles formation

The emulsion, formed in the previous stages at high temperature, is continuously fed into a flash drum (Figure 2.4) where the hexane is flashed and the rubber particles are formed. Prior to the flash drum, calcium stearate is added which act as antioxidant and

stabiliser (McDonald et al., 2000). Furthermore, CaSt<sub>2</sub> acts as a cure modifier on the final product, halobutyl rubber, which helps in the vulcanization process downstream (NIIR Board of Consultants and Engineers, 2016). In the flash drum, there is a holdup of water, kept at constant level, and steam and hot water provide heating, as shown in Figure 2.4. The emulsion is introduced into the flash drum through a pipe at high speed. The operating temperature and pressure are between 105 and 120 °C and 2 and 3 atm respectively, which is above the boiling point of pure hexane of 68 - 90 °C, depending on pressure (Kresge and Wang, 2000; McDonald et al., 2000). The process understanding was that hexane evaporates from the emulsion stream in the headspace, resulting in rubber particles entering the water phase, where CaSt2 is present to prevent further agglomeration (McDonald et al., 2000). This thesis aim was to investigate if there is sufficient residence time in the headspace for fully evaporation of the hexane, such that particle formation is almost complete before entering into the water phase. An outlet in the flash drum, located lower than the water level, removes the particles and feeds them to the next stage of the process, where removal of water is achieved, and the rubber is packed in blocks for shipping. The evaporated hexane is removed from the top of the flash drum and recycled in order to be used again in an earlier stage of the process. The rubber particles formed have irregular shapes, as shown in Figure 2.5 (Arlanxeo, 2017). Due to poor control of the process within the previous stages, the final product has a wide particle size distribution, which results in two main problems, namely: (1) blockages in the pipes due to agglomeration of the rubber particles and (2) value product losses while draining the water due to the small size of the rubber particles. (Kowalski et al., 1987). An experimental configuration was developed and built in the lab to be able to mimic the industrial flash drum and formulate the similar rubber particles, as described in Section 3.7.2.

The next parts of this review discuss the relevant literature on emulsions, emulsification and interfacial mass transfer, as these topics provide the underpinning science for the research conducted in this thesis.

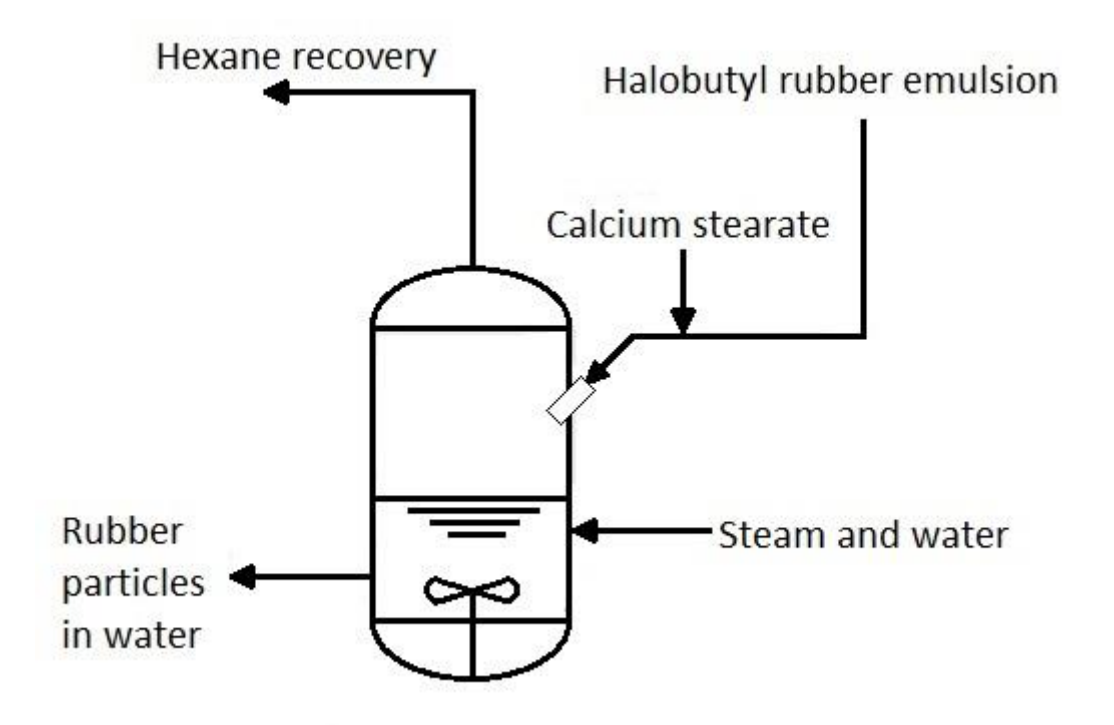


Figure 2.4. Schematic drawing of the industrial flash drum vessel.

(McDonald et al., 2000)



Figure 2.5. Halobutyl rubber dried particles (Arlanxeo, 2017)

#### 2.2. Emulsions

Emulsions play an important role during the halobutyl rubber production process, as both the neutralisation and the rubber particles formation steps depend on the properties of the emulsion. Therefore, this section is a brief introduction to emulsions and a literature review, that covers their types, sizes and applications, as well as the role of surfactants, the viscosity of the continuous phase and the emulsion breaking.

#### 2.2.1. Introduction to emulsion types

An emulsion is a stabilised colloidal dispersion of one liquid dispersed in another in the form of droplets and occurs when the interfacial tension between the two phases is low. Two liquids that are used to form an emulsion are immiscible, like water and oil. The simplest types of emulsions are the O/W and W/O, where the water (W) and oil (O) are the continuous phases, respectively. Several factors can affect the type of the emulsion, such as volume phase fraction, type and concentration of the emulsifier (hydrophobic or hydrophilic), temperature, etc (Binks, 1998; Binks and Horozov, 2006; Wu and Ma, 2016). Multiple emulsions can also form, such as the W/O/W and O/W/O, as shown in Figure 2.6 (Schramm, 2005).

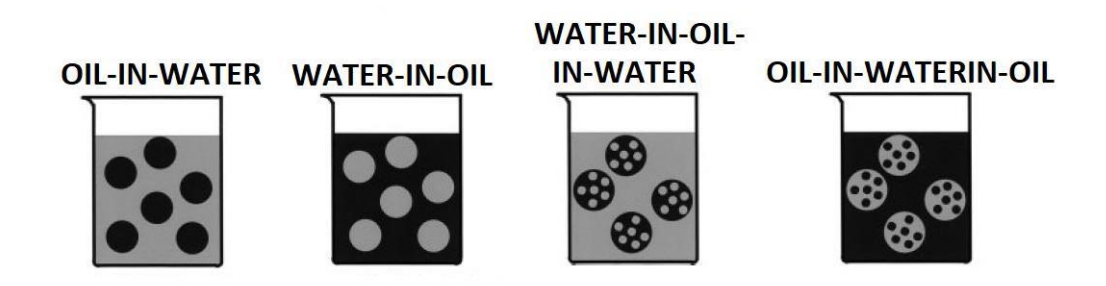


Figure 2.6. Types of emulsions. (Schramm, 2005)

Emulsions find applications in various industry sectors, such as cosmetics, pharmaceuticals, petroleum, agricultural, personal care and food (Albert et al., 2019; Berton-Carabin and Schroën, 2019; Dickinson and Pawlowsky, 1996; Krasodomska and Jungnickel, 2015; Rayner et al., 2012; Sakamoto et al., 2017). In addition, emulsions are important in chemical processes, including halobutyl rubber production process (Rodgers, 2015), because they provide a high specific contact area and promote faster interfacial mass transfer (Pandolfe, 1981). The emulsions can be categorized by the size of the dispersed phase drops as shown bellow (Bai et al., 2016; Coneac et al., 2015; Gupta et al., 2016; Tadros, 2013):

- Macroemulsions are usually emulsions with drop size between 1 and 100 µm.
   These size of emulsions are not thermodynamically stable in the absence of stabilising compounds.
- Microemulsions have usually 10 to 100 nm and they are thermodynamically stable.

 Nanoemulsions have drops in the size range of 100 – 500 nm and they are kinetically stable. These types of emulsions are stabilised by an amphipathic surfactant and they can be either W/O or O/W.

#### 2.2.2. Emulsification techniques

The formation of an emulsion could be achieved by the following emulsification techniques:

- Propeller stirrer.
- Homogenizer/rotor-stator mixer.
- Ultrasonic emulsification.
- Microfluidic devices.
- Membrane emulsification.

The first two types of emulsification techniques are most commonly used in industrial scale applications and, more specifically, the propeller stirrer technique is often applied (Cheremisinoff, 2000). Both techniques apply high shear rate to mix the two liquids. In the rotor-stator mixer high kinetic energy is applied on the liquids by the rotor, forcing them towards the rotor-stator where high shear is applied due to the small size gaps (Harmsen, 2019; Jain and Soni, 2011; Zhang et al., 2012). Ultrasonic emulsification, based on ultrasound waves that travel through the liquids and cause microturbulences and interfacial movement, results in an unstable interface between the two phases and droplets of the dispersed phase are formed (Cha et al., 2019). In the microfluidic devices for the preparation of emulsions, the dispersed phase is pumped through a microchannel containing the continuous phase. Spherical droplets are formed when the dispersed phase exits the microchannel. The main advantage of the microfluidic devices is the uniform emulsions, but it cannot be used in large scale production (Xu et al., 2005). On the other hand, membrane emulsification is a promising technique to achieve uniform emulsion in larger scale productions. In order to formulate the emulsion, the dispersed phase is pressed or injected through the membrane inside a stirred continuous phase. (Alliod et al., 2018; Dragosavac et al., 2012).

As mentioned above, the propeller stirrer technique is the most common technique used in the industry. In order to mimic the industrial process, the same technique was

used in the lab for this study to form the halobutyl rubber emulsion. Furthmore, due to the high viscosity of the organic phase, high shear rate was required.

#### 2.2.3. The role of surfactants/emulsifiers in the emulsions

The stabilization of emulsions is achieved by emulsifying agents (emulsifiers or surfactants), which are amphipathic molecules, with two different ends, one end of is hydrophilic and the other is hydrophobic. An emulsion could be stable even for months or years under the correct use of the emulsifier (Cao et al., 2014; Garti and Katz, 1985; Wong et al., 2015). The emulsifiers decrease the interfacial tension between the two phases, which leads to an increase of the contact area by reducing the dispersed phase drop size (Adebayo and Adeyemi, 2018; Lucassen-Reynders and Kuijpers, 1992). They arrange themselves at the interface of the oil and water phase by creating a protective film which helps the emulsion to be formed and prevent it from breaking (Binks and Horozov, 2006). An important consideration in choosing a suitable emulsifier is its hydrophilic-lipophilic balance (HLB) value, which can be calculated by Equation 2.5. The HLB value indicates if the emulsifier is suitable for W/O or O/W emulsion. The emulsifier should be physically and chemically stable and should not interact with other substances in the emulsion (Tadros, 2013; Zheng et al., 2015), with exceptions such as in the production of the halobutyl rubber where the surfactant acts as cure modifier to the final product (NIIR Board of Consultants and Engineers, 2016).

$$HLB = 20 \frac{MW_{hydrophobic part}}{MW_{total}}$$
 (2.5)

Where: *MW* is the molecular weight.

## 2.2.4. Emulsion breaking

The main problems of emulsions are coalescence, flocculation, creaming, breaking and sedimentation. Figure 2.7 shows the effect of each problem on the emulsions by comparing it with a stable one. In the creaming problem, the less dense dispersed phase rises to the top and forms a creamy phase. Sedimentation is the graviational settling of the dispersed phase due to high-density difference of the two liquids. During coalescence, the droplets of the dispersed phase merge and forms bigger droplets. In

flocculation, the small droplets could stick together due to Van der Waal forces or due to the reduction of free energy and in order to overcome this problem, addition of the correct amount of emulsifier is needed (Alvarado et al., 2011; McMullen et al., 2014; Schramm, 2005). In the halobutyl rubber production process, emulsion breaking could result in low interfacial mass transfer area, as well as on wider rubber particle size distrubution on the final stage of the process.

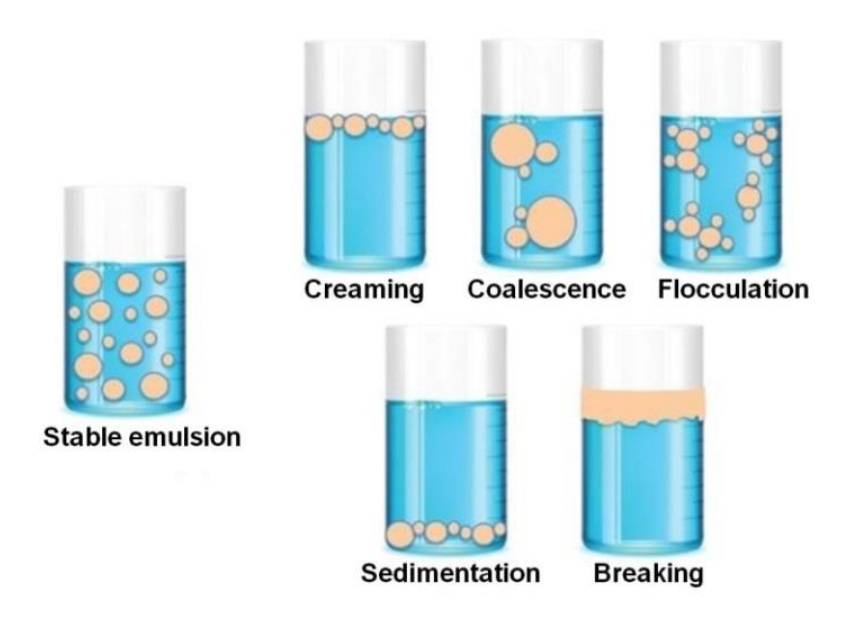


Figure 2.7. Emulsion breaking processes.

(McMullen et al., 2014)

# 2.2.5. The role of viscosity of the continuous phase in the emulsions

The viscosity of the continuous phase of an emulsion plays an important role in its stability and the droplet size. Increasing the viscosity of the continuous phase reduces the coalence and creaming of the dispersed phase drops (Schramm, 2005). As viscosity modifiers, polymers or non-surface active macromolecules could be used in the lab (Behrend et al., 2000). Tesch and Schubert (2002) examined the effect of the continuous phase viscosity on short-term stability of protein stabilized emulsions (Tesch and Schubert, 2002). They concluded that the increase of the viscosity decreased the average diameter of the dispersed phase drops and increased the stability of the emulsion. In their experiments, polyethylene glygol was used to modify the viscosity.

In the halobutyl rubber production process, the rubber acts as a viscosity modifier and with the application of intense agitation, an emulsion is formed (Happ et al., 2012).

#### 2.2.6. Pickering emulsions

In Pickering emulsions, solids are used to stabilise the droplet of the dispersed phase. These types of emulsions are called Pickering and were named by S.U. Pickering in 1907. Originally, these types of emulsions where described by Walter Ramsden four years earlier in 1903 (McMullen et al., 2014; Pickering, 1907). In Pickering emulsions, the solid particles must be smaller than the droplet size of the dispersed phase in order to create a barrier at the interface of the two phases (Alvarado et al., 2011). Pickering emulsions have higher resistance to coalescence and Ostwald ripening (high long-term stability) compared to classic emulsions, which make them the right canditate for the applications which are described in the next paragraph (Chevalier and Bolzinger, 2013). The wettability of the solid particles is responsible for the formation of either W/O or O/W emulsion and is going to be analysed further later in this section.

Pickering emulsions find applications where the regular emulsifiers show adverse effects, like in biomedical products for drug delivery (Frelichowska et al., 2009; Simovic and Prestidge, 2007; Wu et al., 2016), in food industry (Berton-Carabin and Schroën, 2015; Dickinson, 2010; Kargar et al., 2012; Rayner et al., 2014; Rayner and Dejmek, 2015), in cosmetics (Binks et al., 2010) and in catalytic engineering (Shan et al., 2015; Zhao et al., 2016). The advantage of the greater stability of Pickering emulsions is due to the strong attachment of the solid particles between each other. For example, Timgren et al. (2013) managed to form a food-grade Pickering emulsion with high stability of more than 2 years with the use hydrophobic starch granules (Timgren et al., 2013). Another property of Pickering emulsions is their permeability. Due to the large size of the solid particles (compared to common surfactant molecules), Pickering emulsions have higher permeability to interfacial mass transfer. Their permeability is mainly affected by the size and the concentration of the solid particles.

The wettability of the solid particles is responsible for the formation of either W/O or O/W emulsions and also plays important role in the stability of the emulsion (Hunter et al., 2008; Taherpour and Hashemi, 2018). The liquid which wets better the solid particles becomes the continuous phase. A hydrophilic solid particle is more wetted by

the aqueous phase (Figure 2.8) and, as a result, the contact angle is greater than 90° and the system forms an O/W emulsion. On the other hand, the contact angle for hydrophobic solid particles is lower than 90° and the system is W/O emulsion. The reduction of the interfacial area between the two phases is the driving force of the assembly of the solid particles in such structure. The Equation 2.6 shows the adhesion energy (G, Jm<sup>-2</sup>) as a function of the contact angle ( $\theta$ ) and the interfacial tension of the interface ( $\sigma_{ow}$ ). This free energy is what required to remove one particle from the interface between the two phases (French et al., 2016; Low et al., 2020).

$$G = \pi R^2 \sigma_{ow} (1 + \cos \theta)^2 \tag{2.6}$$

Where:  $\sigma_{ow}$  is the interfacial tension of the interface between the two phases.

*R* is the radius of a solid particle.

 $\theta$  is the contact angle between the solid particle and the interface, as shown in Figure 2.8 (measured from the aqueous phase).

The subscripts o and w refer to the oil and water phases respectively.

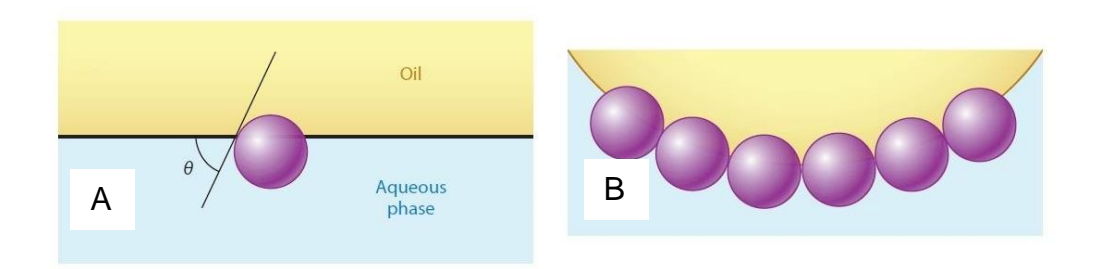


Figure 2.8. A. Contact angle between the solid particle (purple sphere) and the interface, B. Arrangement of the solid particles at the interface on an O/W emulsion.

(Berton-Carabin and Schroën, 2015)

It should be mentioned that, when the solid particles are small enough, it is assumed that the effect of gravity is negligible. Young's equation (Equation 2.7), which is given below, gives the relation between the solid-oil, oil-water and solid-water interfacial tensions and can be used in the prediction of the type of the emulsion (French et al., 2015; Sharifzadeh et al., 2017).

$$\cos\theta = \frac{\sigma_{so} - \sigma_{sw}}{\sigma_{ow}} \tag{2.7}$$

Where:  $\sigma_{so}$  is the interfacial tension of the interface between the solid particle and the oil.

 $\sigma_{sw}$  is the interfacial tension of the interface between the solid particle and the water.

The formation of the Pickering emulsions is based on the following factors:

- The partial wetting of the solid particles by the two phases at the interface.
- The total concentration of the solid particles.
- The size of the solid particles.
- The shape of the solid particles.
- The surface properties of the solid particles (e.g. particle's roughness).

The concentration of the solid particles plays an important role in the stabilisation of a Pickering emulsion. An increase of the concentration favours the surface coverage and improves the stability of the system. However, in some cases, a higher solids concentration decreases the droplet size and forms a network structure (bridges) of solids around the dispersed phase, as shown in Figure 2.9 (Aveyard et al., 2003; Wu and Ma, 2016).

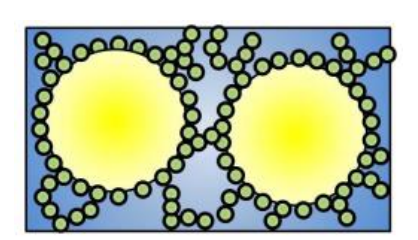


Figure 2.9. Network structure of the solids particles around the dispersed phase. (Reed, 2011)

The size of the solid particles has a major effect on the stability and the size of the droplets in a Pickering emulsion. An decrease of the solid particle diameter favours the formation of more stable emulsions, as it decreases the size of the droplets of the dispersed phase (Qi et al., 2014).

The solid particles can have different shapes, like rods, fibres, cubes and others, which affect the stabilisation of the Pickering emulsion. For example, De Folter et al. (2013) created a Pickering emulsion with the use of novel solid particles in the shape of cubic and peanut shapes, as shown in Figure 2.10 (De Folter et al., 2014). There are different types of solid particles, such as carbon nanotubes, silica, calcium carbonate, block copolymer micelles, bacteria, spores and others that can be used for the formation of Pickering emulsions (Chevalier and Bolzinger, 2013).

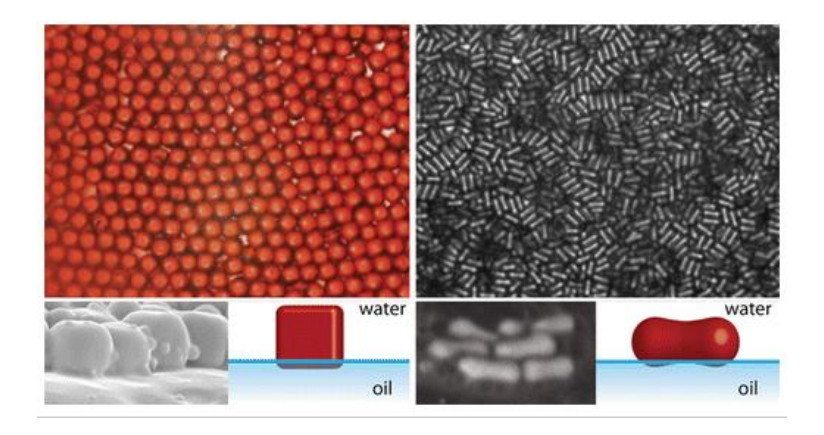


Figure 2.10. Two different shapes of solid particles used in Pickering emulsions. (De Folter et al., 2014)

The surface properties of the solid particles play an important role in the stability of a Pickering emulsion. San-Miguel and Behrens (2012) proposed that the particle roughness improves the stability of the emulsions against coalesce, as it changes the wetting of the particles (San-Miguel and Behrens, 2012). Also, the surface properties (chemical composition) of the solid particles can contribute in the formation of W/O or O/W emulsion. For example, as shown in Figure 2.11, the hydrophilic surface of a particle could be modified by using alkylchlorosilanes in order to become hydrophobic and, as a result, to change the form of the emulsion (Horozov et al., 2003; Reed, 2011).

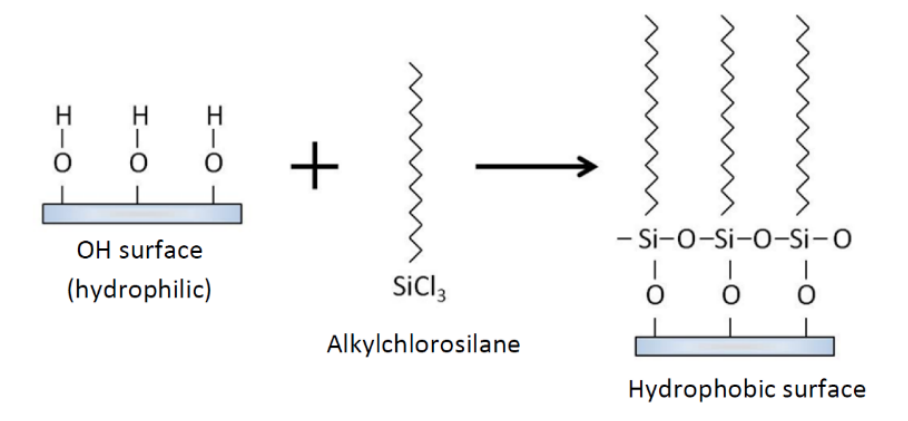


Figure 2.11. Chemical modification of a hydroxylated surface (hydrophilic surface) with alkylchlorosilane to form a hydrophobic surface.

(Reed, 2011)

#### 2.2.7. Calcium stearate as a solid stabilised particle

CaSt<sub>2</sub> is part of the metallic soaps family and used as emulsifying agent in a variety of industies, such as the cosmetics sector. The stearates derive from natural resources and are also used as lubricant and water repellent in various industries (Barker et al., 1977; Sikora, 2019). The CaSt<sub>2</sub> molecule has two long fatty acid chains connected with a metal part, calcium in this case, as shown in Figure 2.12. The two long chains are the hydrophobic group and the metal part is the hydrophilic one and, as a result, it stays at the interface when is present in an emulsion. The CaSt<sub>2</sub> tends to form W/O emulsions due, to two the hydrocarbon chains, which gives a triangular shape to the molecule, as shown in Figure 2.13 (Knowlton and Pearce, 1993; Sharma, 1991). In addition, the calculated HLB value of CaSt<sub>2</sub> is 1.32, using Equation 2.5, indicating that it forms W/O emulsions (Jirgensons and Straumanis, 1962). As mentioned in Section 2.1.6, the CaSt<sub>2</sub> is already added in the halobutyl rubber production process prior to the flash drum; it acts as a curing agent in the final product (ExxonMobil, 2017; Happ et al., 2012; McDonald et al., 2000). This research was focused on an investigation of CaSt<sub>2</sub> as an emulsifier in the halobutyl rubber process, as well as its effect on the interfacial mass transfer of the by-products in the neutralisation step.

#### Hydrophobic part

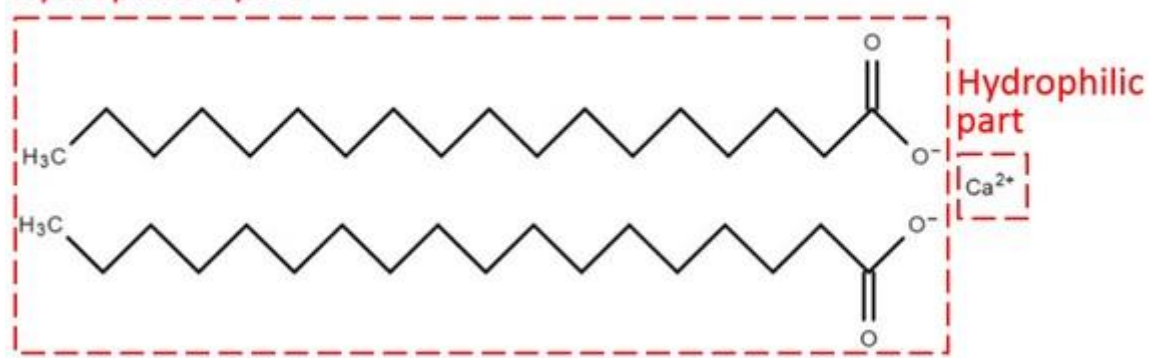


Figure 2.12. Calcium stearate molecule

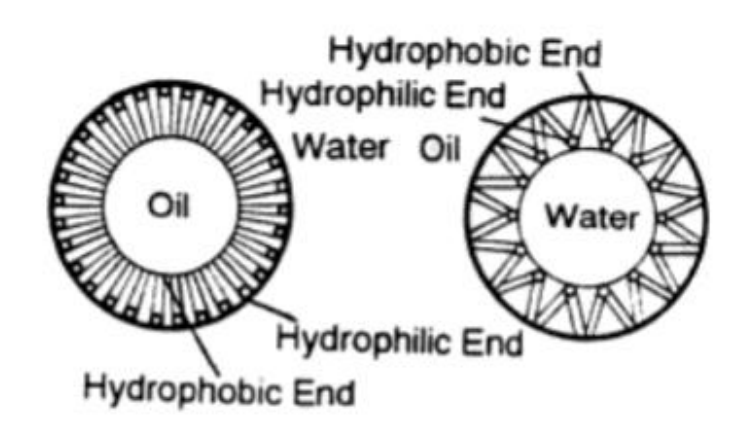


Figure 2.13. The function of the CaSt<sub>2</sub> molecule around the water drops in a W/O emulsion (example on the right) and comparison to a single hydrocarbon chain emulsifier (example on the left).

(Sharma, 1991)

#### 2.3. Interfacial mass transfer

The interfacial mass transfer of the acids in the halobutyl rubber production is a crucial step in order to achieve the neutralisation. This section is dedicated to fundamental theory of the interfacial mass transfer and solvent extraction of metals, as well as on the description of an experimental technique for calculating the mass transfer coefficient. The emulsions, like the one in the halobutyl rubber production process, are the ideal environment for intefacial mass transfer of a solute, due to the high contact area between the two phases (Hussein et al., 2019).

### 2.3.1. Two-film theory

The concentration difference of the solute between the two phases close to the interface is the driving force of the interfacial mass transfer in order to achieve equilibrium in the system. The simplest theory for explaining the mass transfer phenomenon is the two-film theory (Lewis and Whitman, 1924). This theory was developed by Lewis and Whitman and is based on the assumption that the resistance to mass transfer depends on two films, one at each side of the interface, as well as the resistance of the interface, as shown in Figure 2.14.

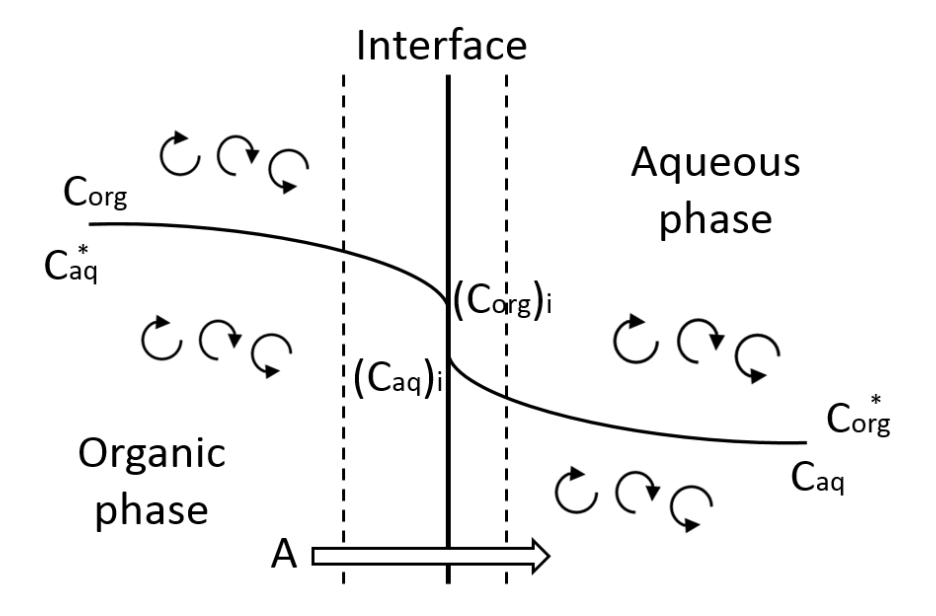


Figure 2.14. The transfer of the solute (A) in a ternary system between organic and aqueous phase.

In addition, the two-film theory is based on the assumptions, that there is not accumulation of the transferred species at the interface and the concentration of the transferred species are uniformed in the well-mixed bulk areas of each phase. Equation 2.8 shows the mass transfer flux of A ( $N_A$ ) between the organic and the aqueous phase, defining the **overall** mass transfer coefficient with respect to the organic phase ( $K_{Oorg}$ ).

$$N_A = K_{Oorg} \left( C_{org} - C_{org}^* \right) \tag{2.8}$$

Where:  $C_{org}$  is the concentration of A in the organic phase bulk area

 $C_{org}^*$  is the concentration of A in the organic phase in equilibrium with the concentration of A in the aqueous phase, as described by the Equation 2.9.

$$C_{ora}^* = mC_{aa} \tag{2.9}$$

Where: m is the distribution coefficient which defined as the ratio of the concentration of A in the organic phase with the one in the aqueous phase at equilibrium.

By expanding the mass transfer flux equation of A to include the concentration of A at the organic phase interface  $(C_{orgi})$  it concluded to the Equation 2.10.

$$N_A = K_{Oorg} [(C_{org} - C_{orgi}) + (C_{orgi} - C_{org}^*)]$$
 (2.10)

Where:  $C_{aqi}$  is the concentration of A in the aqueous phase at the interface.

 $C_{aq}$  is the concentration of A in the aqueous phase bulk area.

By taking into account the Equations 2.11 and 2.12, where the  $C_{orgi}$  and  $C_{org}^*$  are expressed in concentrations of A in the aqueous phase at equilibrium, the Equation 2.10 takes the following form (Equation 2.13).

$$C_{orgi} = mC_{aqi} (2.11)$$

$$C_{org}^* = mC_{aq} \tag{2.12}$$

$$N_A = K_{Oorg} [ (C_{org} - C_{orgi}) + (C_{aqi} - C_{aq})m ]$$
 (2.13)

In a steady-state the fluxes through all films are equal as shown bellow.

$$\frac{N_A}{k_{org}} = \left(C_{org} - C_{orgi}\right) \tag{2.14}$$

$$\frac{N_A}{k_{aq}} = (C_{aqi} - C_{aq}) {(2.15)}$$

Where:  $k_{org}$  and  $k_{aq}$  are the **film** mass transfer cofficient in the organic and aqueous phase respectively.

By taking into consideration the Equations 2.13, 2.14 and 2.15 the overall mass transfer coefficient with respect to the organic phase could be expressed on the indvidual **film** mass transfer coefficients ( $k_{org}$  and  $k_{aq}$ ), as shown in Equation 2.16.

$$\frac{1}{K_{Oorg}} = \frac{1}{k_{org}} + \frac{m}{k_{ag}} \tag{2.16}$$

Low interfacial mass transfer efficiency can be the result of low diffusivity of the solute in one phase, due to the high viscosity of the phase, like in the case of the halobutyl rubber production process. The high concentration of rubber results in high viscosity and, as a consequence, low mass tranfer rate. The molecular diffusion coefficient (*D*, m<sup>2</sup> s<sup>-1</sup>) can be estimated by the Equation 2.17, where it could be seen that is inversely proportional with the viscosity of the solvent (Wilke and Chang, 1955).

Wilke-Chang equation:

$$D = \frac{7.4 \ 10^{-8} T \sqrt{\alpha MW}}{\mu V^{0.6}} \tag{2.17}$$

Where:

*a* is the association coefficient of the solute which is used to take into consideration the molecular weight of the solvent in the diffusion (Miyabe and Isogai, 2011; Wilke and Chang, 1955).

*MW* is the molecular weight of the solvent.

*T* is the absolute temperature.

 $\mu$  is the viscosity of the solvent.

*V* is the molar volume at the normal boiling point of the solute.

In addition, the high viscosity will reduce the diffusivity of the solute in the film of the viscous phase. The relationship between the film mass transfer coefficients ( $k_{org}$  and  $k_{aq}$ ) and the diffusivity ( $D_{org}$  and  $D_{aq}$ ) of the solute on each phase is shown in Equation 2.18.

$$k_{org} = \frac{D_{org}}{\delta_{org}} \qquad k_{aq} = \frac{D_{aq}}{\delta_{aq}} \tag{2.18}$$

Where:  $\delta_{org}$  and  $\delta_{aq}$  are the film thickness on each phase.

Resistance on the interface could be the result of the presence of solids, such as surfactants and emulsifiers, as shown in Figure 2.8 where solid emulsifier particles are attached at the interface to form a Pickering emulsion. For example, inert solids could obstruct the solute at the interface, such as in the work of Ferreira A. et al, (2010), who investigated the effect of polycinyl chloride and polystyrene particles on the interfacial mass transfer between gas and liquid phase. The experiments were conducted in a bubble column and they concluded that the presence of solids increases the resistance in the liquid phase (Ferreira et al., 2010). When there is resistance at the interface ( $R_i$ ), the Equation 2.18 could be written as follows.

$$\frac{1}{K_{Oorg}} = \frac{1}{k_{org}} + \frac{m}{k_{ag}} + R_i \tag{2.19}$$

Finally, the increase of the contact area between the two phases increases the interfacial mass transfer, as it was proved by Kasaie M. et al, (2017) on the solvent extraction of copper in a Lewis-cell apparatus, which is discussed in the following section.

# 2.3.2. Lewis-cell technique

In order to understand the kinetics and the mechanism of the mass transfer between two phases, several experimental procedures have been proposed (Volkon, 2001). The aim of these experimental procedures is to estimate the mass transfer coefficient and reduce the number of experiments in a pilot scale apparatus, as they are time consuming and expensive. The most widely used experimental procedure is the Lewis-cell technique (Huang et al., 2016; Kaplanow et al., 2019). Lewis developed in 1954 an apparatus where the two liquids come in contact at a constant interfacial area, as shown in Figure 2.15, which is used to measure the interfacial mass transfer rate of a solute (Hanna and Noble, 1985; Volkon, 2001).

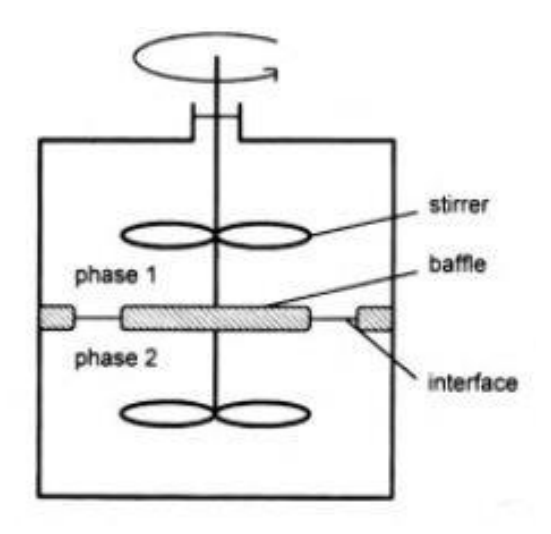


Figure 2.15. Lewis–cell schematic apparatus. (Volkon, 2001)

In the centre of every phase, stirrers are located, able to mix each phase separately without mixing the two liquids together or disturb the interface by creating a vortex. In addition, in order not to create a vortex and preserve the flat interface, a baffle is placed in the centre between the two liquids. Both phases are stirred at the same rate and direction. The heavier phase is introduced first into the cell and then, the lighter one, without disturbing the interface or mixing them (Bandyopadhyay et al., 1996).

However, since the first appearance of the Lewis-cell, several modifications have been made in order to overcome some problems, such as the insufficient mixing of each phase, resulting in lower diffusion of the solute, and not controllable temperature in the system during the experiment. Therefore, reasearchers modified the original apparatus by using stirrers rotating separately in different directions and speeds, applicable in phases with different viscosities. Also, heating/cooling jacket around the cell in order to keep the temperature constant can be added (Stevens and Perera, 1997).

In order to calculate the mass transfer coefficient in the Lewis-cell, the effect of the stirring speed on the interfacial mass transfer should be reduced. In a fixed Lewis-cell and for given liquid phases, the extraction rate is constant after a certain increase of the stirring speed, as shown in Figure 2.16. In the zone A, the extraction rate depends on the stirring rate. On the contrary, in the zone B, the stirring rate has lower effect on the extraction rate (Rydberg et al., 2004).

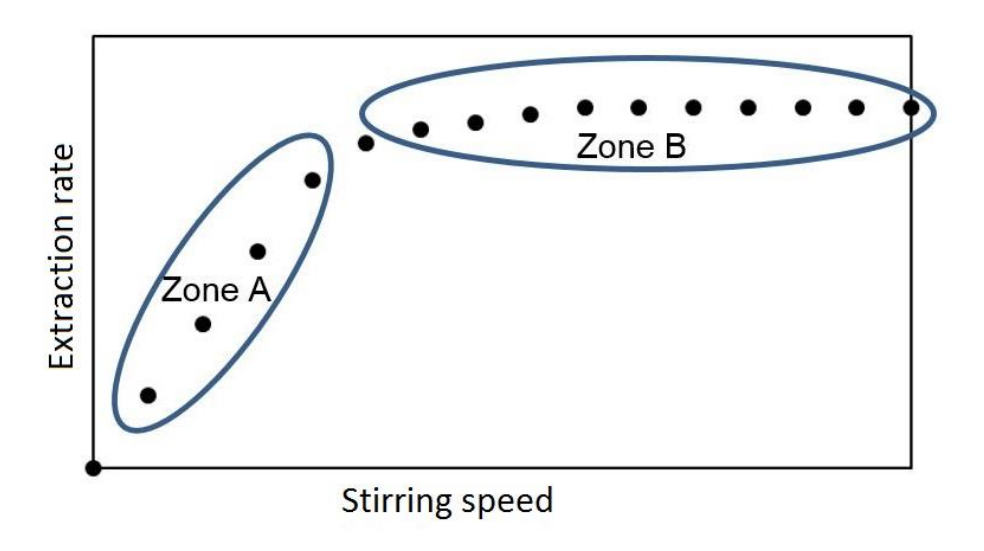


Figure 2.16. The effect of stirring speed on the extraction rate in the Lewis-cell.

Kasaie Maryam et al, (2017) used the Lewis-cell device to perform a kinetic study on the solvent extraction of copper, using Cupromex-3302 as extractant in the organic phase. They concluded that the increase of the stirring speed on each phase up to a certain value increases the copper extraction. By increasing further the stirring speeds there was very low effect on the extraction rate and the extraction process was controlled by the interfacial resistance, the chemical reaction and film thickness. The film thickness, where the diffusivity of the solute depends on the visocsity of the phase, cannot be eliminated (Kasaie et al., 2017). The same observation was made by Sepideh J. et al, (2012) with the solvent extraction of gold in the Lewis-cell (Javanshir et al., 2012). In the case of two phases with different viscosities, different stirring speeds should be applied in every phase in the Lewis-cell aiming for flat interface.

### 2.3.3. Solvent extraction of metals

As in this study metals (copper and chromium) were used initially to safely mimic the interfacial mass transfer of strong acids in the halobutyl rubber production process, this section is dedicated to the solvent extraction of metals and how it is achieved. Solvent extraction of metals relates to hydrometallurgy, which is a chemical process used to recover metals from their ores or industrial wastes, such as copper, uranium, chromium and others (Ritcey, 2006; Schlesinger et al., 2011). Nowadays, the separation and recovery from waste materials is necessity due to the high demand in metals, as well as for the protection of the environment, as they are hazardous and toxic (Chang, 2016). The recovery is achieved by the contact of the aqueous phase

containing a dissolved metal and the organic phase containing an extracting agent, like Aliquat 336. The solvent extraction is the method with the highest efficiency for separation of several metals, including copper and chromium. There are three types of extractant that can be used. Acidic extractants, such as organophosphorus compound (Di-(2-ethylhexyl)phosphoric acid) and carboxylic acids, are used for the extraction of the metals in the first transition series of the periodic table (Chemical Reaction 2.20) (Belkhouche et al., 2005; El-Nadi, 2017; Zhang et al., 2016). As basic extractant can be used an alkylammonium salt (Aliquat 336) to extract chromium and platinum (Chemical Reaction 2.21) (Fontàs et al., 1999; Nayl and Aly, 2015; Wionczyk and Apostoluk, 2005). Elements, such as uranium and thorium, can be extracted by Cyanex 925 by using the solvation mechanism (Chemical Reaction 2.22) (Mhaske and Dhadke, 2002).

Acidic:

$$M_{(aq)}^{z+} + zHA_{(org)} \leftrightarrow MA_{z(org)} + zH_{(aq)}^{+}$$
 (2.20)

Basic:

$$(n-z)R_4N_{(org)}^+ + MX_n^{(n-z)-} \underset{(org)}{\longleftrightarrow} (n-z)R_4N^+MX_n^{(n-z)-} \underset{(org)}{\longleftrightarrow} (2.21)$$

Solvating:

$$MX_{z(aq)} + mS_{(org)} \leftrightarrow MX_zS_{m(org)} + mH_2O$$
 (2.22)

Devi (2016) managed to extract and separate copper from base metals with the solvent extraction method by using ionic liquids (Devi, 2016). The aqueous phase consisted of copper (II) sulphate and sodium sulphate diluted in distilled water. The organic phase used was a mixture of equal volumes of trioctylmethylammonium chloride (Aliquat 336) and bis 2,4,4-trimethylpentylphosphinic acid (Cyanex 272), dissolved in kerosene. When the solvent extraction took place without the presence of the extractants, the extraction rate of copper was insignificant. 100% extraction rate of copper was achieved when the mixture of extractants was used. The solvent extraction of metals is affected by various parameters, such as mixing time, pH, extractants

concentration and organic to aqueous phase ratio. The increase of the extractants' concentration favours the copper extraction. Also, an increase on the extraction was observed with the increase of pH, because the hydrogen ion reacts with the alkaline environment forcing the Chemical Reaction 2.20 to the right (Figure 2.17). The copper solvent extraction depends on pH on the aqueous phase. As in this study the organic to aqueous phase transfer of copper was studied, the copper could be potentially transferred back to the aqueous phase by using a new aqueous phase with the desired pH value. By achieving distribution coefficient equal to zero, the effect of parameters, such as the viscosity of the organic phase and the presence of solids (CaSt<sub>2</sub>) on the interface, on the organic to aqueous phase extraction rate could be examined.

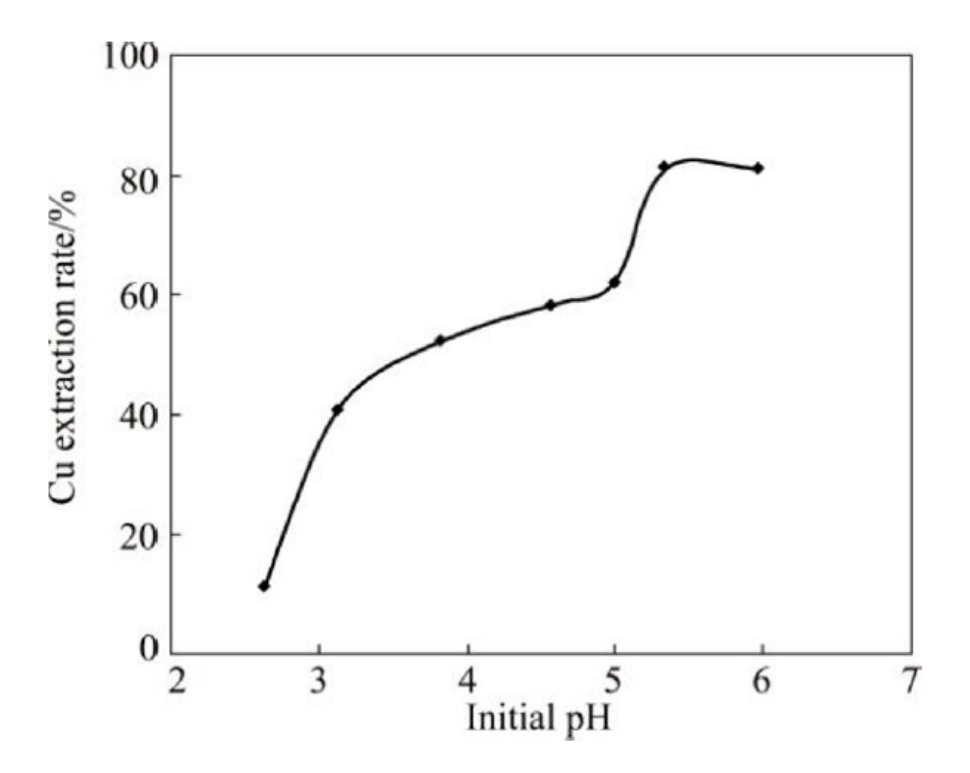


Figure 2.17. Effect of pH on the extraction of copper from the organic to aqueous phase with 0.02 mol/L Aliquat 336 and Cyanex 272 (0.005 mol/L Cu(II), 0.05 mol/L Na<sub>2</sub>SO<sub>4</sub>).

(Devi, 2016)

In the work of Kumar et al. (2013), the interfacial mass transfer of copper by solvent extraction was reported, using as extractant LIX 664N in kerosene (Kumar et al., 2013). The Chemical Reaction 2.23 shows how the copper reacts with the extracting agent. The  $R_{org}$  represents the extracting agent.

$$2HR_{org} + Cu_{aq}^{2+} \leftrightarrow CuR_{2org} + 2H_{aq}^{+} \tag{2.23}$$

It was proved that the copper extraction is favoured by an increase of the extractant concentration. However, at high concentation of LIX 664N, the viscosity of the organic phase decreases the extaction efficiency. It was concluded that the diffusion of the solute in the organic phase was slow and, as a consequence, the extraction efficiency was reduced. The difussivity of the solute in a viscous phase dominates the overall extraction efficiency, similarly to the halobutyl rubber production process, where, due to high butyl rubber concnetration, the viscosity of the organic phase is extremely high. The extractants (e.g. Aliquat 336) used in the solvent extraction of metals have high viscosity (Aguilar and Cortina, 2008). In order to reduce the effect of the viscosity of the organic phase and achieve higher extraction efficiency, the extractants are diluted in organic solvents, such as kerosene, hexane and heptane. It was reported that very low extractant concentration can reduce the extraction efficiency. In the solvent extraction of metals, there is a minimum extractant concentration in the organic solvent able to achieve 100% extraction (Deferm et al., 2016; Huang et al., 2016; Saien and Daliri, 2012; Wellens and Binnemans, 2012).

Wionczyk et al. (2011) studied the extraction of chromium (III) from alkaline aqueous solutions, which were prepared by the following chromium (III) compounds: Cr(ClO<sub>4</sub>)<sub>3</sub>, Cr(NO<sub>3</sub>)<sub>3</sub> and KCr(SO<sub>4</sub>)<sub>2</sub>, with Aliquat 336 (Wionczyk et al., 2011). They investigated the effect of the alkalinity of the auqeous phase (NaOH concentration) on the extraction efficiency. They concluded that, at low concentration of NaOH (0.2 M), 100% extraction of chromium (III) from aqueous to organic phase can be achieved. The increase of sodium hydroxide in the aqueous phase increases its ionic strength, resulting in the decrease of the chromium (III) extraction from the aqueous to the organic phase. The contanct of the organic phase containing the Cr-Aliquat 336 complex with a new aqueous phase with high ionic strength could result in transferring the Cr to the aqueous phase. This organic to aqueous phase extraction of Cr could be potentially used in this study for further investigation of parameters, as described in the case of copper.

### 2.4. Emulsion evaporation and aggregate formation

As described in the halobutyl rubber production process in Section 2.1.6, emulsion evaporation and rubber particles formation take place when excessive heat of the flash drum contents is transferred to the emulsion. Emulsion solvent evaporation is a widely used technique for the formation of various shapes particles from O/W emulsions (Hwisa et al., 2013; Paulo and Santos, 2018; Safari et al., 2018). The desired solid (product) is dissolved in the dispersed phase, i.e. a volatile organic solvent, which evaporates resulting in solid particles. This method finds applications in various sectors, such as the pharmaceutical and the food industries.

In the halobutyl rubber production process, the rubber is dissolved in the hexane (Happ et al., 2012). The solvent evaporation takes place in a flash drum at high temperature. The emulsion stream is injected into the flash drum where it comes in contact with hot water and / or steam at 105 - 120 °C and 2 - 3 atm (McDonald et al., 2000). It is expected in a matter of seconds, before the emulsion stream hits the water, the organic phase to evaporate, and 3D solid particles of random shape to form and drop in the water. This would require very high heat and mass transfer rate from the flash drum to the emulsion stream, due to its low surface area to volume ratio. A partial evaporation of the hexane before the emulsion stream hits the water surface could potentially lead to agglomeration of the rubber particles, as discussed in Section 4.6.2

A similar work has been done by Strizhak and his team (2017) without the presence of a dissolved solid (Strizhak et al., 2017). They created an experimental rig, where a pendant emulsion drop was heated in an air stream of temperature of 1250 °C approximately at 1200 L/min in a temperature resistant quartz glass chamber. The emulsion drop consisted of a water drop covered by kerosene. It was found that the increase of the kerosene content resulted in more rapid explosion of the drop due to the higher amount of vapours generation internally. Antonov and his team (2019) tested the effect of high temperature on a water in diesel emulsion pendant drop in a heated chamber (Antonov et al., 2019). They concluded that the increase of the diesel content leads to lower total heat capacity due to lower water content. This leads the drop to reach faster its boiling point. In addition, it was concluded that the increase of the exposed temperature decreases the breaking time of the emulsion.

The heating of an emulsion pendant drop in a controlled environment is a promising technique to understand the evaporation mechanism of the industrial W/O rubber emulsion in laboratory scale. Furthermore, in this study, it was developed an experiment configuration able to mimic the industrial flash drum, where the evaporation of the emulsion and the rubber particles formation is taking place, to understand further the process. Both experimental setups are described in Section 3.7.

### Chapter 3

### 3. Materials and Methods

In this section, the materials and methods used in this research are presented. The experimental conditions used in this research aim to be within the range of the operating conditions that were reported in the open literature, as described in Section 2.1. However, many commercial processes operate at higher temperature, higher pressure and higher BR content than cannot be easily used in the laboratory. Initially, the experimental configuration and development of a Lewis-cell, which was used to investigate the interfacial mass transfer of the acids in the halobutyl rubber production, are presented. As it was mentioned on the description of the industrial process, hydrogen bromine (HBr) and hydrogen chloride (HCI) were the by-products of the halogenation, which needed to be transferred to the aqueous phase in order to be neutralised. However, in the initials stages of this research alternative solutes were used in the lab due to the following reasons: HBr is a hazardous material that could cause severe health problems to humans and as a result decided not to be used. On the other hand, HCl is less hazardous compare to HBr but it has low solubility in alkanes (Foog et al., 1990; Stavert et al., 1991). Two alternative solutes (copper and chromium) were tested during the initial investigation in order to find the most appropriate one to mimic the industrial process. As described in Sections 4.1 and 4.2, there were problems using copper and chromium and a third solute, namely acetic acid, was considered (Section 4.4). The viscosity of the organic phase and the CaSt<sub>2</sub> concentration in the aqueous phase were the two parameters that examined their effect on the interfacial mass transfer rate of a solute in the Lewis-cell. In addition, a set of experiments are presented to understand how the acidic and alkaline environments in the industrial process, as well as the high temperatures, are affecting calcium stearate (CaSt<sub>2</sub>) (Section 3.4).

The emulsion size and stability are important in the industrial process. The effect of viscosity of the organic phase and the calcium stearate on the size and stability of the emulsion were tested, as described in Section 3.6. The viscosity was modified with the dilution of butyl rubber in the organic phase. The emulsions were formed in the lab by propeller mixing, the most common industrial technique, and their sizes were

measured from microscope images. Also, the stability of these emulsions under gentle stirring was examined.

In the industrial process, the formation of the rubber particles is achieved with the evaporation of the emulsion in the flash drum. Initially, an experiment was conducted, where a single emulsion drop exposed at high temperatures, like in the flash drum, to understand the fundamentals of the emulsion evaporation, as well as the effect of the CaSt<sub>2</sub>, as described in Section 3.7.1. In addition to that, an experimental rig was developed and built in the lab (Section 3.7.2) to mimic the industrial flash drum aiming to formulate similar to the industrial process rubber particles. This experimental rig will give the opportunity to examine parameters that could affect the size and shape of those rubber particles.

For this research, a non-halogenated butyl rubber (BR) was supplied by ExxonMobil in the form of "cement" (rubber dissolved in hexane) at high concentration, which was then dried (total removal of the hexane) and re-dissolved in a pure solvent in the lab to achieve the desired concentration. The calcium stearate was in a dispersion form containing a small amount of an industrial surfactant; various grades are available commercially with a range of particle of sizes. The CaSt<sub>2</sub> dispersion used in this research is typical of those used in a halobutyl rubber production process. Fresh deionised water was obtained from an Elix Essential water purification system.

# 3.1 Lewis – cell experimental configuration

The interfacial mass transfer problem was addressed in a Lewis-cell, which was built in the lab. An updated version of the Lewis-cell was developed to deal with the highly viscous organic phase, caused by the dissolved BR. Three different solutes were used in the Lewis-cell experiments (copper, chromium and acetic acid), as described previously.

The first experimental configuration consisted of an unbaffled glass tube with a polytetrafluorethylene (PTFE) base. The working capacity of the vessel was 100 mL. An opening at the top of the tube was used for the stirrer, which was a single shaft with paddles at two different heights. The two paddles were mixing each phase

separately, as shown in Figure 3.1. Samples could be withdrawn from the aqueous phase from a line at the bottom of the PTFE base.

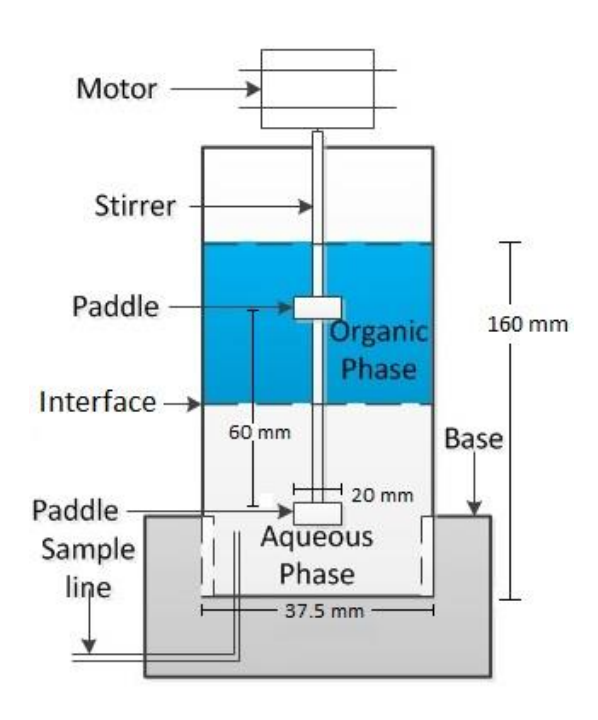


Figure 3.1. Schematic drawing of the Lewis-cell with single stirring shaft (not to scale).

Due to limitations of the single stirrer speed and direction, it was necessary to update the Lewis-cell for effective mixing of the two phases. On the updated Lewis-cell, two motors were used, having two separate coaxial shafts, which could rotate in opposite directions at different rotational speeds. The stirring speeds and different directions helped to overcome the problem of the high viscosity organic phase, which was the result of the dissolved BR. The effect of BR concentration in the organic phase viscosity is described in Section 4.4.2. Various stirring speeds on each phase were used in order to reduce their effect on the extraction rate in the Lewis-cell and be able to compare experiments with different viscosities (Kasaie et al., 2017; Melgarejo-Torres et al., 2012). In addition, a PTFE ring was introduced at the interface in order to reduce the turbulence in the area, contributing by minimising the disruption due to mixing. A schematic drawing of the updated Lewis-cell, including the dimensions, is shown in Figure 3.2. All Lewis-cell experiments were conducted at room temperature (20±1 °C) in a fume cupboard.

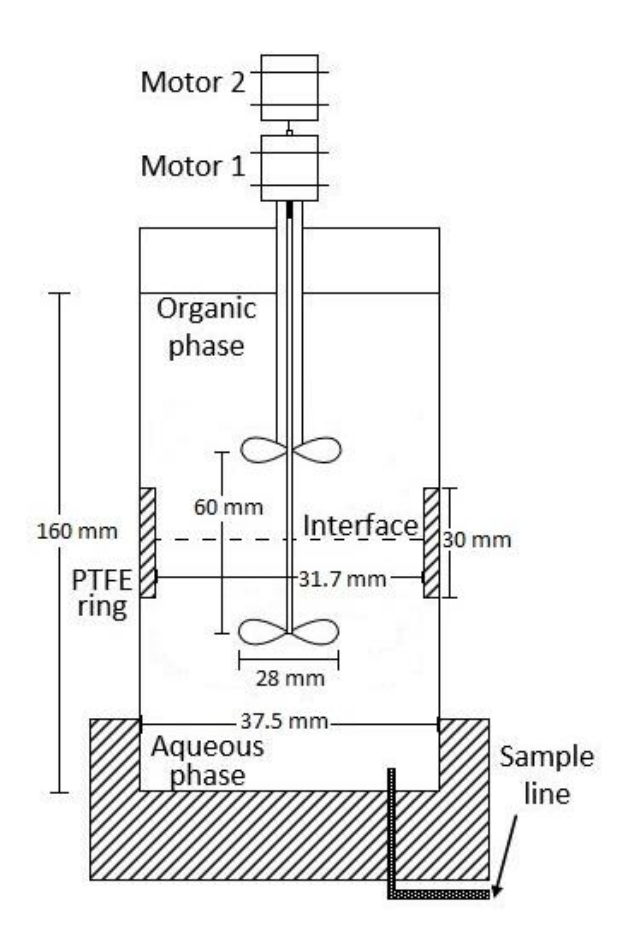


Figure 3.2. Schematic drawing of the updated Lewis-cell (not to scale).

# 3.2. Copper solvent extraction

The first solute chosen to investigate the interfacial mass transfer of the acids in the halobutyl rubber production was the copper (Cu). Cu was used as solute as it could be easily transfer towards each phase with the use of an extracting agent, Bis(2-ethylhelyx) phosphate (D2EHPA), by changing the pH (Zhongqi et al., 2007).

The organic solvent used in the solvent extraction experiment of Cu was kerosene (low odour) from Fisher Scientific. As solute and extracting agent, copper (II) sulphate pentahydrate (CuSO<sub>4</sub>.5H<sub>2</sub>O) (159.61 g/mol) and Bis(2-ethylhelyx) phosphate (95%, 322.43 g/mol molecular weight) were used respectively, both purchased from Sigma Aldrich. As background salt for extraction, sodium sulphate (Na<sub>2</sub>SO<sub>4</sub>) was used and purchased from Sigma Aldrich (Reffas et al., 2009). As pH modifiers, sulfuric acid (H<sub>2</sub>SO<sub>4</sub>, 1M) and sodium hydroxide solution 1M (NaOH) were used and supplied by Fisher Scientific.

Main aim of this study was to examine the effect of various parameters, such as organic phase viscosity and CaSt<sub>2</sub> concentration, on the organic to aqueous phase mass transfer rate. The initial step in the experimental procedure was to find the relationship between the distribution coefficient of Cu and the pH of the aqueous phase.

The CuSO<sub>4</sub> dissolved in water produces Cu<sup>2+</sup>. The solvent extraction of Cu is pH dependent, because protons in the D2EHPA are exchanged with Cu ions and the process can be facilitated by neutralising the released H<sup>+</sup> using an alkaline solution, as shown in Chemical Reaction 2.23, where RH represents the extracting agent (Kasaie et al., 2017). In order to find the dependency between the pH and the extraction efficiency, initially the two phases were prepared as shown in Table 3.1.

Table 3.1. Initial concentrations of the two phases for the investigation of the effect of pH on the extraction efficiency of Cu.

	Organic	phase	
CuSO <sub>4</sub> .5H <sub>2</sub> O 0.039 M		D2EHPA	0.151 M
Na <sub>2</sub> SO <sub>4</sub> 0.5 M			
H <sub>2</sub> SO <sub>4</sub>	Small amount to achieve pH of 1.5		

The Na<sub>2</sub>SO<sub>4</sub> was added in the aqueous phase to achieve a uniform and controlled ionic strength, which helps the reaction between the metal and the extractant (Reffas et al., 2009). Equal volumes of each phase were mixed in a 2 L glass reactor at 300 rpm for 5 minutes. The emulsion was then left for 20 minutes to fully separate. The glass reactor had a valve at the bottom allowing to take samples from the aqueous phase to be analysed in the UV-Vis spectrophotometer. Prior to the analysis, every experimental sample was centrifuged for 30 minutes at 1500 rpm in order to eliminate any organic drop. The samples were diluted with dilution factor of 0.4 by the addition of 25% ammonia solution and distilled water. The principal theory that the UV-Vis spectrophotometer is based is described in Appendix 1. In Appendix 1.1, the calibration of the UV-Vis instrument for Cu analysis is presented, as well as the error of the calibration curve that is added in the experimental results. The procedure was repeated several times while gradually increasing the pH with the addition of NaOH, until reaching the value of pH 4. The experiment was repeated 3 times. In Section 4.1, results showing the dependence of Cu extraction efficiency from the organic to the aqueous phase with pH are presented.

The next step was to prepare an organic phase with Cu-D2EHPA complex which would be used as the organic phase on the Lewis-cell experiments. In order to achieve that, aqueous phase containing 0.039 M CuSO<sub>4</sub>.5H<sub>2</sub>O, 0.5 M Na<sub>2</sub>SO<sub>4</sub> and NaOH was mixed for 5 minutes in the glass reactor with organic phase (kerosene) containing 0.151 M D2EHPA. The used amount of NaOH was appropriate to achieve a pH of 4, as it was concluded from the previous experiment (Figure 4.1). The same procedure was followed to prepare the organic phase containing Cu with the presence of BR, as the effect of the organic phase viscosity on the interfacial mass transfer needed to be examined. A mixture of kerosene and BR was used (50 g/L) as organic solvent instead of pure kerosene.

A new aqueous phase was prepared, containing only 0.5 M Na<sub>2</sub>SO<sub>4</sub> and a small amount of H<sub>2</sub>SO<sub>4</sub>, enough to achieve pH of 1.5, as, under these conditions, all the Cu could be transferred back to the aqueous phase when it will be in contact with an organic phase with the Cu-D2EHPA complex (Figure 4.1). This aqueous phase was used in the Lewis-cell experiments for the investigation of the organic to aqueous phase extraction as the distribution coefficient is zero for Cu between the organic and aqueous phase at pH of 1.5. Equal volumes (50 mL) of each phase were used on the Lewis-cell experiments. The Lewis-cell version with the single motor and shaft was used in the Cu extraction investigation. The aqueous phase (heavy phase) was introduced first into the apparatus. Then, the organic phase containing the Cu-D2EHPA complex was introduced slowly into the glass tube without disturbing the interface and avoiding mixing the two phases. Finally, the shaft with the two paddles was adjusted, as shown in Figure 3.1. Figure 3.3 shows the Lewis-cell loaded with both phases (organic phase containing Cu-D2EHPA complex at the top and aqueous phase at the bottom) at the start of the experiment. Several stirring speeds (Table 3.2) were tested to reduce the stirring effect on the extraction rate and allow comparison of the mass transfer results between different organic phase viscosities (0 and 50 g/L BR in kerosene), as discussed in Section 2.3.2. Samples from the aqueous phase were taken every several minutes to be analysed in the UV-Vis spectrophotometer as described above. The total duration of each experiment was 330 minutes and repeated three times.

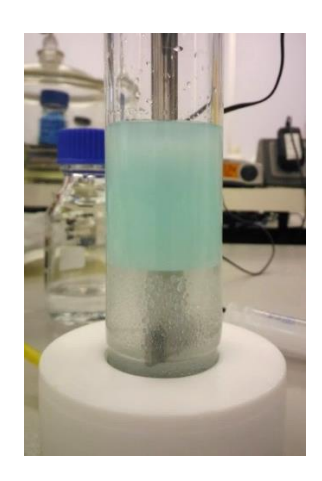


Figure 3.3. The two phases in the Lewis-cell at the start of the experiment.

Table 3.2. Stirring speeds tested on Lewis-cell according to BR concentration in the organic phase.

Organic phase	0 g/L BR	50 g/L BR
Stirring speed (rpm)	100	200
	125	250
	175	300
	200	350

At the end of each Lewis-cell experiment (330 min), the two phases were mixed intensively for 5 min, as no equilibrium was established by that time. By mixing the two phases, all the Cu was transferred to the aqueous phase, achieving 100% extraction. The concentration of Cu in the aqueous phase at the end was equal to the concentration of Cu in the organic phase at the start of the experiment, as both phases had the same volume. The reduction of the aqueous phase volume during the Lewis-cell experiments, occurring due to the samples taken for analysis, was taken into account in the final calculations of Cu concentration in the organic phase. The results of those experiments are analysed and discussed in Section 4.1.

In addition to the effect of the organic phase viscosity on the extraction rate, the effect of CaSt<sub>2</sub> was also investigated. To commence this part of the study, it was important to investigate the chemical compatibility of the CaSt<sub>2</sub> with D2EHPA, CuSO<sub>4</sub>.5H<sub>2</sub>O, NaOH and H<sub>2</sub>SO<sub>4</sub>. An initial investigation took place on the effect of H<sub>2</sub>SO<sub>4</sub> and NaOH on the CaSt<sub>2</sub>: 4 samples with the same concentration of CaSt<sub>2</sub> (5 g/L) were prepared and, for samples 3 and 4, H<sub>2</sub>SO<sub>4</sub> was added to low the pH to 2. For samples 1 and 2, a small amount of NaOH was added to achieve pH of 12. In Section 4.1, Figure 4.6

shows the visual effect of H<sub>2</sub>SO<sub>4</sub> and NaOH on the CaSt<sub>2</sub> suspension. Further investigation of the effect of the acidic environment on the CaSt<sub>2</sub> is presented in Section 3.4.1.

### 3.3. Chromium solvent extraction

Due to the reaction of  $CaSt_2$  with the  $H_2SO_4$  and the formation of stearic acid (discussed in Section 4.1), it was concluded that an alternative solute should be used that could be extracted in alkaline environment. Chromium (Cr) could be extracted from the aqueous phase to the organic phase with the Aliquat 336 (a quaternary ammonium salt) at alkaline environment (pH = 12) (Chemical Reaction 3.1) (Wionczyk and Apostoluk, 2005). First aim of this stage was to achieve organic to aqueous phase extraction and then to investigate the effect of  $CaSt_2$  on the extraction during the Lewis-cell experiment.

$$R_4 NCl_{(org)} + [Cr(OH)_4]_{(aq)}^- \leftrightarrow [(R_4 N)Cr(OH)_4]_{(org)} + Cl_{(aq)}^-$$
 (3.1)

As organic solvents n-heptane (99+% purity) and 1-decanol (>98% purity) were used, supplied by Fisher Scientific and Sigma Aldrich accordingly. Chromium (III) nitrate nonahydrate (Cr(NO<sub>3</sub>)<sub>3</sub>.9H<sub>2</sub>O) (99% purity, 400.14 g/mol molecular weight) and Aliquat 336 (methyltrioctylammonium chloride) (404.17 g/mol molecular weight) were supplied by Sigma Aldrich. When the Cr(NO<sub>3</sub>)<sub>3</sub> is present in an aqueous phase with NaOH, they react and form the following ion: [Cr(OH)<sub>4</sub>]<sup>-</sup> (Rai et al., 1987; Wionczyk and Apostoluk, 2005). Sodium hydroxide solution (NaOH, 1M) and sodium chloride (NaCl, >99% purity) were purchased from Fisher Scientific.

Table 3.3 shows the initial concentrations of the aqueous and organic phases prior to the aqueous to organic phase extraction by mixing. Equal volumes (50 mL) of each phase were used and the mixing took place for 10 minutes using a stirring magnet at high speed. At the end of the experiment, the emulsion was transferred to a separation funnel to fully separate.

Table 3.3. Initial composition of the aqueous and organic phases at the aqueous to organic phase extraction of Cr.

Aqueous phase		Organic phase	e (heptane)
Cr(NO <sub>3</sub> ) <sub>3</sub> .9H <sub>2</sub> O 0.005 M		Aliquat 336	0.151 M
NaOH	0.1 M		

The analysis of the Cr concentration in the aqueous phase was conducted using Flame Atomic Absorption Spectroscopy (FAAS). Prior to the analysis every sample was filtered with a 0.2 µm syringe filter and then diluted accordingly to achieve concentration within the calibration range. In Appendix 2 the FAAS instrument is briefly described and on Appendix 2.1 the calibration procedure of FAAS for Cr is shown as well as the error of the calibration curve that is added in the experimental results. 100% extraction of Cr from the aqueous to organic phase was achieved, but it was observed the formation of a third phase, as shown visually in Figure 3.4



Figure 3.4. Third phase formed after the separation of the two phases.

According to Wionczyk and Apostoluk (2004) the formation of the third phase can be avoided by changing the solvent with the addition of 1% v/v 1-decanol in heptane. Thus, in the following aqueous to organic phase experiments, it was achieved elimination of the third phase, when 1-decanol was added in the organic phase.

As the main aim of this study was to investigate the effect of CaSt<sub>2</sub> on the organic to aqueous phase extraction of a solute, first it was important to achieve the best conditions to conduct the extraction of Cr from the organic, where was present in a Cr-Aliquat 336 complex form, to a clean aqueous phase. Several aqueous phases were tested in order to check which one will give the highest organic to aqueous phase extraction efficiency. To achieve that, organic phase with Cr-Aliquat 336 complex was prepared as described above and mixed with several aqueous phases. Table 3.4 shows the concentrations of NaOH and NaCl in those aqueous phases examined,

aiming for high % of Cr extraction from the organic to the aqueous phase. The concentration of NaOH was kept constant at 0.4 M during the experiments, based on the work of Wionczyk and Apostoluk who concluded that 0.5 M NAOH, high ionic strength, results in low efficiency on the aqueous to organic phase extraction, assuming high efficiency to the opposite extraction (Wionczyk and Apostoluk, 2004). NaCl was added as it is the product of the Chemical Reaction 3.1 and by increasing its concentration will force the reaction to the left.

Table 3.4. Concentrations of the aqueous phase aiming to achieve high organic to aqueous phase extraction efficiency.

Aqueous phase			
NaOH (M) NaCl (M)			
0.4	0.00		
0.4	0.01		
0.4	0.10		
0.4	0.15		
0.4	0.20		

Every experiment was conducted 3 times by mixing the two phases for 10 minutes with a magnetic stirrer. The formulated emulsion was then transferred into a separation funnel for 10 min for the phases to be separated. The samples prepared as described above and analysed in the FAAS (Appendix 2.1). The aqueous phase that achieved the highest extraction efficiency from the organic to aqueous phase was the one used in the Lewis-cell experiments to investigate the effect of the prementioned parameters. In addition, it was tested the effect of CaSt<sub>2</sub> on the organic to aqueous phase extraction by mixing the two phases. 5 g/L CaSt<sub>2</sub> was added in the aqueous phase, which achieved the highest extraction efficiency of organic to aqueous phase transfer, and mixed with the organic phase containing Cr-Aliquat 336 complex for 10 minutes with a magnetic stirrer. The phases were separated and sample from the aqueous phase was analysed in the FAAS as explained above (Appendix 2.1). On Section 4.2, the results of the organic to aqueous phase extractions with different aqueous phase are presented and discussed.

An initial Lewis-cell experiment was conducted with the presence of CaSt<sub>2</sub> in the aqueous phase. As Lewis-cell apparatus, the updated version with the individual stirrers in each phase was used. An aqueous phase containing 0.4 M NaOH, 0.1 M

NaCl and 5 g/L CaSt<sub>2</sub> was used. The aqueous phase was sonicated for 10 minutes prior to the experiment to break and prevent any agglomeration of the CaSt<sub>2</sub> that could block the sample line of the Lewis-cell apparatus. As organic phase was used the one mentioned above containing Cr-Aliquat 336 complex. Equal volumes of each phase were used. The same procedure of loading the two phases in the Lewis-cell was followed as in Cu experiments described in Section 3.2. The two stirrers in each phase were operated at opposite directions, but at the same speed (150 rpm), as no BR was used, and the viscosities of each phase were similar. The total time of the experiments was 60 minutes and samples from the aqueous phase were taken every 10 minutes. On Section 4.2, the outcome of the Lewis-cell experiment with Cr and the effect of CaSt<sub>2</sub> are discussed.

### 3.4. Calcium stearate

Due to the problems that CaSt<sub>2</sub> caused on solvent extraction with Cu and Cr, its behaviour required further investigation in various conditions. This section considers the effect of acidic and alkaline environments, as well as high temperature, on the chemical stability of CaSt<sub>2</sub>. Also, the size and morphology of the calcium stearate agglomerations were investigated.

As mentioned in start of Chapter 3, the third solute that was used in the experiments was the AcOH. It was important to understand if the AcOH has the same effect on CaSt<sub>2</sub> with the HCI, which is the solute in the industrial process. In addition to that, the effect of alkaline environment (presence of NaOH) was tested on the CaSt<sub>2</sub>, as in the industrial process NaOH is used for the neutralisation of the acids and the pH after the emulsification reactor is approximately equal to 13. High temperatures could impact the CaSt<sub>2</sub> structure and it was important to examine if there was any dissociation happening at high temperatures.

Acetic acid (AcOH) (>99.7% purity), sodium hydroxide solution 1M (1N) and hydrogen chloride (HCI, 37% v/v) were purchased by Fisher Scientific. As mentioned in the start of Chapter 3, the calcium stearate (CaSt<sub>2</sub>) was in the form of suspension at concentration equal to 50% w/v and with dilution the desired concentrations were achieved in the lab.

# 3.4.1. Effect of acetic acid, hydrogen chloride, alkaline environment and high temperature on the calcium stearate

Initially, the effect of AcOH was examined on CaSt<sub>2</sub> at various molar ratios, between 0 and 4. The reaction between CaSt<sub>2</sub> and AcOH produces stearic acid and calcium acetate, as shown in Chemical Reaction 3.2.

$$(C_{17}H_{35}COO)_2Ca + 2CH_3COOH \rightarrow 2C_{17}H_{35}COOH + Ca(CH_3COO)_2$$
 (3.2)

The concentration of calcium stearate was constant between the experiments and equal to 0.025 M (15 g/L). The appropriate amount of AcOH and CaSt₂ added in distilled water, as shown in Table 3.5, to achieve the desired molar ratio, and mixed by shaking the solution for 2 minutes. Every sample was then filtered with a 0.2 μm syringe filter to eliminate any solids and then diluted accordingly. The concentration of calcium in the samples was measured by the FAAS (Appendix 2.2) and then the % of CaSt₂ reacted with the acid was calculated. Each experiment was repeated three times to check the accuracy of the results.

Table 3.5. Concentrations of AcOH and CaSt<sub>2</sub> in solution.

#	AcOH (M)	CaSt <sub>2</sub> (M)	Molar ratio (-)
1	0	0.025	0
2	0.01	0.025	0.4
3	0.025	0.025	1
4	0.05	0.025	2
5	0.1	0.025	4

In addition to the above experiment, the excess of acid in the solution, above molar ratio of 4, was used to examine if there is an increase on the % of CaSt<sub>2</sub> that react with the acid. The acids used in this experiment were AcOH and HCI. In the halobutyl industrial process, the CaSt<sub>2</sub> reacts with HCI, producing stearic acid and calcium chloride, as shown in Chemical Reaction 3.3.

$$(C_{17}H_{35}COO)_2Ca + 2HCl \rightarrow 2C_{17}H_{35}COOH + CaCl_2$$
 (3.3)

The concentration of calcium stearate was constant between the experiments and equal to 0.0005 M (0.3 g/L). Table 3.6 shows the concentrations of AcOH, HCl and

CaSt<sub>2</sub> that used in every solution, alongside with the final pH of each solution. The experimental procedure was the same as above with the exception that there was no dilution of the sample prior to the analysis as the measured concentration of calcium was within the calibration range. The results of the reaction between the CaSt<sub>2</sub> and the acids are presented and discussed in Section 4.3.1.

Table 3.6. Concentrations of CaSt<sub>2</sub>, AcOH and HCl in each solution with their respective pH.

#	CaSt <sub>2</sub> (M)	AcOH (M)	рН	#	CaSt <sub>2</sub> (M)	HCI	рН
						(M)	
A1	0.0005	0	7.40	B1	0.0005	0	7.40
A2	0.0005	0.01	3.65	B2	0.0005	0.01	2.28
А3	0.0005	0.1	3.05	B3	0.0005	0.1	1.47
A4	0.0005	0.2	2.84	B4	0.0005	0.2	1.02
A5	0.0005	0.3	2.79	B5	0.0005	0.3	0.82

As mentioned above, the effect of the alkaline environment was tested on the CaSt<sub>2</sub>, as the pH of the industrial process after the neutralisation of the acids is approximately equal to 13 and NaOH (0.1 M) was used in the Lewis-cell in (Section 3.5.3). The same procedure on preparation of the solutions and analysis of the samples was followed like in the previous experiment with the acids. Table 3.7 shows the concentrations of NaOH and CaSt<sub>2</sub> in each solution and their final pH.

Table 3.7. Concentrations of CaSt<sub>2</sub> and NaOH in each solution with their respective pH.

#	NaOH (M)	CaSt <sub>2</sub> (M)	рН
C1	0.0	0.0005	7.40
C2	0.1	0.0005	12.91
C3	0.3	0.0005	13.25
C4	0.5	0.0005	13.40
C5	1	0.0005	13.58

Finally, in order to investigate the temperature effect on the dissociation of CaSt<sub>2</sub>, the following experimental procedure was followed. A solution of 1.5 g/L of CaSt<sub>2</sub> was prepared and heated from room temperature up to 70 °C over a period of 20 minutes. Every 10 °C increase of temperature, a sample was taken. The same preparation and analysis of the samples was followed like in the previous experiments. The experimental results are presented and discussed in Section 4.3.1.

### 3.4.2. Size and morphology of the calcium stearate

The CaSt<sub>2</sub> morphology was analysed using a Scanning Electron Microscope (SEM). Prior to the SEM analysis, a sample of a CaSt<sub>2</sub> suspension was dried overnight in a vacuum oven at room temperature and then, the remained powder was covered with a thin layer of gold (~10 nm). In addition, the size of the CaSt<sub>2</sub> particles, at various pH values, was measured using the Malvern Mastersizer 2000, which is a particle size analyser. The pH was modified with the addition of H<sub>2</sub>SO<sub>4</sub> or NaOH accordingly. On Appendix 8, the Malvern Mastersizer 2000 principle theory is described as well as the operating procedure. The results and their discussion are presented in Section 4.3.2.

### 3.5. Acetic acid solvent extraction

The third solute used, was the acetic acid (AcOH), as it is a weak acid and simulates better the interfacial mass transfer of the by-products at the neutralisation step in the industial process. An initial experiment was to calculate the distribution coefficient of AcOH between water and heptane. N-Heptane was used as organic solvent, due to its lower evaporation rate compared to hexane which is used in the industry. Next step was to examine the effect of CaSt<sub>2</sub> and BR on the mass transfer efficiency of AcOH from the organic to aqueous phase by mixing the two phases, i.e. to achieve equilibrium between the phases. Finally, the effect of viscosity of the organic phase and CaSt<sub>2</sub> concentration in the aqueous phase on the extraction rate of AcOH in the Lewis-cell were investigated. Acetic acid (AcOH, >99.7% purity) and sodium hydroxide solution (NaOH, 1M) were purchased by Fisher Scientific. N-heptane (99+% purity) was supplied by Fisher Scientific.

# 3.5.1. Distribution coefficient of AcOH between water and heptane

The experiment for the calculation of the distribution coefficient of AcOH between water and heptane is presented below, as well as the effect of BR and CaSt<sub>2</sub> in extraction efficiency when the two phases were mixed.

Table 3.8 shows the concentration of AcOH, BR and CaSt<sub>2</sub> that were used in each phase. The dilution of AcOH in heptane (organic phase) was done be mixing. When

BR was present in the organic phase, BR was dissolved first and then, the AcOH was added. The aqueous phase with  $CaSt_2$  was prepared by adding the appropriate amount from the supplied  $CaSt_2$  suspension to achieve concentration of 10 g/L. In every experiment, equal volumes (50 mL) of each phase were mixed with a magnetic stirrer for 10 minutes and then the two phases were separated in a separation funnel. Every experiment was conducted three times, to check the accuracy of the results The AcOH concentration was measured with High Performance Liquid Chromatography (HPLC). The principal theory that the HPLC is based on is described in Appendix 3. In Appendix 3.1, the calibration of the instrument for Cu analysis is presented, as well as the error of the calibration curve that is added in the experimental results. Prior to the analysis, every sample was filtered with a 0.2  $\mu$ m syringe filter. The % of extraction of every experiment is presented on Section 4.4.1.

Table 3.8. Initial concentrations of the organic and aqueous phases for the calculation of the distribution coefficient.

#	Organic phase		Aqueous phase	
#	AcOH (M)	BR (g/L)	CaSt <sub>2</sub> (g/L)	
1	0.09	0	0	
2	0.09	50	0	
3	0.09	50	10	

# 3.5.2. Viscosity of the organic phase – Lewis-cell

The viscosity of the organic phase is an important parameter which affects the interfacial mass transfer of the solute. Typically, halobutyl rubber production process use high concentrations of the BR (200 - 250 g/L) (ExxonMobil, 2017). Consequently, the viscosity of the organic phase is high, which potentially has an effect on the diffusivity of the solutes towards the interface. The viscosity of heptane with various concentrations of dissolved BR (0 – 200 g/L) was measured in the lab by the HAAKE Viscotester iQ Rheometer at two different temperatures: room temperature (20 °C) and 50 °C, which were the experimental and industrial process temperatures, respectively, as shown in Appendix 5. For the rheometer analysis of each solution, a range of shear rates was applied, and the shear stress was measured in order to understand their rheology behaviour. Three different concentrations of BR in heptane were tested in the Lewis-cell, as shown in Table 3.9. BR concertation higher than 100

g/L was not used in the Lewis-cell due to the very high viscosity, which made the organic phase difficult to work with. In this experiment, the aqueous phase contained no CaSt<sub>2</sub> or NaOH, as only the effect of organic phase viscosity was examined here.

Table 3.9. BR and AcOH concentrations in the organic phase on Lewis-cell experiments examine the effect of the organic phase viscosity on the extraction rate of AcOH.

#	Organic phase		
#	BR (g/L)	AcOH (M)	
1	0	0.09	
2	50	0.09	
3	100	0.09	

The same procedure for the introduction of both phases in the Lewis-cell was followed, similar to the Cu experiments in Section 3.2. The stirring of each phase started simultaneously at different speeds and opposite directions. The stirring speed of the aqueous phase was constant at 150 rpm through every experiment, while the stirring speed of the organic phase was chosen according to its viscosity, which depends on BR concentrations. Table 3.10 shows the stirring speed of the organic phase according to the BR concentration. In order to find the appropriate stirring speeds, the stirrer was set to the maximum speed that could be achieved in the Lewi-cell without disturbing the interface and creating vortex. Lower values of stirring speeds of the organic phase were tested to make sure that the Lewis-cell was operating at the Zone B, as shown in Figure 2.16.

Table 3.10. Stirring speed of the organic phase in the Lewis-cell at various concentration of BR.

BR (g/L)	Stirring Speed (rpm)
0	150
50	500
100	700

Samples from the aqueous phase were taken every 10 or 20 minutes in order to measure the AcOH concentration in the HPLC (Appendix 3.1). The total time of the experiment was 60 minutes and no equilibrium was achieved until that time. On Sections 4.4.2, the experimental results showing the effect of organic phase viscosity on the extraction rate of AcOH are presented and discussed.

### 3.5.3. Calcium stearate in the aqueous phase – Lewis-cell

The effect of the CaSt<sub>2</sub> in the aqueous phase on the interfacial mass transfer rate of AcOH was tested in the Lewis-cell. Table 3.11 shows the concentration of each phase for the four experiments that conducted.

Table 3.11. The concentrations of each species in each phase in the Lewis-cell experiment for the investigation of the effect of CaSt<sub>2</sub> on the interfacial mass transfer rate.

#	Aqueous phase		Organic phase	
#	CaSt <sub>2</sub> (g/L)	NaOH (M)	AcOH (M)	BR (g/L)
1	0	0	0.09	0
2	5	0	0.09	0
3	10	0	0.09	0
4	15	0	0.09	0

The stirring speed of each phase was 150 rpm for all the experiments, as both phases had similar viscosities. The AcOH concentration was measured in the HPLC (Appendix 3.1) and the results are presented and discussed in Section 4.4.3. Every experiment was conducted 3 times to check the reproducibility of the results and the average values of concentrations are reported.

To mimic better the interfacial mass transfer taking place in the halobutyl rubber production, both  $CaSt_2$  and NaOH were present in the aqueous phase during the Lewis-cell experiment. 0.1 M NaOH and 5 g/L  $CaSt_2$  were added in the aqueous phase. The amount of 0.1 M NaOH, that was chosen, was the appropriate to achieve alkaline environment (pH  $\sim$  12) at the equilibrium.

# 3.6. Butyl rubber water-in-oil emulsion

The size and the stability of the W/O emulsion was investigated, as it is critical for the halobutyl rubber production. The emulsion's surface area plays an important role in the neutralisation step, as higher contact area between the two phases results in better interfacial mass transfer of the acids. The organic phase viscosity and the concentration of CaSt<sub>2</sub> as solid emulsifier were the two parameters that were examined. An organic solvent hexane (specified reagent for general laboratory work) was used, which was supplied by Fisher Scientific. The ratio between the organic and

the aqueous phase in the laboratory experiments was 4:1 organic to aqueous phase by volume. Table 3.12 shows the concentration and volume of each phase that used to formulate the emulsions. Each emulsion was formulated by mixing, using a double blade mixer at high speed (2500 rpm) for 2 minutes and then, maintaining them by gently mixing (500 rpm) for 40 minutes. Samples were taken every 10 minutes to measure the size of the aqueous drops and, consequently, the stability of the emulsion was determined.

Table 3.12. Concentration of CaSt<sub>2</sub> and BR in each phase for the formation of the W/O emulsions.

	Aqueous phase		Organic phase	
#	Volume	CaSt <sub>2</sub>	Volume	•
	(mL)	(g/L)	(mL)	BR (g/L)
1	20	5	80	50
2	20	5	80	100
3	20	5	80	150
Α	20	0	80	100
В	20	5	80	100
С	20	10	80	100
D	20	15	80	100

Initially, it was attempted to analyse the emulsion with a Jorin ViPa analyser. The Jorin ViPa analyser is a visual process analyser which is capable of particles size analysis in a continuous flow system, as shown in Figure 3.5 (Jorin, 2006). It could be potentialy used in line at the rubber particles formation experiment, which is described in the Section 3.7.2. As shown in Figure 3.5, the emulsion passes through a flow cell where, with the use of a high speed digital video camera, the detection of the aqueous drops is taking place. At high BR concentrations, the emuslion became cloudy and, as a result, the camera could not detect any aqueous drops, as shown in Figure 3.6 which is an example photo taken by the instrument. Due to the above concerns, it was decided to use a static image analsis with a microscope (GX Microscope GXML3201) instead, in order to be able to measure the emulsion size.

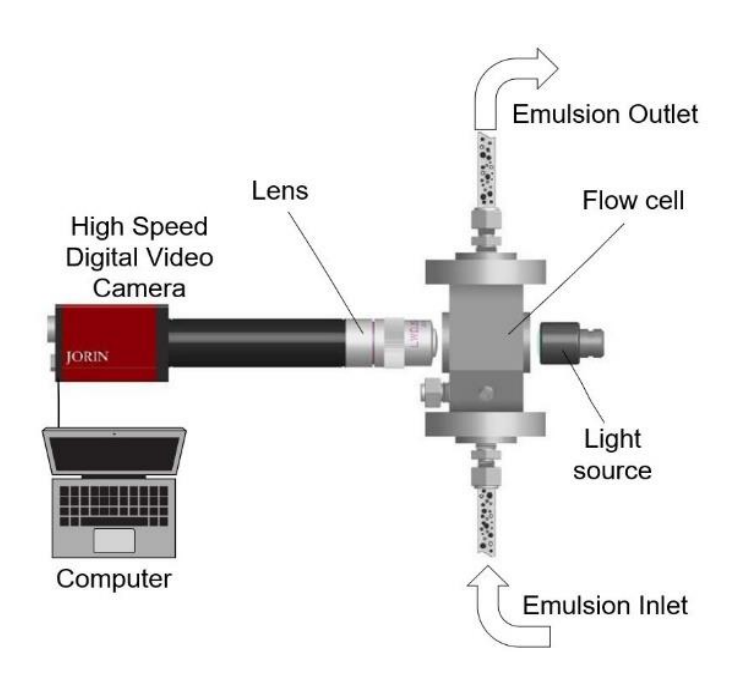


Figure 3.5. Schematic of the Jorin ViPa image analysis technique working configuration.

(Jorin, 2006)

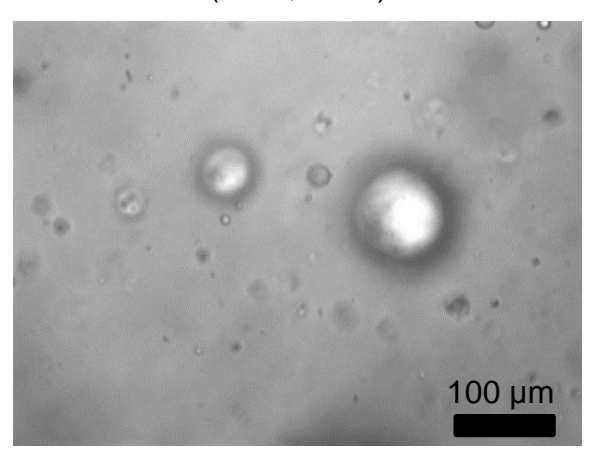


Figure 3.6. Photo taken from the Jorin ViPa analyser in the lab.

The images, taken by the microscope, were then analysed on the ImageJ (Software for image analysis). 250 aqueous drops were measured per sample and the average diameter by number was calculated. The image analysis on the ImageJ is presented in Appendix 7. On the Section 4.5, the results are presented and the effect of BR and CaSt<sub>2</sub> on the size and the stability of the emulsion is discussed.

In addition, it was measured the effect of the BR in the organic phase and the CaSt<sub>2</sub> in the aqueous phase on the interfacial tension. The interfacial tension was measured with Drop Shape Analyser (DSA 100 – KRUSS) using the technique of the pendant drop as it is analysed in the Appendix 6.

Table 3.13 shows the concentrations of the species in each of the two phases for each system prepared for the analysis of the interfacial tension. On Section 4.5, the interfacial tension for every system is presented with function of time until the equilibrium interfacial tension was achieved.

Table 3.13. Combination of aqueous and organic phases that used to measure the interfacial tension.

#	Aqueous phase	Organic phase	
	CaSt <sub>2</sub> (g/L)	BR (g/L)	
1	0	0	
2	0	50	
3	0	100	
4	0	150	
5	0	0	
6	5	0	
7	10	0	
8	15	0	

### 3.7. Rubber particles formation

In the halobutyl production process, a rapid solvent evaporation of the emulsion in a flash drum is taking place resulting in rubber particles with wide size distribution, as described in Section 2.1.6. Controlling the distribution of the particles and understanding their formation mechanism is important for the industry. The aim of this study was to understand the emulsion evaporation mechanism and build an experimental configuration that could mimic the industrial flash drum, which will enable to investigate parameter that could affect the size and shape of these particles.

In these experiments, as solvent, hexane was used, due to the lower boiling temperature compared to kerosene and heptane that were used in the Lewis-cell experiments (Joshi and Adhikari, 2019). Also, hexane is the industrial organic solvent due to its low heat that needs to be evaporated (boiling point of 68 °C). The hexane (specified reagent for general laboratory work) and sodium hydroxide solution (NaOH, 1M) were purchased by Fisher Scientific.

### 3.7.1. Evaporation of a W/O emulsion pendant drop

This experimental procedure was as a preliminary study to understand the impact of high temperature on a W/O emulsion drop containing BR, as well as the effect of CaSt<sub>2</sub> on the evaporation mechanism, in a controlled environment.

Table 3.14 shows the two W/O emulsions that were used on this experiment. The phase ratio of the emulsion was equal to the industrial one. The emulsion was formed by mixing the two phases with a two bladed stirrer for 2 minutes at 2500 rpm. NaOH was added in order to mimic better the industrial process, assuming that the aqueous phase has alkaline environment after the neutralisation of the acids.

Table 3.14. Concentration of each species in each phase and their volumes that used in the emulsion pendant drop experiment.

#	Organic phase		Aqueous phase		
	Volume (mL)	BR (g/L)	Volume (mL)	CaSt <sub>2</sub> (g/L)	NaOH (M)
1	80	100	20	0	0.1
2	80	100	20	15	0.1

After the formation of the emulsion, a small amount was taken using a glass syringe. The glass syringe was then transferred to the KRUSS Drop Shape Analyser (DSA 100) instrument where the experiment took place. An emulsion drop, volume of approximately 10  $\mu$ L, was formed outside and then lowered inside the preheated chamber in order to start the experiment. Figure 3.7 shows the experimental configuration, where the emulsion drop is located inside a heating chamber of the KRUSS DSA 100 instrument. The heating chamber had two opposite sides made from glass for the camera and the light source. The chamber was sealed from all sides, except two holes at the top, used for the syringe and the thermostat.

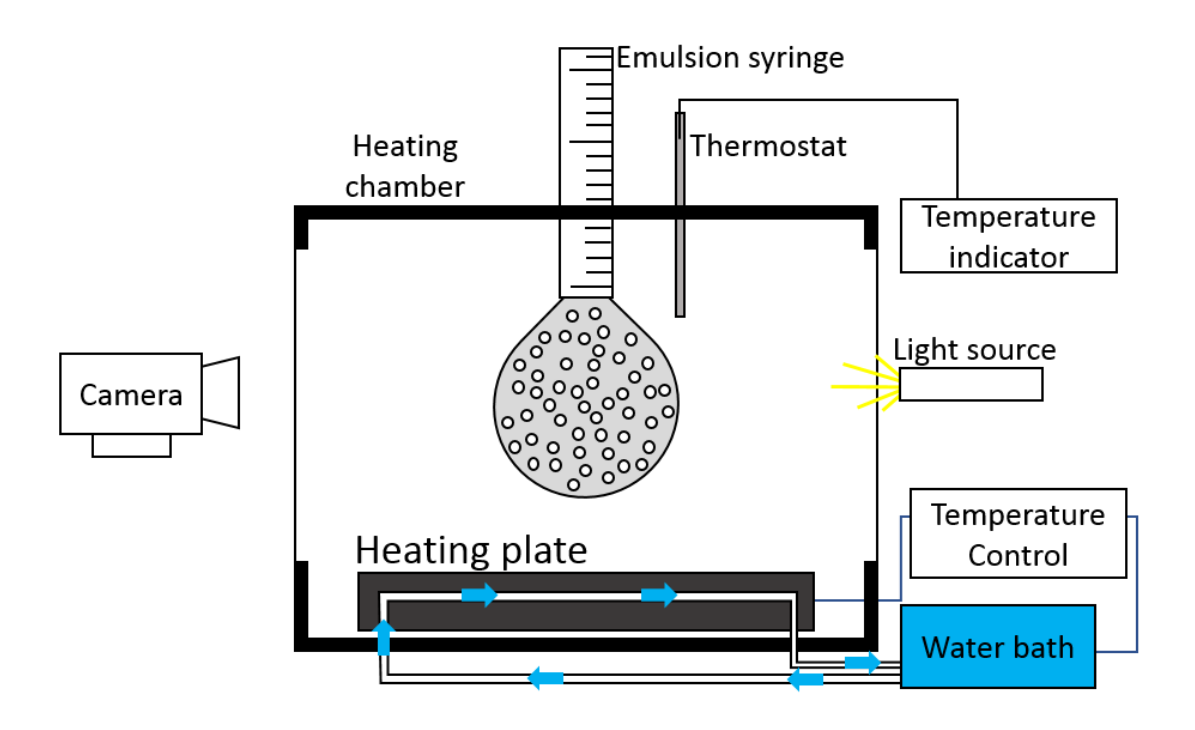


Figure 3.7. Experimental configuration of the pendant emulsion drop evaporation (not to scale).

The chamber was heated by a heating plate and the temperature controlled with circulation of cooling water. The temperature was stable for 5 minutes prior to every experiment. A separate thermostat was used to measure the temperature on the area of the drop, as shown in Figure 3.7, because the instrument was measuring the temperature of the heating plate and it will not be accurate to use it as the experimental temperature. The camera was used to detect volume and shape change of the drop through time and to understand where the evaporation is staring on the emulsion. Each emulsion was exposed at the following temperatures: 70, 80, 100 and 130 °C. Due to the limitation of the instrument, 130 °C was the highest temperature that was used. It should be noted that calibration of the KRUSS DSA 100 was achieved by setting the outside diameter of the needle on the instrument.

On Section 4.6.1, the normalised volume change of every emulsion in every experiment is presented and discussed. In addition, images taken every couple of seconds showing visually the effect of high temperature (130 °C) on the W/O emulsion drop are presented.

### 3.7.2. Flash evaporation of the water-in-oil emulsion

In addition to the above experiment (Section 3.7.1), an experimental configuration was built in the lab, aiming to mimic the industrial flash drum in order to be able to form similar rubber particles in the laboratory scale by emulsion evaporation.

Figure 3.8 shows the schematic drawing of the initial experimental configuration. The apparatus consisted of two main parts: an emulsification vessel and a "flash drum". The emulsification vessel consisted of a 0.5 L glass container with a 4 bladed propeller stirrer. The vessel was sealed from the top to eliminate hexane evaporation. In addition, a heating jacket was used to heat the emulsion at 50 °C. A thermocouple was used to measure the emulsion temperature. A peristaltic pump (Watson Marlow 603S) was used to transfer the emulsion at approximately 1 m/s into the "flash drum" through a 200 mm metallic pipe, as shown in Figure 3.8. The "flash drum" consisted of a stainless-steel vessel, 20 L volume, filled with water and 5 g/L CaSt<sub>2</sub>. CaSt<sub>2</sub> in the "flash drum" was used to prevent any agglomeration of rubber particles in the water after their formation. An induction heater was used to heat the vessel up to the boiling point of water. The vessel was insulated, to minimize the heat loses, and there was an opening on the lid to allow the introduction of the emulsion, as well as the escape of the hexane vapours towards the lab extraction. The temperature close to the inlet of the emulsion into the "flash drum" was approximately 98 °C. A stepper motor with a 3blade propeller was used to mix the water during the experiment to prevent agglomeration of the rubber particles. This type of motor was used due to the fact that it could be operated in flammable environment without any safety concerns. The stirring speed was 300 rpm. The experiment ran as batch process, while the industrial process is a continuous operation. When all the emulsion was transferred to the "flash drum", the experiment was completed, and the rubber particles were collected from the water and left to dry overnight in the fume cupboard at ambient temperature. The dried rubber particles' size and shape were analysed.

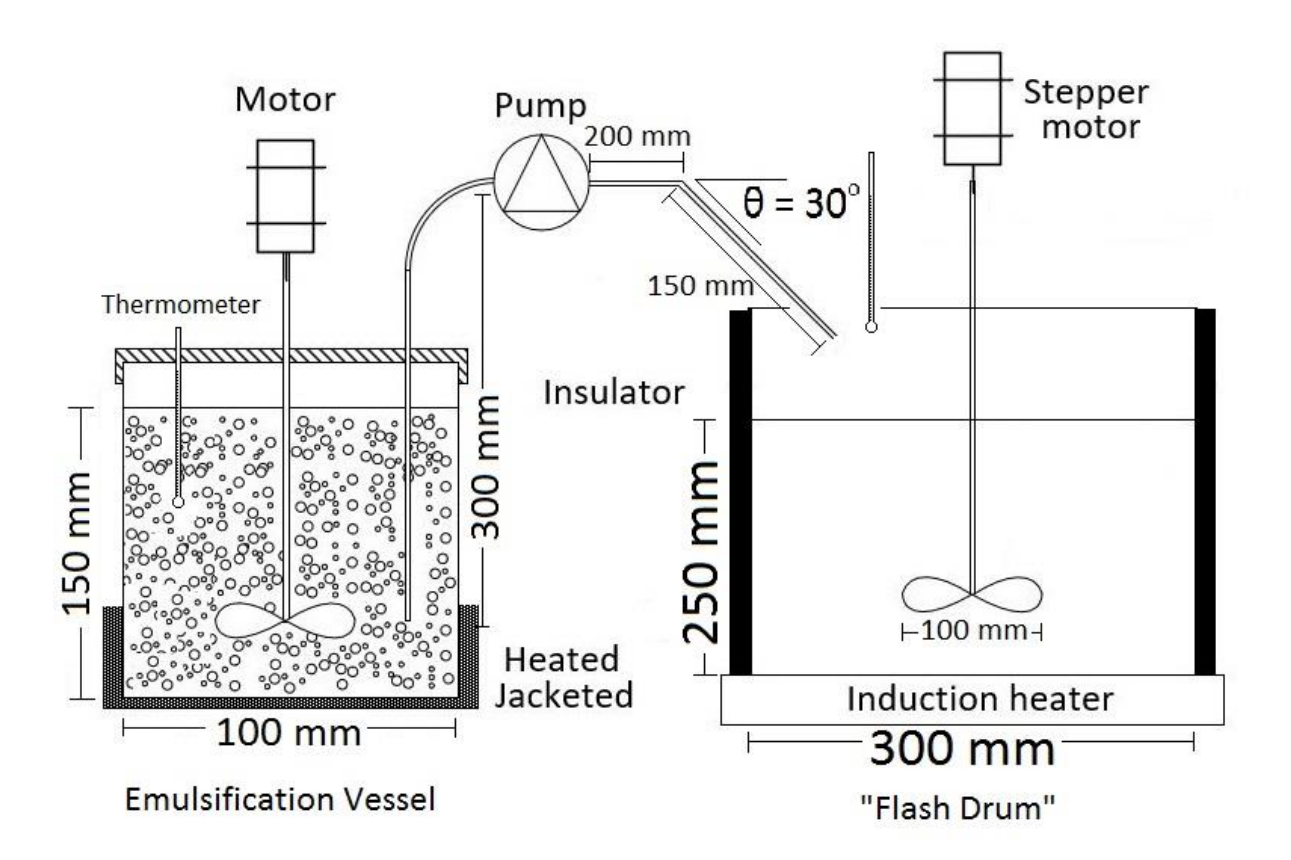


Figure 3.8. Schematic drawing of the initial rubber particles formation experimental configuration (not to scale).

Prior to the experiment, the two phases were prepared separately and then added in the emulsification vessel. The concentration of each phase and their volumes are shown in Table 3.15.

Table 3.15. Concentration and volume of each phase used in the rubber particles formation experiment.

#	Organic phase		Aqueous phase		
#	Volume (mL)	BR (g/L)	Volume (mL)	CaSt <sub>2</sub> (g/L)	NaOH (M)
1	400	100	100	15	0.1
2	250	100	250	15	0.1

The outcome of the above experiments, which is described on Section 4.6.2, resulted in the modification of the discharging system of the emulsion into the "flash drum" to allow better speed control of the discharge emulsion and eliminate the pulsing effect of the peristaltic pump, as well as result in better mixing in the "flash drum". No experiments were conducted with the updated experimental configuration, but it was developed and built for future potential.

The modified experimental rig is shown in shown in Figure 3.9. The emulsification vessel and the peristaltic pump was replaced by a pressurised stainless-steel vessel with an outlet at the bottom, facilitating the discharge of the emulsion into the "flash drum". A stirring shaft with two sets of 4 bladed propeller stirrers at different levels would be used to formulate the emulsion. Heating elements were placed inside the pressurised vessel wall to heat the emulsion at 50 °C. The thickness of the pressurised vessel was 10 mm allowing to be pressurised with the use of nitrogen. The vessel was located at a higher level from the "flash drum" to reduce friction, as less piping was required. A valve at the bottom of the vessel was used in order to discharge the emulsion when the pressure was at the desired level inside the vessel. Due to limited volume of the vessel, the discharged speed of the emulsion should be kept constant during the experimental time. In addition, a second mixer was added in the "flash drum" for more appropriate mixing, which will be discussed in Section 4.6.2.

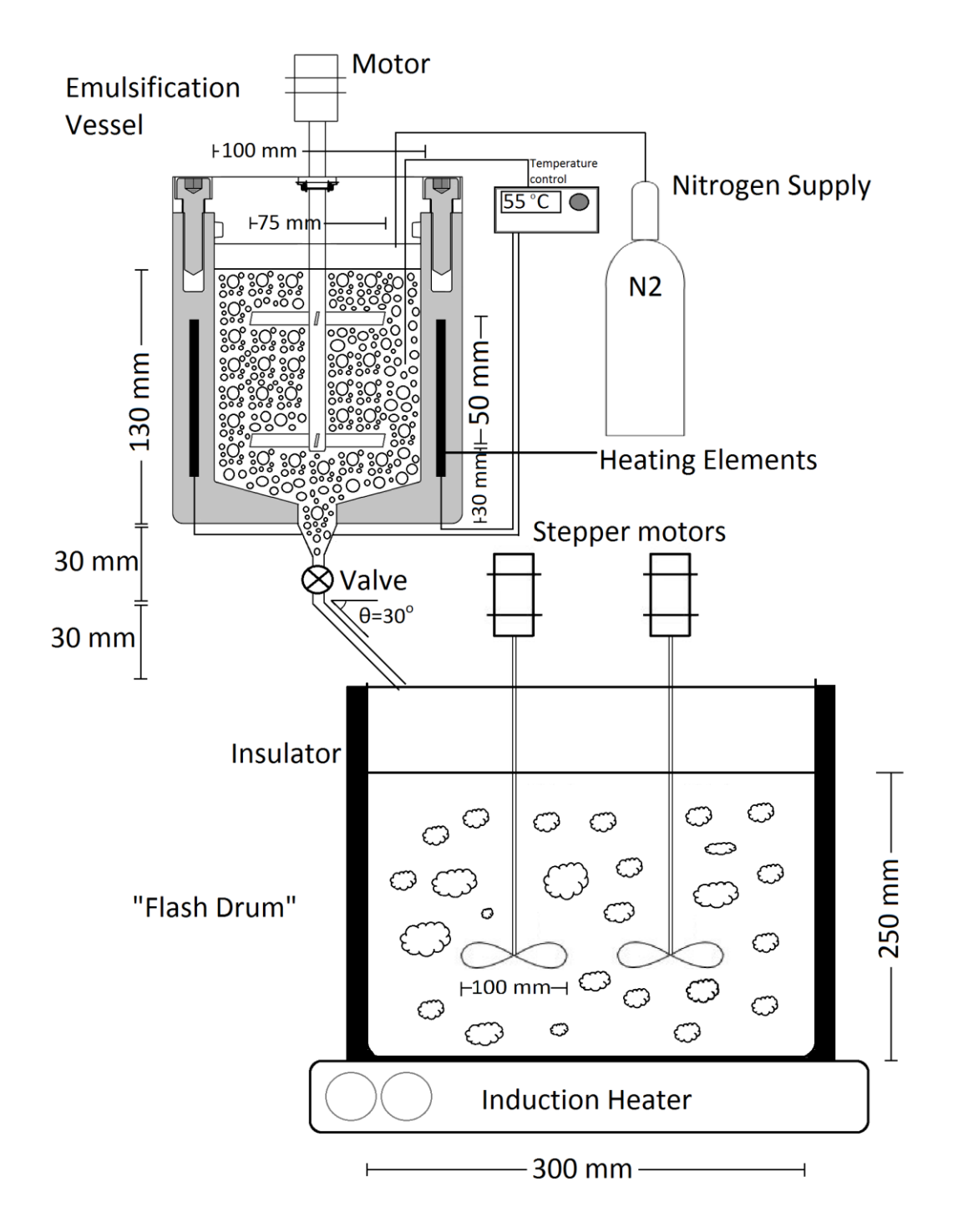


Figure 3.9. Schematic drawing of the updated rubber particles formation experimental configuration (not to scale).

### Chapter 4

## 4. Experimental results and discussion

## 4.1. Copper solvent extraction – Lewis-cell

In this section, the Cu extraction experimental results are presented and discussed, as well as the reasons why it was judged as an inappropriate solute for the investigation of interfacial mass transfer taking place in the halobutyl rubber production process.

Figure 4.1 shows the % of extraction efficiency of Cu from the aqueous to the organic phase at a pH range between 1.5 and 4 (see Section 3.2 for experimental details). The Cu extraction between phases depends on the pH at equilibrium. Up to a pH of 2, Cu extraction efficiency is low and then increases rapidly. For this study, the extreme values of pH, 1.5 and 4, are crucial, as, on these pH values, 100% Cu extraction is achieved from organic to aqueous and from aqueous to organic phase respectively. It could be concluded that the distribution coefficient (m) of Cu between the organic and the aqueous phase can be controlled by the pH.

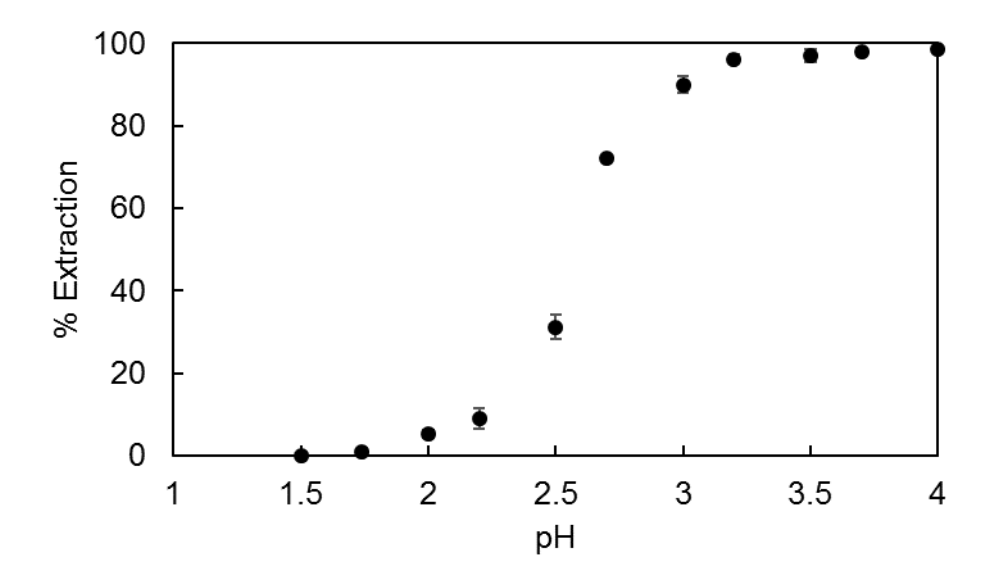


Figure 4.1. % of extracted copper from the aqueous to the organic phase at various pH values (error bars show the spread of results from 3 repeats).

As described in Section 3.2, the next step was to prepare the organic phase with Cu-D2EHPA complex and investigate the extraction rate of Cu in the Lewis cell when the pH of the aqueous phase is 1.5 (distribution coefficient equal to zero). The latter was set up so that mass transfer of the solute occurs from the organic to the aqueous phase, to mimic the neutralisation that occurs during the halobutyl rubber process described in Section 2.1.5. For the two concentrations of BR (0 and 50 g/L) in the organic phase, several stirring speeds were used, as shown in Figure 4.2 and 4.3.

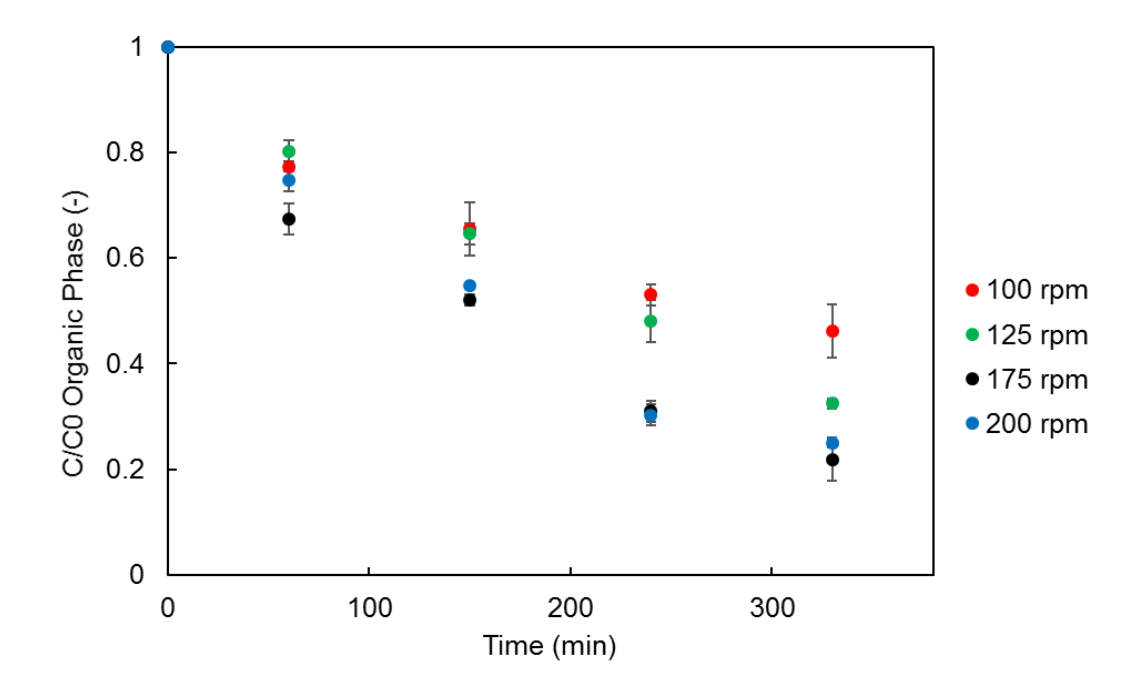


Figure 4.2. Effect of stirring speed on the extraction rate of Cu from the organic to the aqueous phase in the Lewis-cell (0 g/L BR) (error bars show the spread of results from 3 repeats).

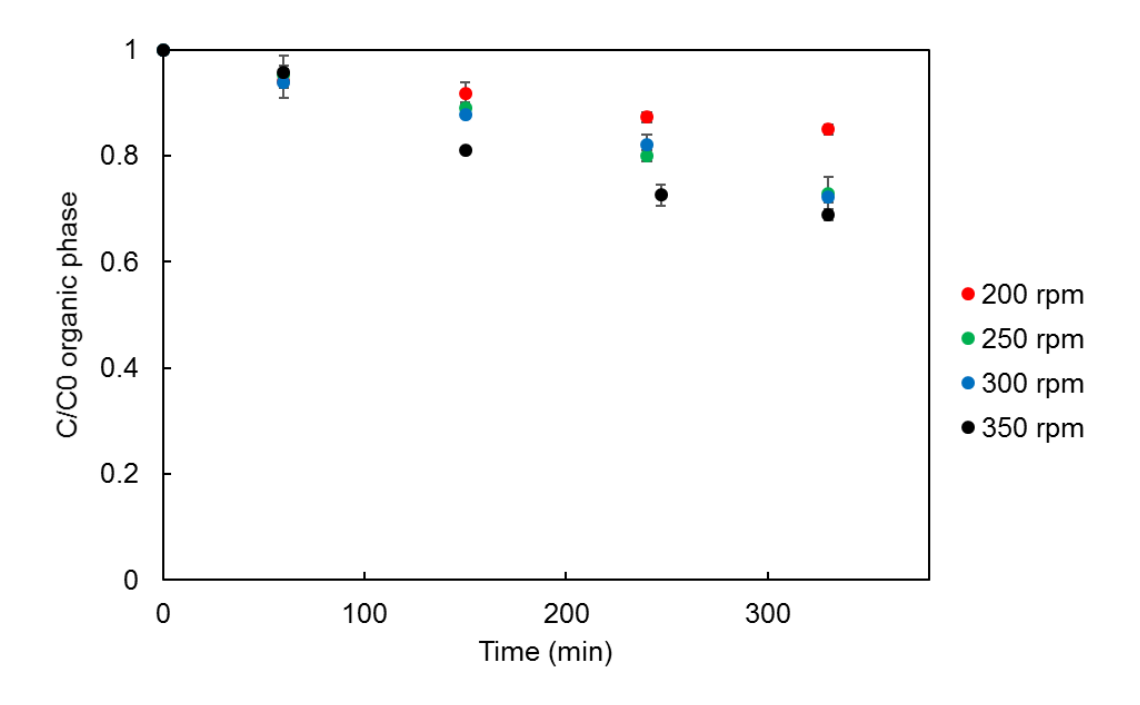


Figure 4.3. Effect of stirring speed on the extraction rate of Cu from the organic to the aqueous phase in the Lewis-cell (50 g/L BR) (error bars show the spread of results from 3 repeats).

The increase of the stirring speed resulted in higher Cu extraction rate from the organic to the aqueous phase in the Lewis-cell (sharper reduction of Cu concentration in the organic phase). Above a certain value of stirring speed for both sets of experiments (~175 rpm for 0 g/L BR and ~300 rpm for 50 g/L BR), the % of extraction efficiency at the 330th minute of the Lewis-cell experiment remained relatively constant, as shown in Figure 4.4. This allowed the comparison between the two experiments, with and without BR in the organic phase, on the solute extraction rate, as shown in Figure 4.5.

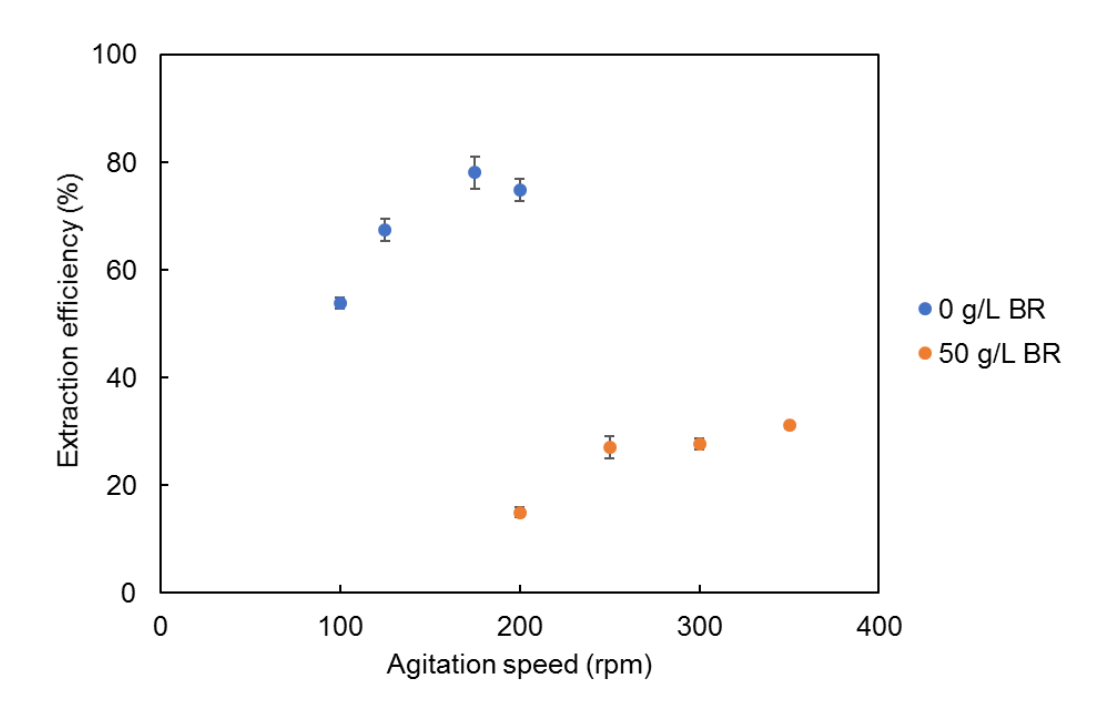


Figure 4.4. Extraction efficiency at 330<sup>th</sup> min of Cu from the organic to the aqueous phase at various stirring speeds for 0 and 50 g/L BR at the end of Lewis-cell experiments.

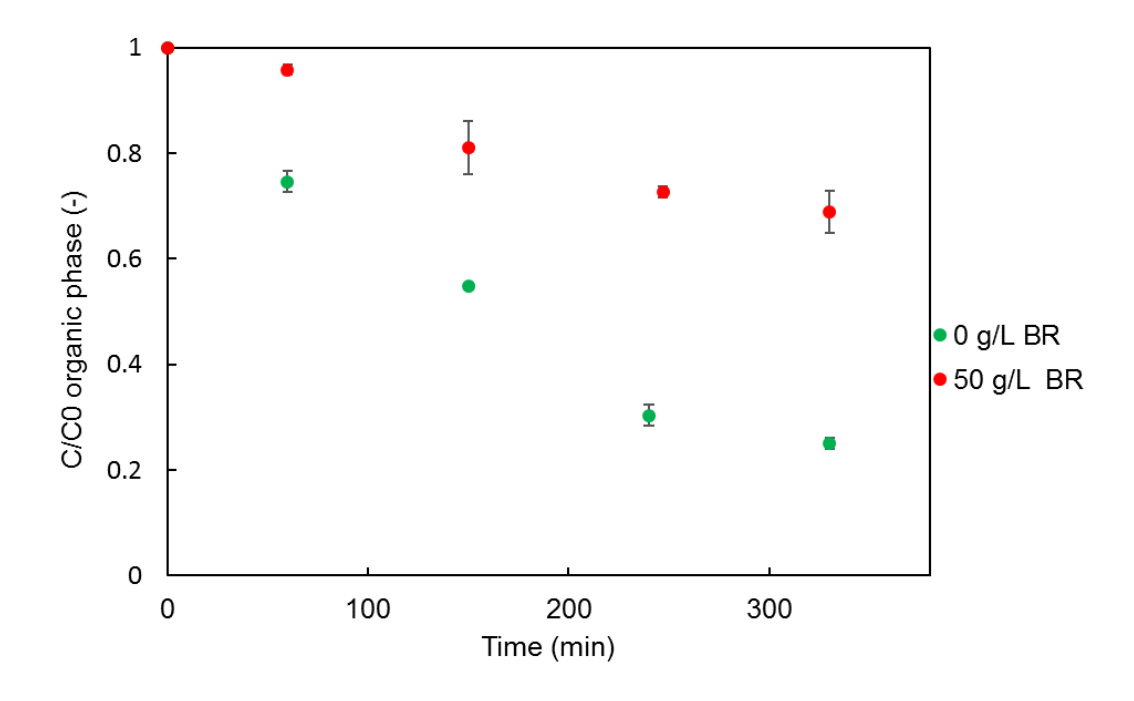


Figure 4.5. Effect of BR concentration in the organic phase on the extraction rate of copper from the organic to the aqueous phase in the Lewis-cell at the highest impeller speeds.

By comparing the highest agitation speeds at the experiments with and without BR, as shown in Figure 4.5, it could be easily concluded that the presence of BR in the organic phase had negative impact on the extraction efficiency, i.e. there is a considerable decrease in the mass transfer rate for the 50 g/L BR organic phase, in comparison with the 0 g/L BR, despite the much increase stirrer speeds for the former. The low extraction rate was the result of the increase in the viscosity, which reduced the diffusivity and increased the film thickness of the organic phase and, hence, reduced the film mass transfer coefficient, as discussed in Section 2.3.

As described in Section 3.2, an initial investigation of the compatibility of CaSt<sub>2</sub> with H<sub>2</sub>SO<sub>4</sub> and NaOH took place. Figure 4.6 shows the 4 samples of a CaSt<sub>2</sub> suspension in water under acidic and alkaline environmental conditions. Visual observation of the low pH sample concluded that the CaSt<sub>2</sub> reacted with the H<sub>2</sub>SO<sub>4</sub> and formed stearic acid agglomerations which floated on the surface. Due to that reaction of CaSt<sub>2</sub> in acidic conditions, it was decided to conduct the Lewis-cell experiment at alkaline environment. Hence, an alternative solute, chromium (Cr), was selected, which is able to be extracted in an alkaline environment, as described in Section 4.2.

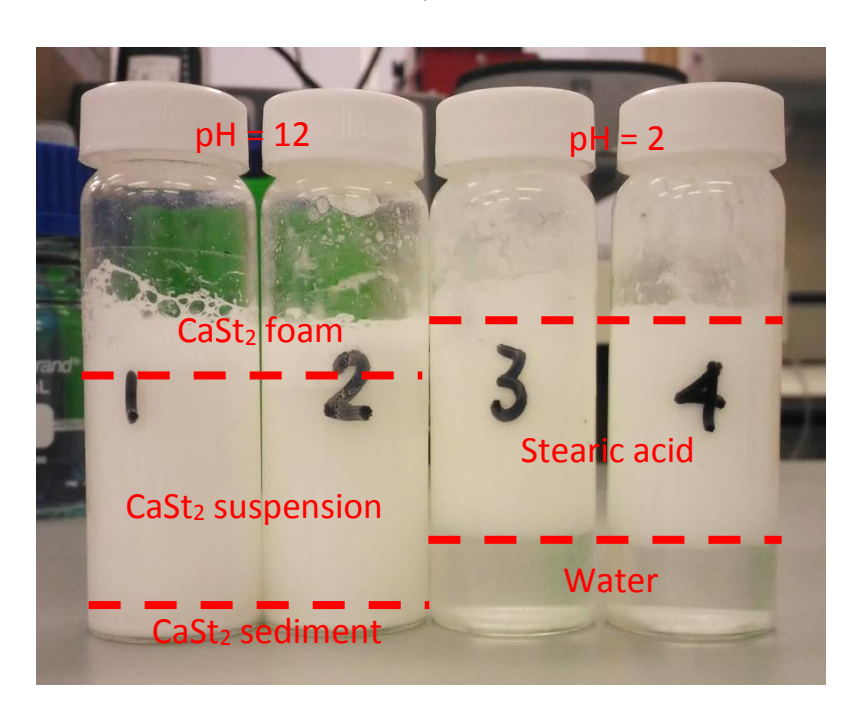


Figure 4.6. Visual observation of the effect of acidic and alkaline environment in the CaSt<sub>2</sub> suspension.

#### 4.2. Chromium solvent extraction – Lewis-cell

This section covers the experimental results from Cr extraction from the organic to the aqueous phase by mixing, as well as the problem in the Lewis-cell caused by the  $CaSt_2$ . As the aqueous to the organic phase extraction of Cr is well described in the literature, the aim of this experiment was to achieve to reverse that extraction by, achieving distribution coefficient (m) equal to zero. This would allow us to investigate the effect of organic phase viscosity and  $CaSt_2$  concentration in the aqueous phase on the extraction rate from the organic to aqueous phase. Experimental materials, methods and conditions are described in Section 3.3.

Figure 4.7 shows the effect of ionic strength on the extraction efficiency at equilibrium of Cr from the organic to the aqueous phase by mixing. The ionic strength (*IS*) was dependent on the concentrations of NaOH and NaCl and calculated by Equation 4.1 (Arnaut et al., 2006). In addition, Table 4.1 shows the calculated ionic strength for each aqueous phase, as well as how it affected the extraction efficiency of Cr.

$$IS = \frac{1}{2} \sum_{i} C_i Z_i^2 \tag{4.1}$$

Where:  $C_i$  is the concentration of each ion i.

 $Z_i$  is the charge of each ion i.

Table 4.1. Concertation of the NaOH and NaCl in the aqueous phases and the respective ionic strength and Cr extraction efficiency.

	Extraction		
NaOH (M)	NaCl (M)	Ionic Strength (M)	efficiency (%)
0.4	0.00	0.40	0.0
0.4	0.01	0.41	2.9
0.4	0.10	0.50	99.5
0.4	0.15	0.55	65.8
0.4	0.20	0.60	68.1

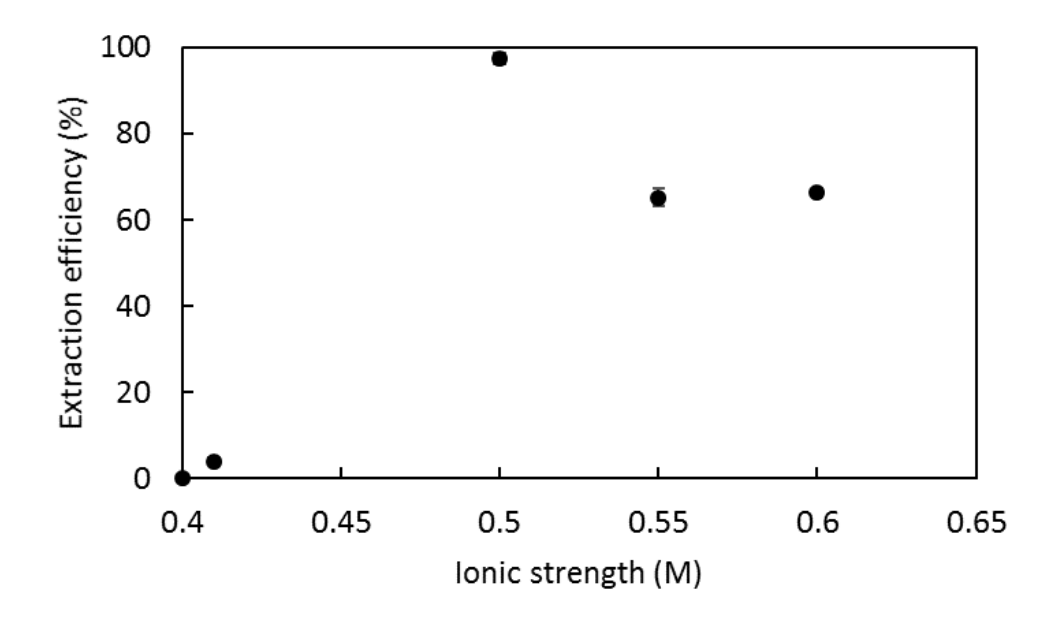


Figure 4.7. Effect of ionic strength on the extraction efficiency of Cr from the organic to the aqueous phase.

The increase of ionic strength from 0.41 to 0.50 M resulted in a dramatic increase of the Cr extraction efficiency from the organic to the aqueous phase. However, further increase of the ionic strength, decreased the extraction. At ionic strength higher than 0.5 M, solids were formed in the aqueous phase after mixing and separating the two phases. These solids, probably containing Cr, were insoluble in the aqueous phase, as shown in Figure 4.8, and thus, they couldn't be measured in the FAAS. This resulted in the low calculated extraction efficiency for an ionic strength of 0.50 M.



Figure 4.8. Cr solid particles formulation at high concentration of NaCl experiment.

As explained above, 0.4 M NaOH and 0.10 M NaCl in the aqueous phase were the ideal conditions to achieve the highest extraction efficiency (distribution coefficient (*m*) equal to zero) in order to run the Lewis-cell experiment. The effect of CaSt<sub>2</sub> in the aqueous phase on the extraction efficiency of Cr from the organic to the aqueous phase was tested by mixing. The CaSt<sub>2</sub> was added in the aqueous phase with 0.4 M NaOH and 0.10 M NaCl and mixed with the organic phase containing Cr-Aliquat 336 complex. The presence of CaSt<sub>2</sub> in the system did not result in Cr-CaSt<sub>2</sub> solids, keeping the extraction efficiency at same value (99.5%). However, in the Lewis-cell experiment, Cr-CaSt<sub>2</sub> solids were observed on the walls, as shown in Figure 4.9, due to their extensive time of contact (60 minutes) compared to the limited time in the mixing experiment. Figure 4.9 A shows the Cr-CaSt<sub>2</sub> solids formed in the Lewis-cell (A) during and (B) at the end of the experiment.

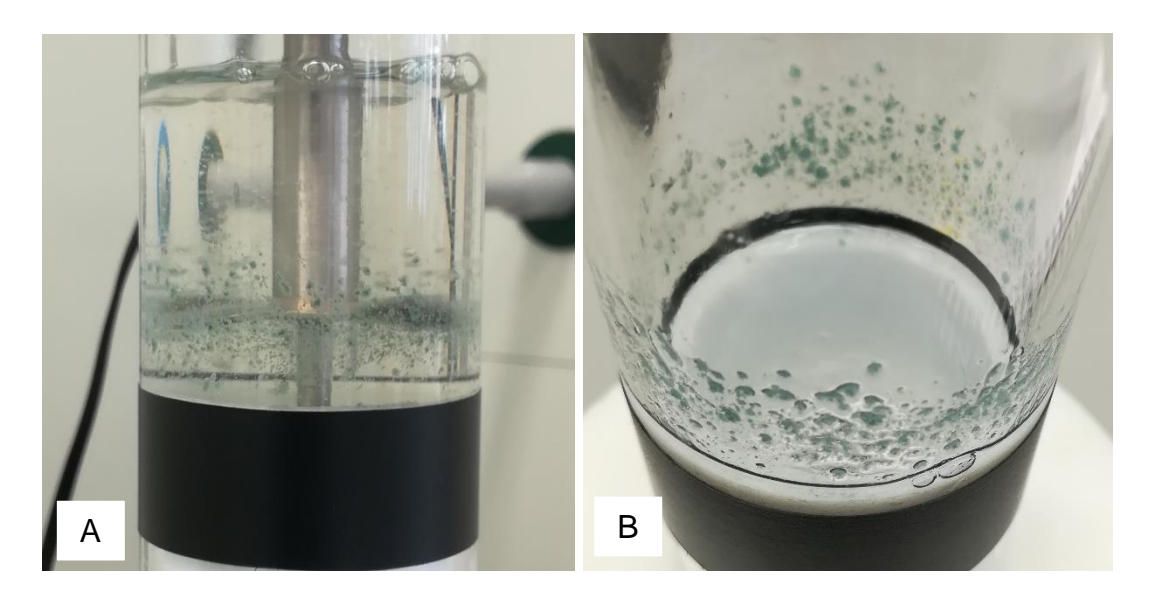


Figure 4.9. (A) Cr-CaSt<sub>2</sub> solids during and (B) at the end of the Lewis-cell experiment.

This undesired result led to the necessity of finding an alternative chemical in order to represent the interfacial mass transfer of the acids from the organic to the aqueous phase in the industrial process. Both Cu and Cr experiments in the Lewis-cell were not successful at the stage of CaSt<sub>2</sub> introduction. A weak acid, acetic acid, was chosen as an appropriate alternative from a health and safety point of view and to better mimic the industrial process.

#### 4.3. Calcium stearate

This section considers the effect of acidic and alkaline environments, as well as the high temperatures, on the CaSt<sub>2</sub>. The industrial emulsifier, CaSt<sub>2</sub>, encounters all these environments in the halobutyl rubber production process and it is important to understand their impact on it. In addition, the morphology and size of the CaSt<sub>2</sub> was determined.

# 4.3.1. Calcium stearate at acidic/alkaline environment and high temperature

This section shows the effect of the acidic and alkaline environment and high temperature on the CaSt<sub>2</sub>. As mentioned in Section 3.4.1, initially the effect of AcOH on CaSt<sub>2</sub> was tested at various mole ratios. Figure 4.10 shows the % of CaSt<sub>2</sub> that has reacted with the weak acid at various molar ratio between AcOH and CaSt<sub>2</sub>.

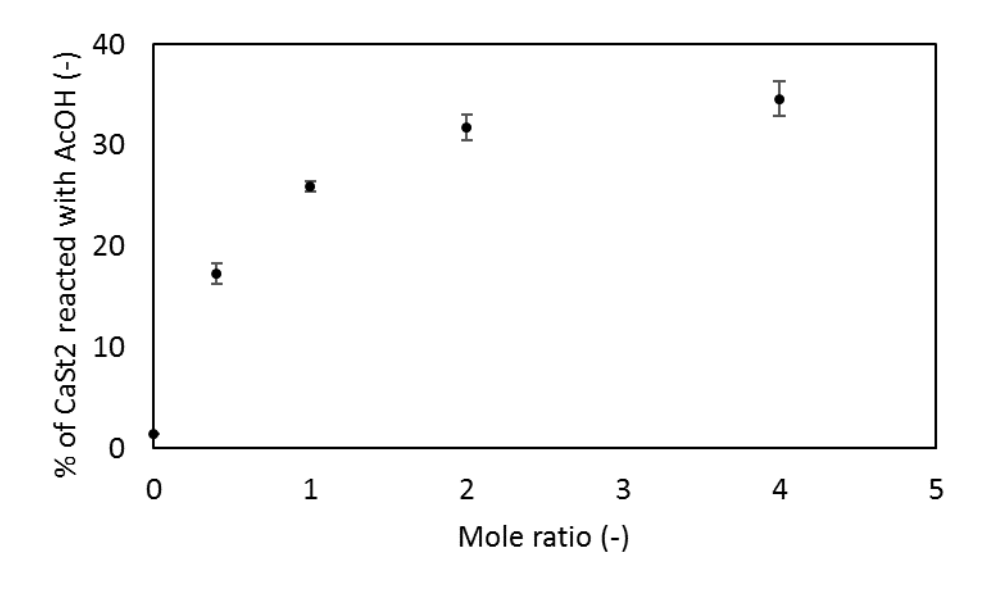


Figure 4.10. Effect of molar ratio (AcOH/CaSt<sub>2</sub>) on the % of CaSt<sub>2</sub> that reacted with the AcOH.

As the CaSt<sub>2</sub> is constant through the experiments (see Section 3.4.1), an increase of AcOH increases the amount of CaSt<sub>2</sub> that reacts (Figure 4.10). For mole ratios above 2 it is observed that the % of CaSt<sub>2</sub> that reacted created a plateau area, showing that there is limited CaSt<sub>2</sub> that could react with the acid. This is in line with the experimental

results that were produced where the CaSt<sub>2</sub> came in contact with excess AcOH or HCl, as show in Table 4.2. Figure 4.11 shows the % of CaSt<sub>2</sub> reacted with various concentration of AcOH and HCl. As indicated by Chemical Reaction (3.2) (reproduced below).

$$(C_{17}H_{35}COO)_2Ca + 2CH_3COOH \rightarrow 2C_{17}H_{35}COOH + Ca(CH_3COO)_2$$
 (3.4)

Table 4.2. Concentrations of CaSt<sub>2</sub>, AcOH and HCl in each solution with their respective pH.

#	CaSt <sub>2</sub> (M)	AcOH (M)	рН	#	CaSt <sub>2</sub> (M)	HCI	рН
						(M)	
A1	0.0005	0	7.40	B1	0.0005	0	7.40
A2	0.0005	0.01	3.65	B2	0.0005	0.01	2.28
А3	0.0005	0.1	3.05	B3	0.0005	0.1	1.47
A4	0.0005	0.2	2.84	B4	0.0005	0.2	1.02
A5	0.0005	0.3	2.79	B5	0.0005	0.3	0.82

At mole ratios above 2 in Figure 4.10, AcOH should be in excess, so a high conversion of CaSt<sub>2</sub> was expected. Figure 4.11 also shows the % of CaSt<sub>2</sub> reacted with various excess concentrations of AcOH and HCl.

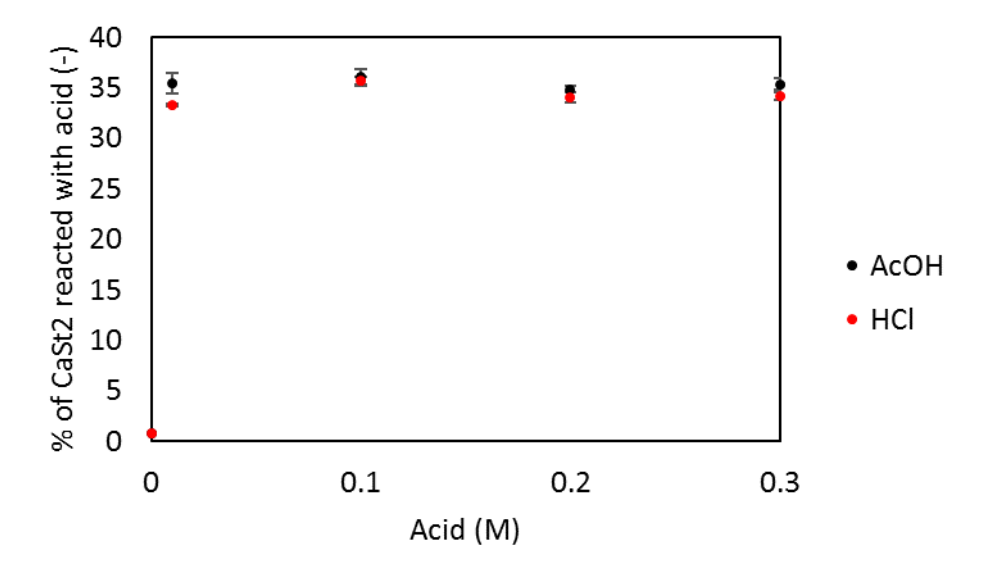


Figure 4.11. The % CaSt<sub>2</sub> that reacted with excess of AcOH or HCl.

Figure 4.11 shows that both acids resulted in the same amount percentage of CaSt<sub>2</sub> that reacted, equal to approximately 35%, in agreement with Figure 4.10. In addition

to the above, Figure 4.12 shows the effect of the final pH on the amount of CaSt<sub>2</sub> that reacted with each acid. The error bars represent the accuracy of the results.

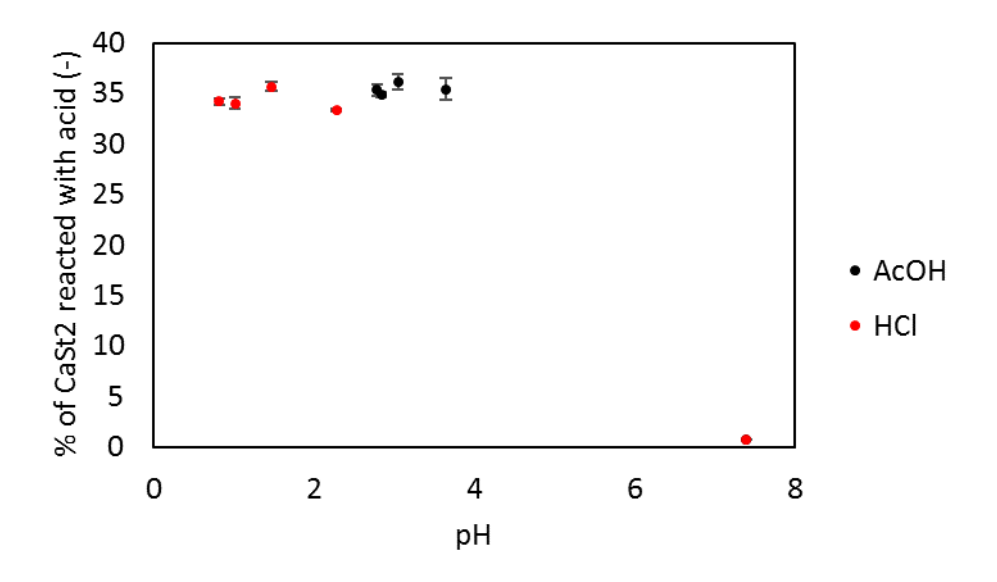


Figure 4.12. Final pH solution (acid and CaSt<sub>2</sub>) is comparison with the % of CaSt<sub>2</sub> that reacted with each acid.

As HCI is a strong acid, with higher dissociation constant, it might be expected that higher amount of CaSt<sub>2</sub> will react with it compared to the acetic acid, a weak acid. It is possible that the limited reaction between the CaSt<sub>2</sub> and each acid is due to low solubility in the water-phase and as a result it cannot react further. From Figure 4.12 it is concluded that pH values lower than 4 resulted in the formation of stearic acid, which is the product of the reaction between the CaSt<sub>2</sub> and an acid. From the above experiments, it could be concluded that in the halobutyl rubber production process there could be a limit on the amount of CaSt<sub>2</sub> that could react with the acid (acidic environment) and initiate the others reactions which result in foaming downstream, as described in Section 2.1. It should be aimed that the CaSt<sub>2</sub> should no encounter acidic environment in the industrial process in order to maintain its structure and consequently its functionality as emulsifier.

As mentioned in Section 3.4.1, the effect of an alkaline environment and high temperature on the dissociation of CaSt<sub>2</sub> were tested. Alkaline environment (pH > 12.91) was achieved with the addition of NaOH as shown in Table 4.3. Figure 4.13 shows the dissociation of CaSt<sub>2</sub> at various NaOH concentrations.

Table 4.3. Concentrations of CaSt<sub>2</sub> and NaOH in each solution with their respective pH values.

#	NaOH (M)	CaSt <sub>2</sub> (M)	рН
C1	0.0	0.0005	7.40
C2	0.1	0.0005	12.91
C3	0.3	0.0005	13.25
C4	0.5	0.0005	13.40
C5	1	0.0005	13.58

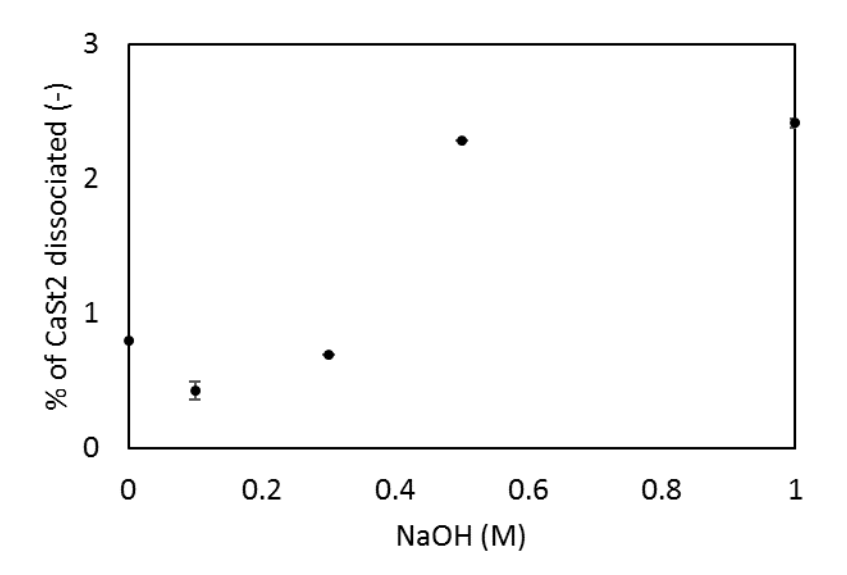


Figure 4.13. Effect of alkaline environment (various concentrations of NaOH) on the dissociation of CaSt<sub>2</sub>.

It is expected that there would be limited dissociation of CaSt<sub>2</sub> in alkaline environments. Figure 4.13 shows the results which indicate that a very low percentage of CaSt<sub>2</sub> has dissociated, which could simply reflect the sensitivity of the instrument at values close to zero. It could be concluded that after the neutralisation of acids in the industrial process, the alkaline environment should have no effect on the CaSt<sub>2</sub>, as there is no reaction between CaSt<sub>2</sub> and NaOH.

Figure 4.14 shows the dissociation of CaSt<sub>2</sub> at temperatures between 30 and 70 °C at pH equal to 7. A solution of 1.5 g/L of CaSt<sub>2</sub> was prepared and heated from room temperature up to 70 °C over a period of 20 minutes without modifying the pH.

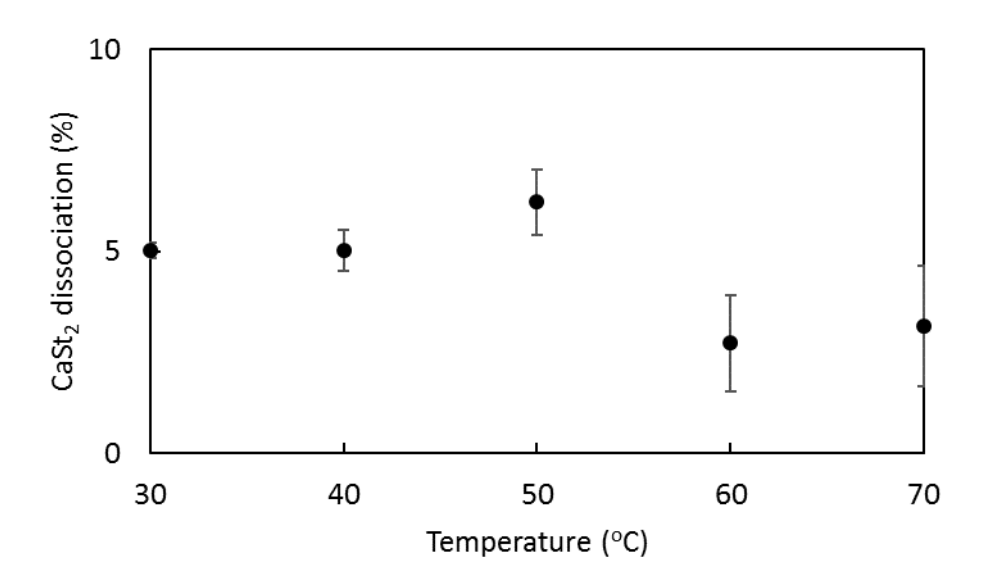


Figure 4.14. Effect of temperature on CaSt<sub>2</sub> dissociation

It is observed, in Figure 4.14, that the % of CaSt<sub>2</sub> dissociated low, but does not show a consistent behaviour. Samples were taken from the same solution during the heating, so the % of dissociation was expected to be accumulative, something that is not shown in Figure 4.14, as there is an initial increase and then decrease on the amount of CaSt<sub>2</sub> that dissociated during the experiment. It is believed that reason for that trend is the sensitivity of the instrument at low values. It should be noted that the neutralisation step in the industrial process takes place at high temperature, 20 - 65 °C (ExxonMobil, 2017; Happ et al., 2012). It is concluded that temperatures in this range have very low effect on the CaSt<sub>2</sub>, as very low dissociation took place (~ 5%) in the laboratory experiment.

# 4.3.2. Calcium stearate morphology

Figure 4.15 shows the CaSt<sub>2</sub> particles morphology used in this study. The SEM image shows that the particles have plate-like shape. Figure 4.16 shows the size distribution of CaSt<sub>2</sub> particles at various pH values. The average diameter (D[3,2]) of the CaSt<sub>2</sub> particles was 9.44 µm at pH of 7.4. There is a slight increase on the average size of the CaSt<sub>2</sub> particles at low pH values, as shown in Table 4.4, due to the formation of stearic acid on the surface of CaSt<sub>2</sub> particles, which is sticky and agglomerates. This cover of the CaSt<sub>2</sub> surface from stearic acid could be the reason of the low % of CaSt<sub>2</sub> reacted with the acids, as observed in Section 4.3.1, providing that the stearic acid could act as barrier. In addition, in an alkaline environment (pH~14), some bigger

particles were observed. However, the particle size did not change significantly at the various pH values.

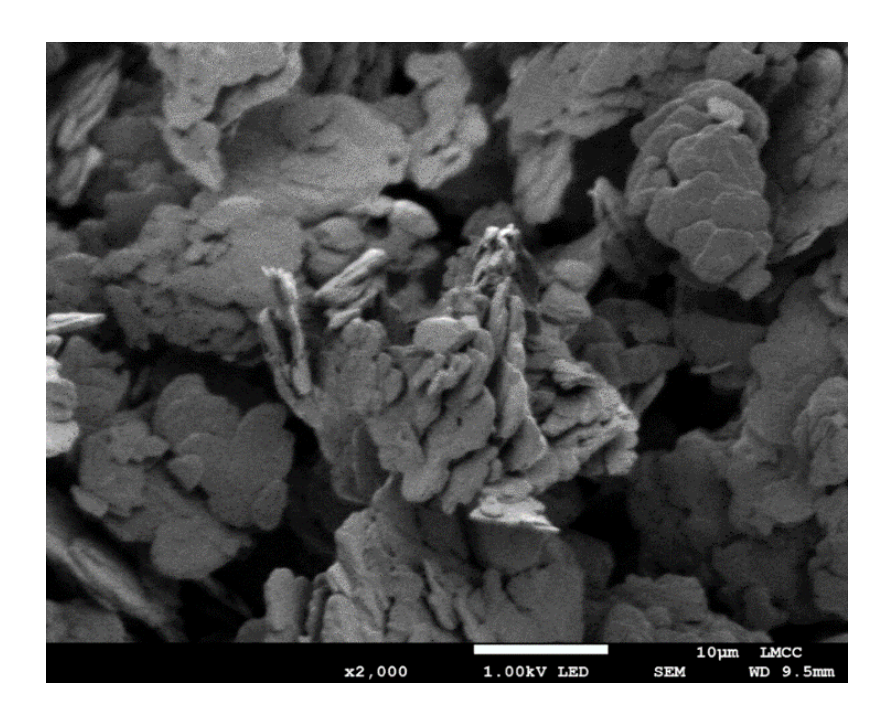


Figure 4.15. Morphology of the CaSt<sub>2</sub> dried particles (SEM image).

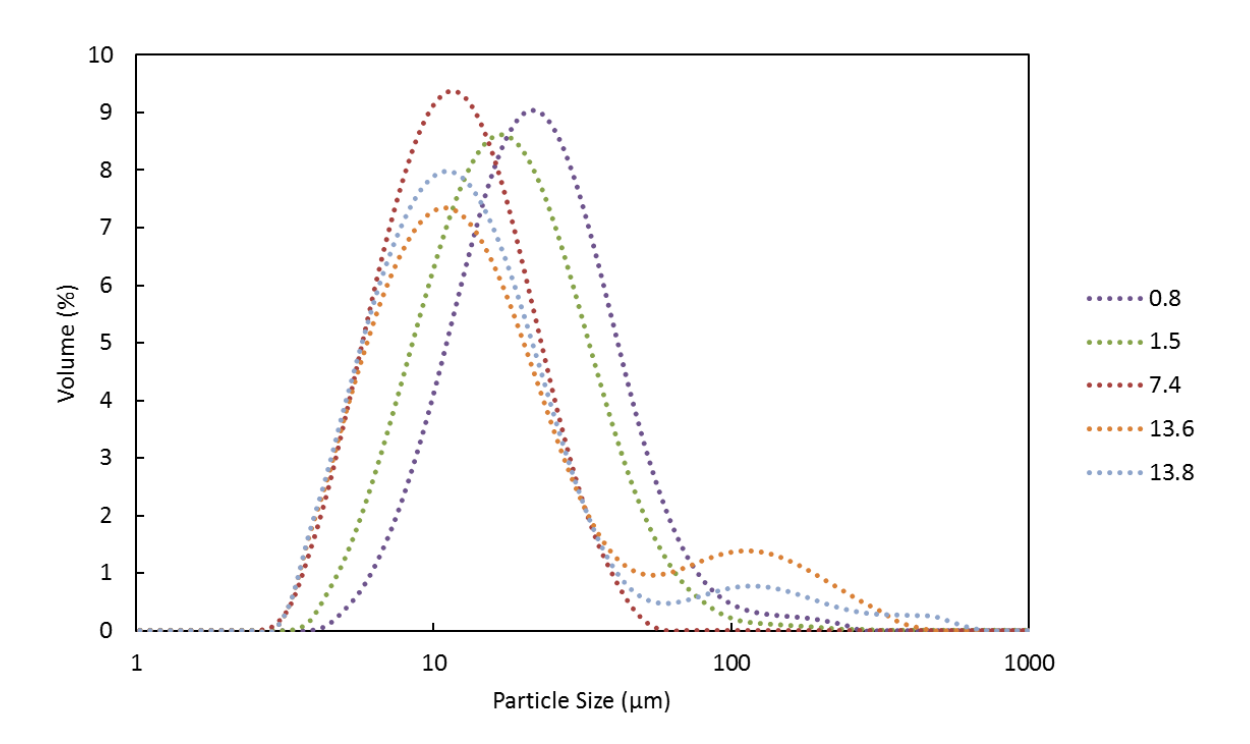


Figure 4.16. Particle size distribution of CaSt<sub>2</sub> at various pH values.

Table 4.4. The average diameter (D[3,2]) of CaSt<sub>2</sub> measured by the Malvern instrument at various pH values.

#	рН	D[3,2] (µm)
1	0.8	17.25
2	1.5	13.53
3	7.4	9.44
4	13.6	10.57
5	13.8	9.97

#### 4.4. Acetic acid solvent extraction

This section, initially shows the experimental results for the determination of the distibution coefficient of the third solute, namely AcOH, between the organic and aqueous phase by mixing the two phases. In addition, the Lewis-cell experiments, with AcOH as the solute, where the effect of organic phase viscosity and CaSt<sub>2</sub> concentration on the extraction rate, are prestented and discussed. The experimental methods and conditions are discussed in Section 3.5.

#### 4.4.1. Distribution coefficient of acetic acid

The Figure 4.17 shows the % of extraction of AcOH and the % of CaSt<sub>2</sub> reacted with the AcOH, during the AcOH interfacial mass transfer from the organic to the aqueous phase by mixing the two phases. The concentration of the species in each phase have been presented in Table 3.8.

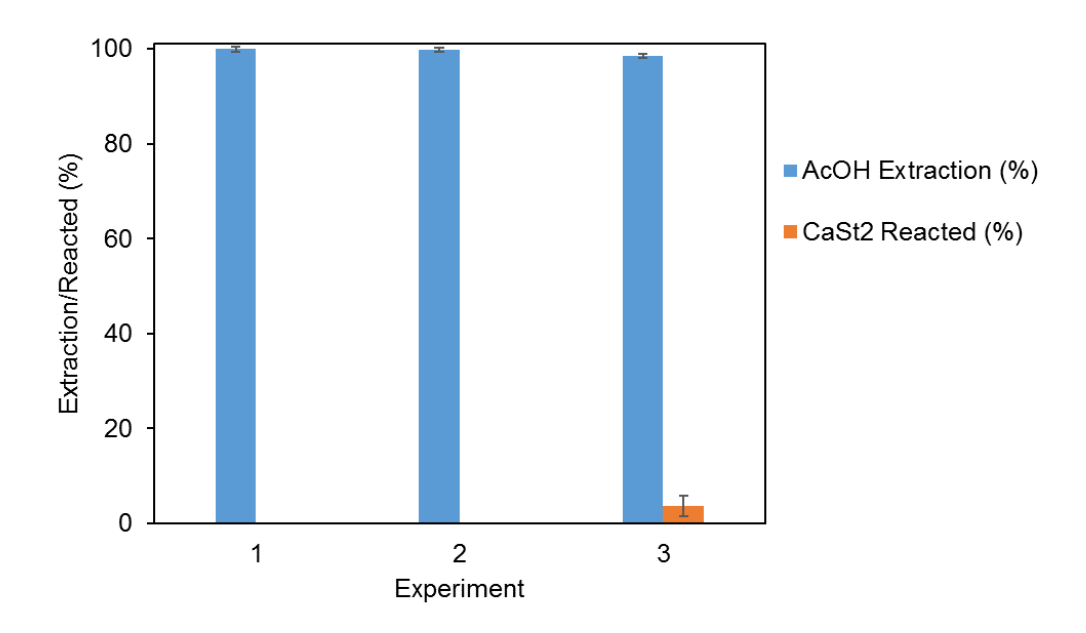


Figure 4.17. Extraction efficiency of AcOH and % of reacted CaSt<sub>2</sub> after the organic to aqueous phase mass transfer of AcOH by mixing.

In experiment 1 (see Table 3.8), where only AcOH was present in the system, the extraction from the organic to aqueous phase was approximately 100%, so it can be concluded that the distribution coefficient of AcOH between the two phases is 0. In addition, both BR and CaSt<sub>2</sub> did not reduce the extraction efficiency significantly, as concluded from the results of experiments 2 (BR was present) and 3 (both BR and CaSt<sub>2</sub> were present) as shown in Figure 4.17. Due to the above reasons, the AcOH was selected as a suitable solute for the investigation of the organic phase viscosity and CaSt<sub>2</sub> concentration on its extraction rate in the Lewis-cell.

# 4.4.2. Effect of butyl rubber concentration on the interfacial mass transfer coefficient

This section discusses the effect of organic phase viscosity on the interfacial mass transfer coefficient of AcOH from the organic to aqueous phase. It should be noted that the BR concentration in the industrial process is around 200 and 250 g/L and hence the viscosity is very high (ExxonMobil, 2017). Figure 4.18 shows how the BR concentration in heptane, between 0 and 200 g/L, affects the viscosity at temperatures of 20 and 50 °C. The viscosity in Figure 4.18 is presented using a logarithmic scale. All the solutions exhibited Newtonian behaviour as the shear stress increased linearly

with the increase of the shear rate, as shown in Appendix 5. It is observed that the increase of BR concentration increases exponentially the viscosity. The increase of the viscosity for concentrations lower than 100 g/L BR is insignificant compared to 200 g/L BR.

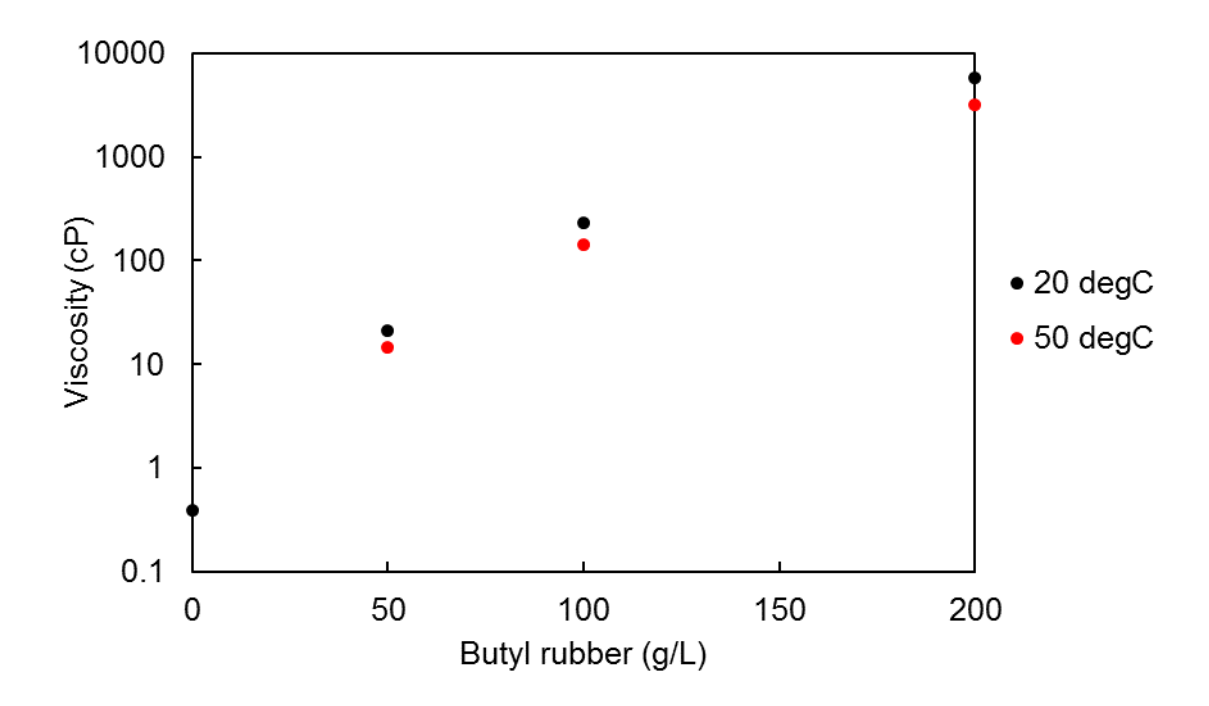


Figure 4.18. Viscosity of the organic phase at various concentrations of BR (0 – 200 g/L in n-heptane) (Logarithmic scale).

The Lewis-cell with the independent stirrers was used to investigate the effect of the organic phase viscosity as described in Section 3.5.2 (Table 3.9) at 20 °C without the presence of CaSt<sub>2</sub>. It should be mentioned that the experimental results were conducted at sufficiently high stirring speeds for there to be little effect and it was concluded that operation was at the Zone B as shown in Figure 2.16. In addition, every experiment was conducted at slightest lower stirring speed and the same extraction rate was observed. Figure 4.19 shows how the AcOH concentration profile in the organic phase is changing with time at various BR concentrations. As shown from the error bars, the reproducibility of the experiment is consistent. No equilibrium was reached during the 60 minutes of the experiment.

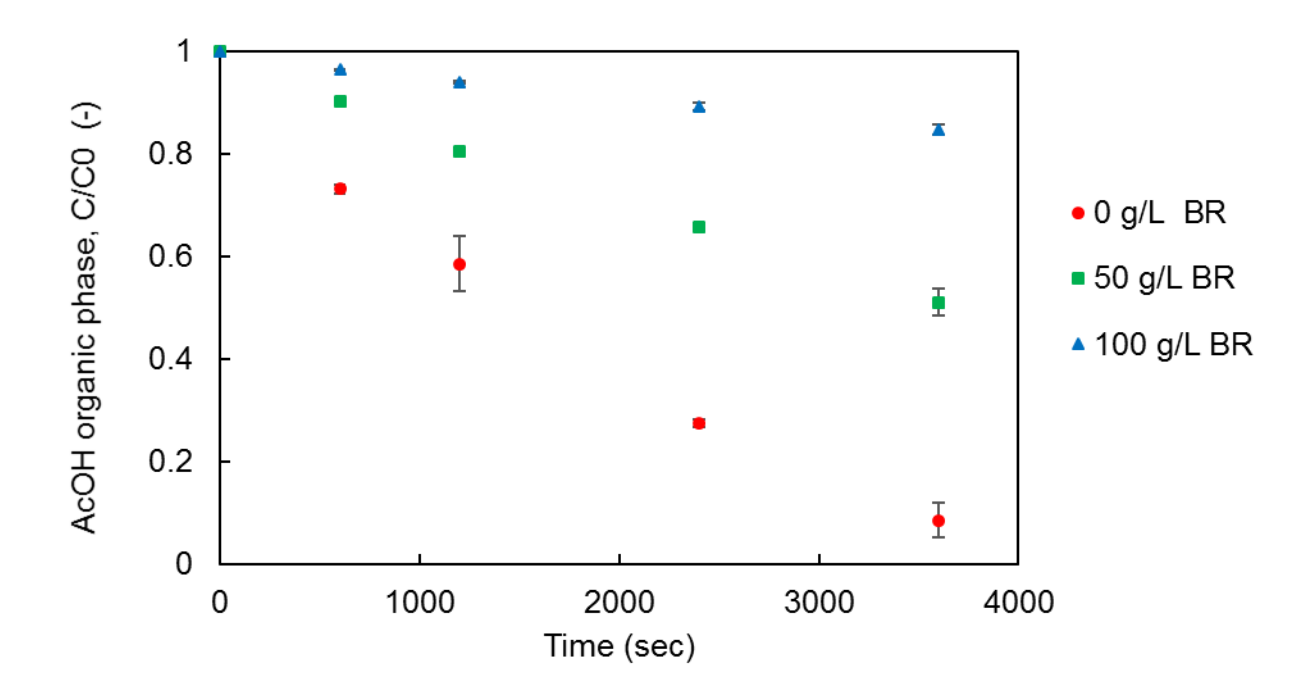


Figure 4.19. AcOH profile organic concentration with time at various concentrations of BR in the organic phase and without CaSt<sub>2</sub> in the aqueous phase.

It is concluded that, as the BR concentration increases, resulting in viscosity increase, the AcOH extraction rate from the organic to aqueous phase is slower. The mass balance on AcOH in the organic phase is shown in Equation 4.2, assuming perfect mixing in the bulk region.

$$V_{org} \frac{dC_{org}}{dt} = -K_{Oorg} A (C_{org} - C_{org}^*)$$
(4.2)

Where:  $V_{org}$  is the volume of the organic phase.

A is the interfacial area between phases.

 $K_{Oorg}$  is the overall mass transfer coefficient with respect to the organic phase.

 $C_{org}^*$  is the concentration of the AcOH in the organic phase in equilibrium with the AcOH concentration in the aqueous phase.

In Section 4.4.1 it was concluded that the distribution coefficient (m) between the two phases, with the presence of BR in the organic phase, was zero. By taking into

consideration the Equation 2.9, the  $C_{org}^*$  is zero. Therefore, separating the variables and integrating Equation 4.2 yields Equation 4.3.

$$-\ln\left(\frac{C_{org}}{C_{org}(0)}\right) = \frac{K_{Oorg}A}{V_{org}}t\tag{4.3}$$

Where:  $C_{org}$  is AcOH concentration in the organic phase with time.

 $\mathcal{C}_{org}(0)$  is the initial AcOH concentration in the organic phase.

Hence, by plotting the  $-ln(K_{oorg}A/V_{org})$  as a function of time (t) the slope of the straight lime will be equal to  $K_{oorg}A/V_{org}$  (Figure 4.20). Both A and  $V_{org}$  are known and constant during the Lewis-cell experiment and hence  $K_{oorg}$  can be calculated for every concentration of BR, as shown in Table 4.5.

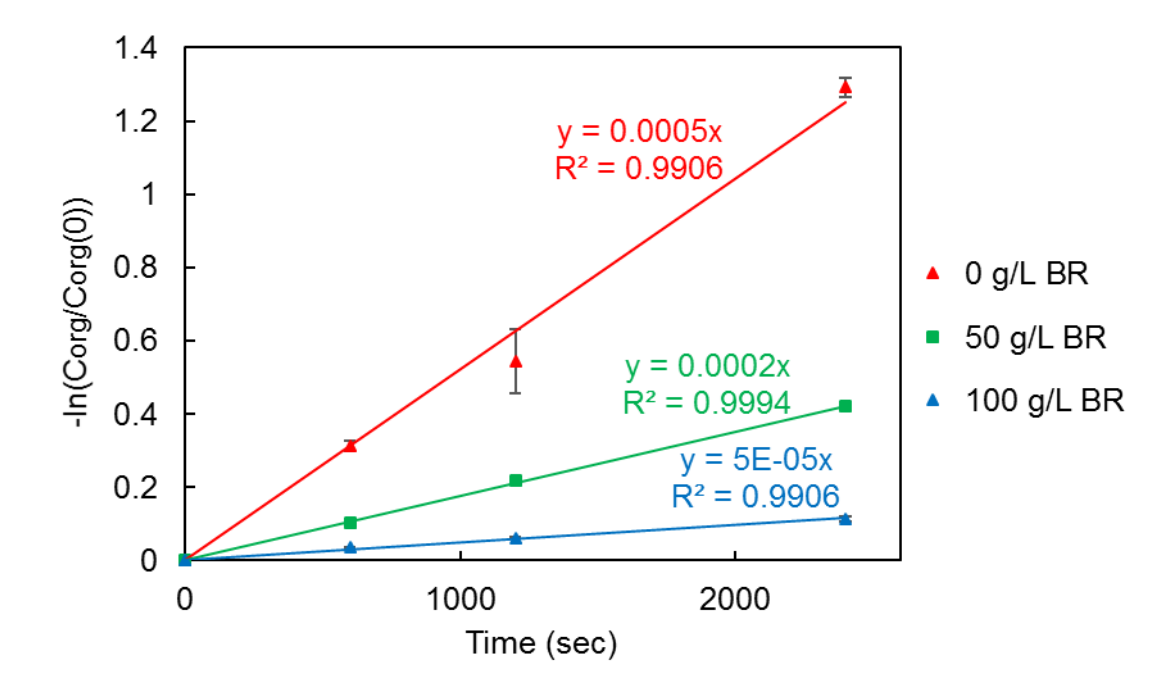


Figure 4.20.  $-ln(K_{Oorg}A/V_{org})$  as a function of time during the Lewis-cell experiments at various concentration of BR in the organic phase and without CaSt<sub>2</sub> in the aqueous phase.

Table 4.5. Effect of BR concentration in the organic phase (organic phase viscosity) on the overall mass transfer coefficient ( $K_{Oorg}$ ).

BR (g/L)	Viscosity	K <sub>Oorg</sub> A/V <sub>org</sub>	K <sub>Oorg</sub> (m/s)	
	(cP)	(s)		
0	0.389	5.346·10 <sup>-4</sup>	3.427·10 <sup>-5</sup>	
50	21.5	1.756·10 <sup>-4</sup>	1.126 ·10 <sup>-5</sup>	
100	229.0	0.466·10 <sup>-4</sup>	0.298-10 <sup>-5</sup>	

As discussed in Section 2.3, in the two-film theory of mass transfer, the resistance to mass transfer occurs two films and the interface. The distribution coefficient (m) for the AcOH in this system is zero and there is no resistance at the interface  $(R_i)$ . By taking into account the Equation 2.16, it is concluded that the overall resistance should depend only in the resistance in the organic phase film due its viscosity.

By plotting (Figure 4.21) the overall mass transfer coefficient against the organic phase viscosity, it could be concluded that the there is a sharp reduction in the  $K_{oorg}$  with a slight increase of viscosity. Further increase of the viscosity does not affect the coefficient significantly, as shown in Figure 4.21. As mentioned before, the BR concentration in the industrial process is between 200 and 250 g/L. A decrease of the BR concentration in the industrial process lower than 50 g/L of BR in order to achieve better interfacial mass transfer of the solute (HCL or HBr) will reduce the production rate, which is an non feasible solution for the industry.

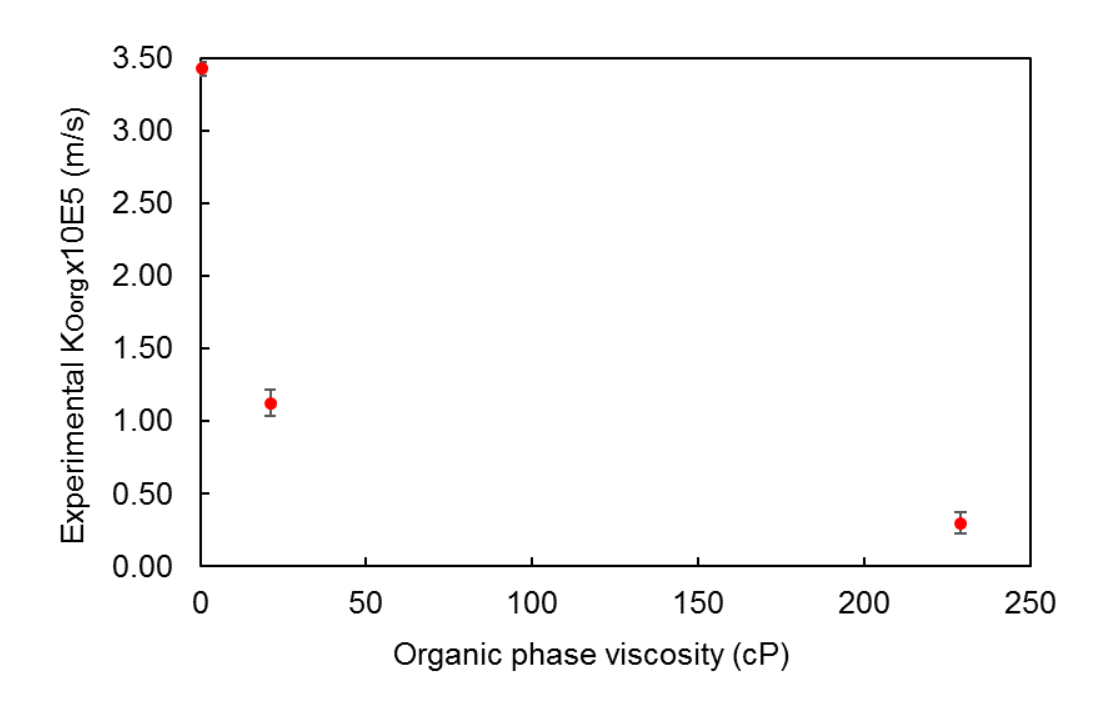


Figure 4.21. Experimental mass transfer coefficient of AcOH at various viscosities of the organic phase.

# 4.4.3. Effect of calcium stearate on the interfacial mass transfer rate of AcOH

This section shows the effect of CaSt<sub>2</sub> on the interfacial mass transfer rate of AcOH in the Lewis-cell during the organic to aqueous phase extraction. As mentioned in Section 3.5.3 (Table 3.11), initially three different concentrations of CaSt<sub>2</sub> were tested without the presence of BR and compare to the case of no CaSt<sub>2</sub>. Figure 4.22 shows how the concentration profile of AcOH in the organic phase is changing during the Lewis-cell experiment at various CaSt<sub>2</sub> concentrations.

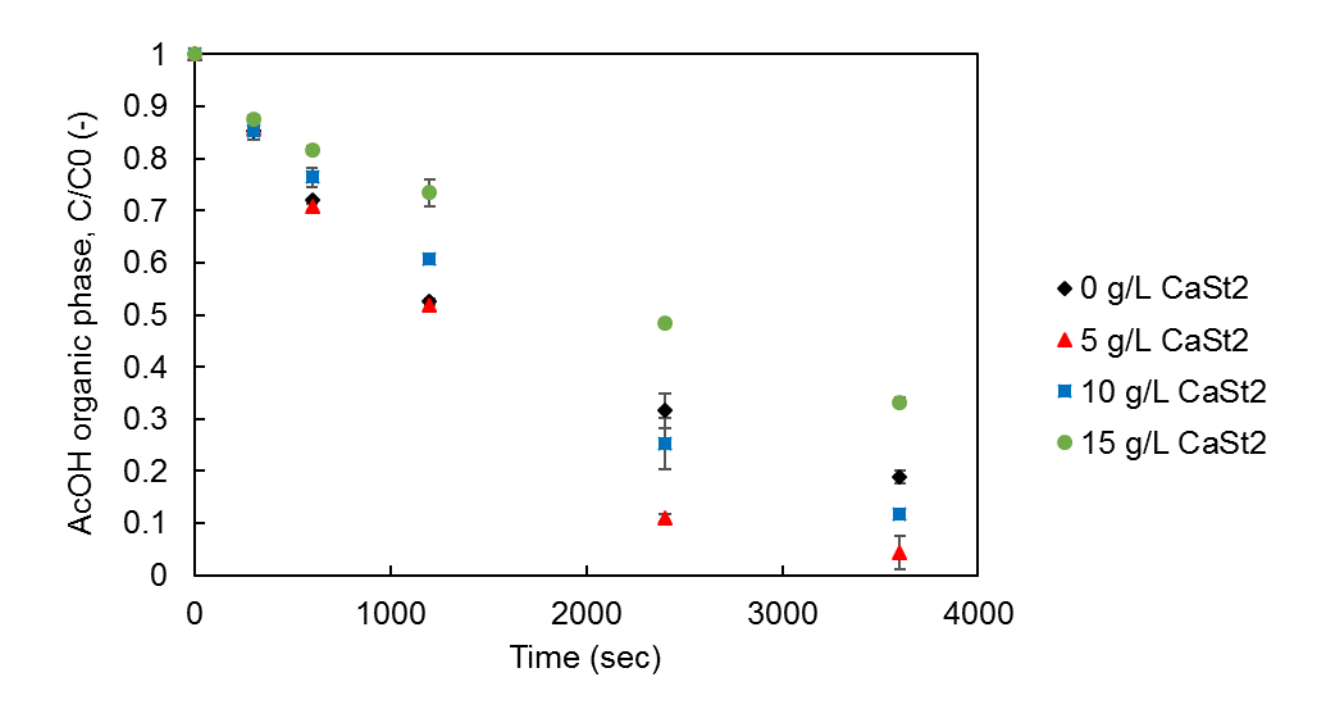


Figure 4.22. Effect of CaSt<sub>2</sub> on the AcOH extraction rate in the Lewis-cell without the presence of NaOH.

By comparing the 0 and 5 g/L CaSt<sub>2</sub> experimental results from Figure 4.22, it may be concluded that the addition of small concentrations of CaSt<sub>2</sub> in the aqueous phase increased the extraction rate of the AcOH from the organic to aqueous phase. It is possible, that the CaSt<sub>2</sub> reacted with the AcOH in the aqueous phase and as a result the concentration difference could increase between the two phases. As mentioned in Section 2.3 the concentration difference was the driving force for the interfacial mass transfer of the solute. A higher concentration difference between the two phases would increase the extraction rate. However, the distribution coefficient m has been shown to be zero (Section 4.4.1), so that is difficult to see why  $C_{org}^*$  (see Equation 4.2) should fall much further because of the chemical reaction.

Further addition of CaSt<sub>2</sub> (>5 g/L) decreased the extraction rate of AcOH in Figure 4.22. During the Lewis-cell experiments, the CaSt<sub>2</sub> reacted with AcOH and formed stearic acid, which agglomerated, forming large particles at the interface. In addition, these particles themselves stayed at the interface. As the concentration of the CaSt<sub>2</sub> increased, the amount of these particles at the interface increased too, resulting in an additional resistance to the mass transfer of AcOH from the organic to the aqueous phase. Therefore, a low concentration of CaSt<sub>2</sub> provided a modest improvement in the

mass transfer rate, but further increase added resistance at the interface and reduce the mass transfer rate.

Figure 4.23 shows the aqueous phase at the start and at the end of the Lewis-cell experiment when 10 g/L CaSt<sub>2</sub> was used. There is visual observation of the stearic acid agglomerations at the end of the Lewis-cell experiment.

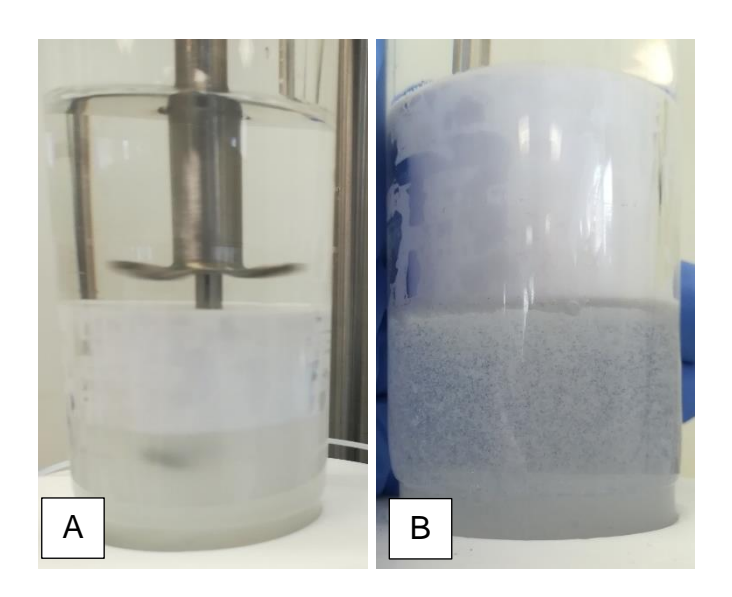


Figure 4.23. Formation of stearic acid during the Lewis-cell experiment. (A) The aqueous phase with 10 g/L CaSt<sub>2</sub> at the start (time: 0 sec) and (B) the end of the Lewis-cell experiment (time: 3600 sec)

As mentioned in Section 3.5.3, to examine also the effect of NaOH in the above experiments and to better mimic the interfacial mass transfer taking place in the halobutyl rubber production, a Lewis-cell experiment with 5 g/L CaSt<sub>2</sub> and 0.1 M NaOH in the aqueous phase was conducted. The addition of the NaOH reduced the visible dissociation of CaSt<sub>2</sub>, as well as increased the mass transfer rate (sharp reduction of concentration in the organic phase) of the AcOH, as shown in Figure 4.24. It could be suggested that, both CaSt<sub>2</sub> and NaOH reacted with the AcOH in the aqueous phase close to the interface, resulting in low AcOH concentration area, similar to the Lewiscell experiment with no NaOH and 5 g/L CaSt<sub>2</sub>. It is possible that the low concentration area increased the concentration difference between the two phases and, as a result, the interfacial mass transfer rate was increased.

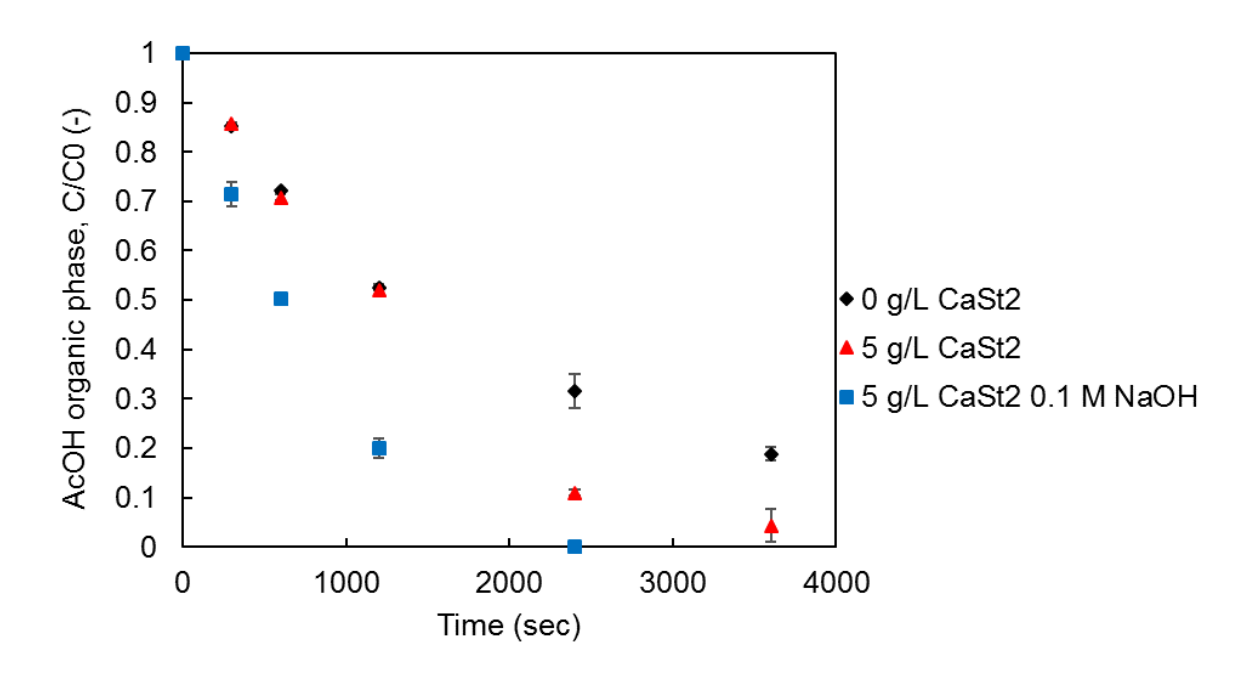


Figure 4.24. Effect of CaSt<sub>2</sub> on the AcOH extraction rate with the presence of NaOH in the Lewis-cell.

To conclude, a small amount of CaSt<sub>2</sub> in the aqueous phase improved the interfacial mass transfer of the solutes in the industrial process, especially when NaOH was present, which reduced the CaSt<sub>2</sub> and the HCl or HBr reaction forming insoluble, fatty stearic acid. Lack of NaOH in the industrial process would result in the formation of stearic acid which would obstruct the interfacial mass transfer of the solutes when high concentration of CaSt<sub>2</sub> is used. In the industrial applications, the ratio between the CaSt<sub>2</sub> and NaOH should be the appropriate aiming for high interfacial mass transfer rate and low formation rate of stearic acid.

# 4.5. Size and stability of the W/O Pickering emulsion

The stability and size of the emulsion that is formed in the industrial process plays an important role on the interfacial mass transfer, as discussed in the previous section; in addition, it is could have an effect on the formation of the rubber particles in the flash drum. In this section, the size and the stability of a W/O emulsion are presented. The BR concentration in the organic phase and the CaSt<sub>2</sub> concentration in the aqueous phase were the two parameters tested. As mentioned in Section 2.2.7, CaSt<sub>2</sub> is a solid emulsifier which forms Pickering W/O emulsions and would be added later to the halobutyl rubber as stabiliser of the product.

The formation method of the emulsion, as well as the analysis of the size of the emulsion and the emulsion stability investigation were described in Section 3.6. Table 4.6 shows the concentration of CaSt<sub>2</sub> and BR in each phase for the formation of the W/O emulsion. Emulsions 1 to 3 were used for the investigation of the effect of BR concentration (continuous phase viscosity) on the emulsion size and stability. In those experiments 5 g/L CaSt<sub>2</sub> was used as 0 g/L resulted in an unstable emulsion within a few minutes after the formation. Emulsion A to D were used to investigate the effect of CaSt<sub>2</sub> on the emulsion size and stability.

Table 4.6. Concentration of CaSt<sub>2</sub> and BR in each phase for the formation of the W/O emulsions.

	Aqueous phase		Organic phase		
#	Volume	CaSt <sub>2</sub>	Volume	DD (a/L)	
	(mL)	(g/L)	(mL)	BR (g/L)	
1	20	5	80	50	
2	20	5	80	100	
3	20	5	80	150	
Α	20	0	80	100	
В	20	5	80	100	
С	20	10	80	100	
D	20	15	80	100	

Figure 4.25 shows how the average diameter (by number) of the aqueous phase drops is changing at various BR concentration in the organic phase as function of time.

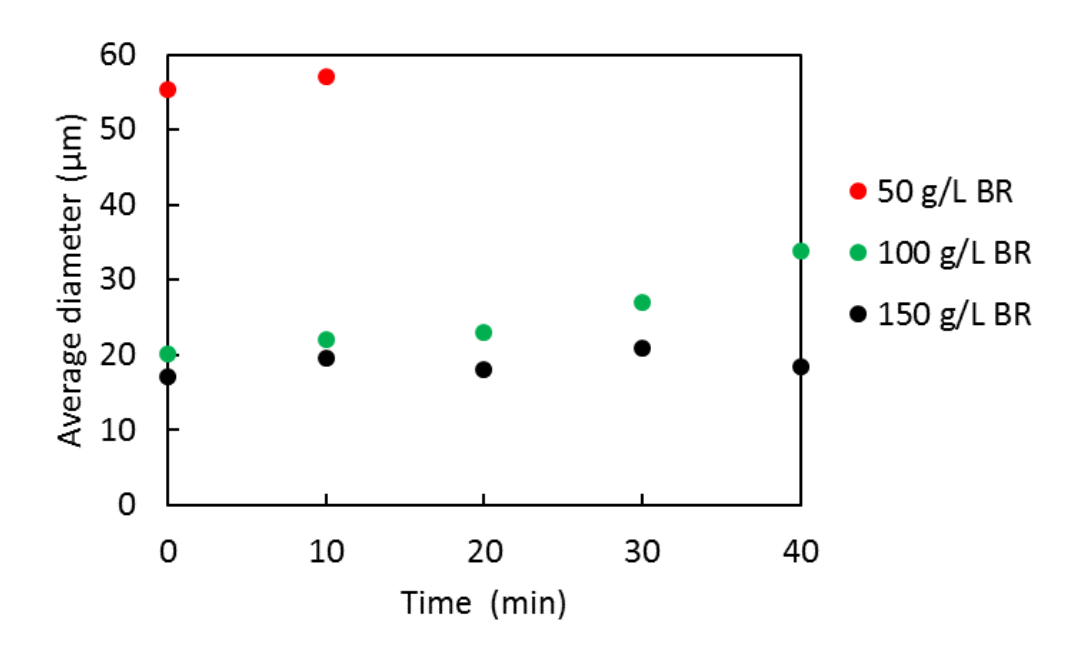


Figure 4.25. Effect of BR content on the emulsion size and stability - with 5 g/L CaSt<sub>2</sub> in the aqueous phase (Experiment: 1 to 3).

Agitation of the low BR concentration (50 g/L) resulted in an average drop size of approximately 55  $\mu$ m in the emulsion. However, the phases separated after 10 minutes, showing that the emulsion was not stable. On the other hand, higher concentrations of BR (100 and 150 g/L), corresponding to higher viscosity of the continuous phase (Figure 4.18), resulted in considerably smaller size of the dispersed aqueous drops (approximately 20  $\mu$ m) and more stable emulsions. At 100 g/L BR, the emulsion is less stable compared to 150 g/L BR, due to the higher viscosity of the organic phase as described also in Section 2.2.5.

Figure 4.26 shows how the dynamic interfacial tension is changing through time until the thermodynamic equilibrium is achieved, at various concentrations of BR in the organic phase and with no CaSt<sub>2</sub> in the aqueous phase (Table 4.6). The presence of the surface tension of water in the graph ensures the correct calibration of the KRUSS DSA 100 instrument.

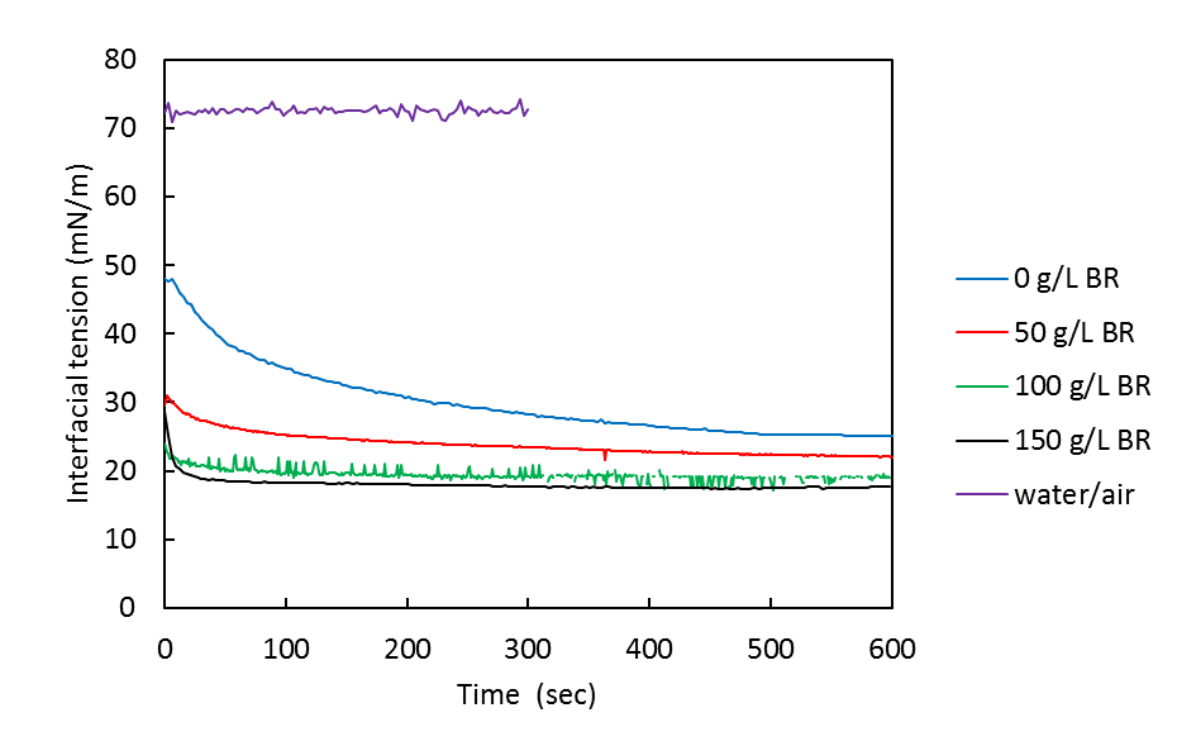


Figure 4.26. Effect of BR content on the interfacial tension between the organic and the aqueous phase without the presence of CaSt<sub>2</sub>.

As shown in the Figure 4.26, for every measurement there is a decrease in the interfacial tension (dynamic) with time until it stabilises (equilibrium interfacial tension). An increase of BR concentration corresponding to an increased viscosity, reducing the interfacial tension. However, the decrease of the interfacial tension is not proportional with the increase of the BR concentration. At concentrations of 100 and 150 g/L the interfacial tension change is almost negligible. At low interfacial tension values, highest BR concentration, the emulsion has better stability through time, as shown in Figure 4.25 (Pandolfe, 1981). It was concluded that the higher the viscosity, the more stable the emulsion during the 40 minutes of testing.

In addition, the effect of the presence of different concentrations of CaSt<sub>2</sub> on the Pickering emulsion size and stability were tested. Based on the conclusions of Figure 4.25, 100 g/L BR concentration was used for this analysis, as it gave a relative stable emulsion to work with. As stated in Table 4.6, the tested emulsion had 100 g/L BR in the organic phase and four different concentrations of CaSt<sub>2</sub> in the aqueous phase were tested (experiments A to D). Figure 4.27 shows the effect of CaSt<sub>2</sub> on the emulsion size and stability for a testing period of 40 minutes.

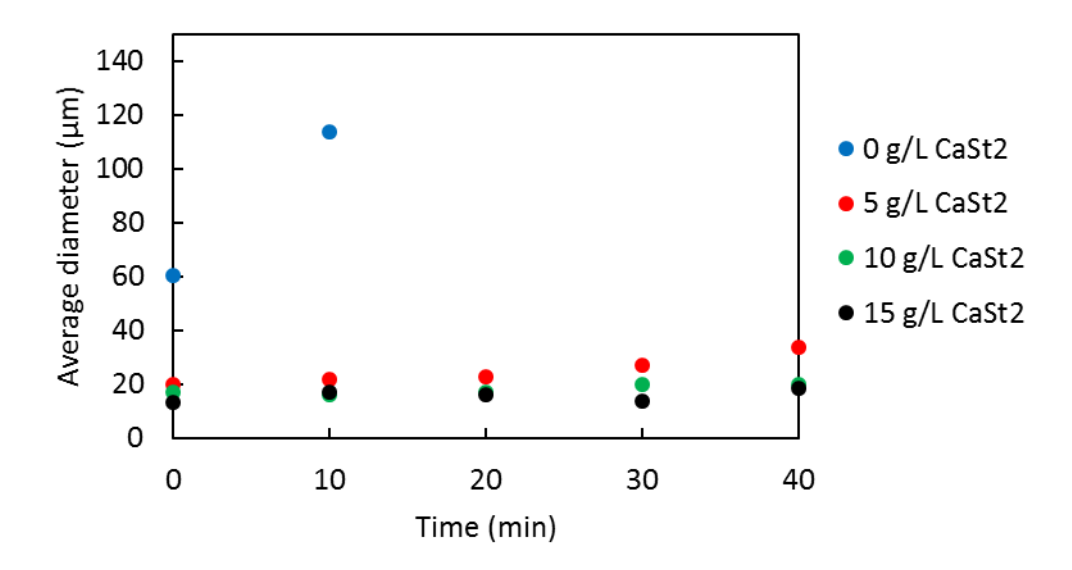


Figure 4.27. Effect of CaSt<sub>2</sub> content on the emulsion size and stabilization – with 100 g/L BR in the organic phase (Experiments: A to D)

As shown in Figure 4.27, the absence of emulsifier (0 g/L CaSt<sub>2</sub>) resulted initially (t = 0 min) in an emulsion with mean size of 60  $\mu$ m. After 10 minutes the mean size increased to 120  $\mu$ m and before the 20<sup>th</sup> minute it was visually observed that the two phases were separated. As there was no CaSt<sub>2</sub>, the viscosity of the organic phase was responsible for the initial formation of the emulsion and its low stability for approximately 10 minutes. On the other hand, even the lowest concentration of CaSt<sub>2</sub> (5 g/L) resulted in a relative stable Pickering emulsion for the 40 minutes of the experiment, with mean size approximately equal to 20  $\mu$ m. Figure 4.28 shows how the fine CaSt<sub>2</sub> particles are arranged on the interface and stabilise the aqueous drops. As the CaSt<sub>2</sub> concentration increased from 5 to 15 g/L the emulsion stability also increased. Figure 4.29 shows the effect of CaSt<sub>2</sub> on the interfacial tension between the two phases, when no BR was present in the organic phase.

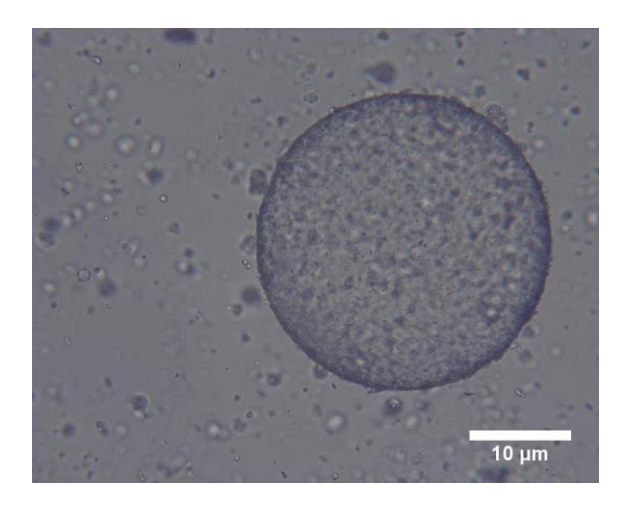


Figure 4.28. Example of the arrangement of fine CaSt<sub>2</sub> particles on the interface

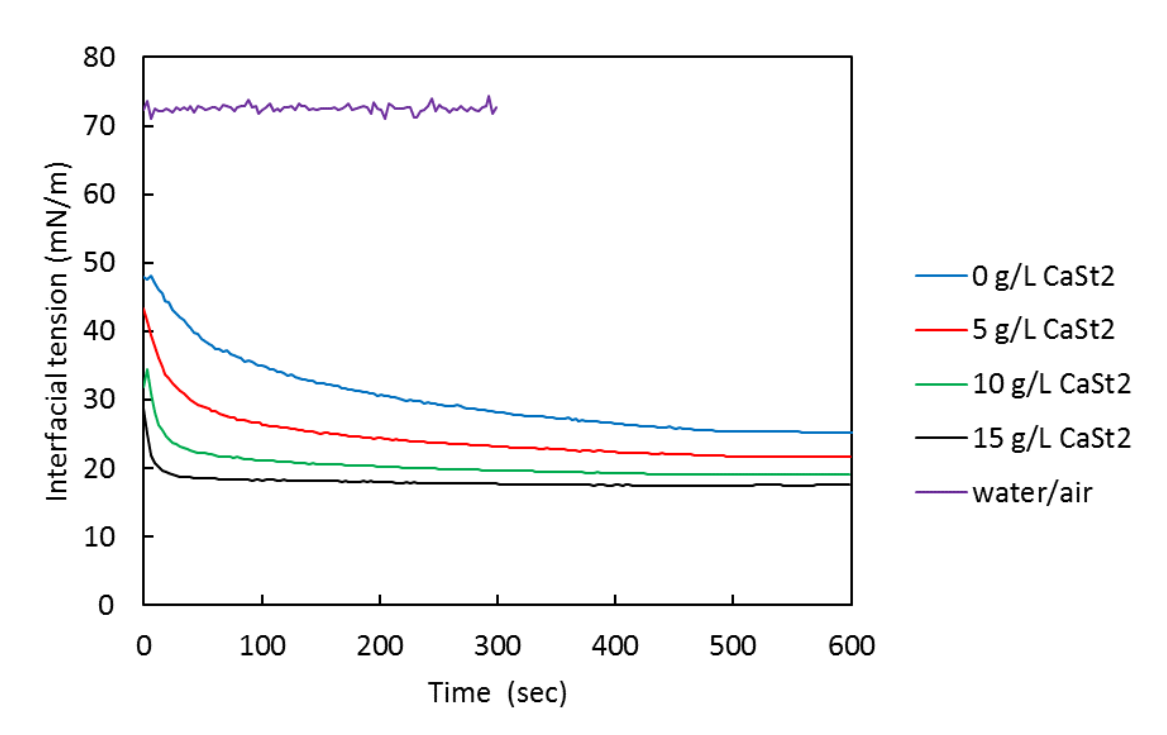


Figure 4.29. Effect of CaSt<sub>2</sub> on the interfacial tension between the aqueous and organic phases without the presence of BR.

The reduction of interfacial tension with time was due slow arrangement of the calcium stearate at the interface or contamination between phases (Maestro et al., 2014). The increase of CaSt<sub>2</sub> concentration reduces the interfacial tension up to a certain point as expected from an emulsification agent. This reduction resulted in a more stable and smaller mean size emulsion, as was described in Section 2.2.3 (Wong et al., 2015).

As noted in Section 2.1, which describes the halobutyl rubber production process, the emulsion is formed by mixing prior to the flash drum. A concentration of BR higher than 100 g/L in the organic phase and the presence of  $CaSt_2$  (>5 g/L) resulted in relative stable emulsions with mean sizes of approximately 20  $\mu$ m during the 40 minutes lab experiment. The  $CaSt_2$ , which is used in the halobutyl rubber production process as stabiliser of the final product, could be potentially used at an earlier stage as a solid emulsifier during neutralisation and emulsification. It may be concluded that the emulsion in the halobutyl rubber production process would be stable in the industrial process prior to the flash drum, as the polymer concentration is greater than 200 g/L.

### 4.6. Rubber particles formation

In this section, the results of the emulsion pendant drop evaporation experiments are presented and discussed, aiming to understand the evaporation mechanism of the W/O emulsion in the industrial flash drum. Experimental results are presented from the development process of a lab scale "flash drum" aiming to replicate the industrial one and achieve the same type of rubber particles, enable to study the effect of various parameters on their size and shape in laboratory scale.

# 4.6.1. W/O emulsion pendant drop evaporation

As was mentioned on the Section 3.7.1, a W/O emulsion pendant drop was exposed to high temperatures in a controlled environment, aiming to understand the evaporation mechanism of the emulsion. Two different emulsions were used in this experiment, as was shown in Table 3.14 and exposed to temperatures between 70 and 130 °C. 68 °C is the boiling point of hexane at atmospheric pressure and that is why the lowest temperature tested was the 70 °C. Figure 4.30 shows the effect of temperature (130 °C) on the W/O emulsion drop, without CaSt<sub>2</sub>, as captured by images taken by the KRUSS DSA 100 instrument's camera.

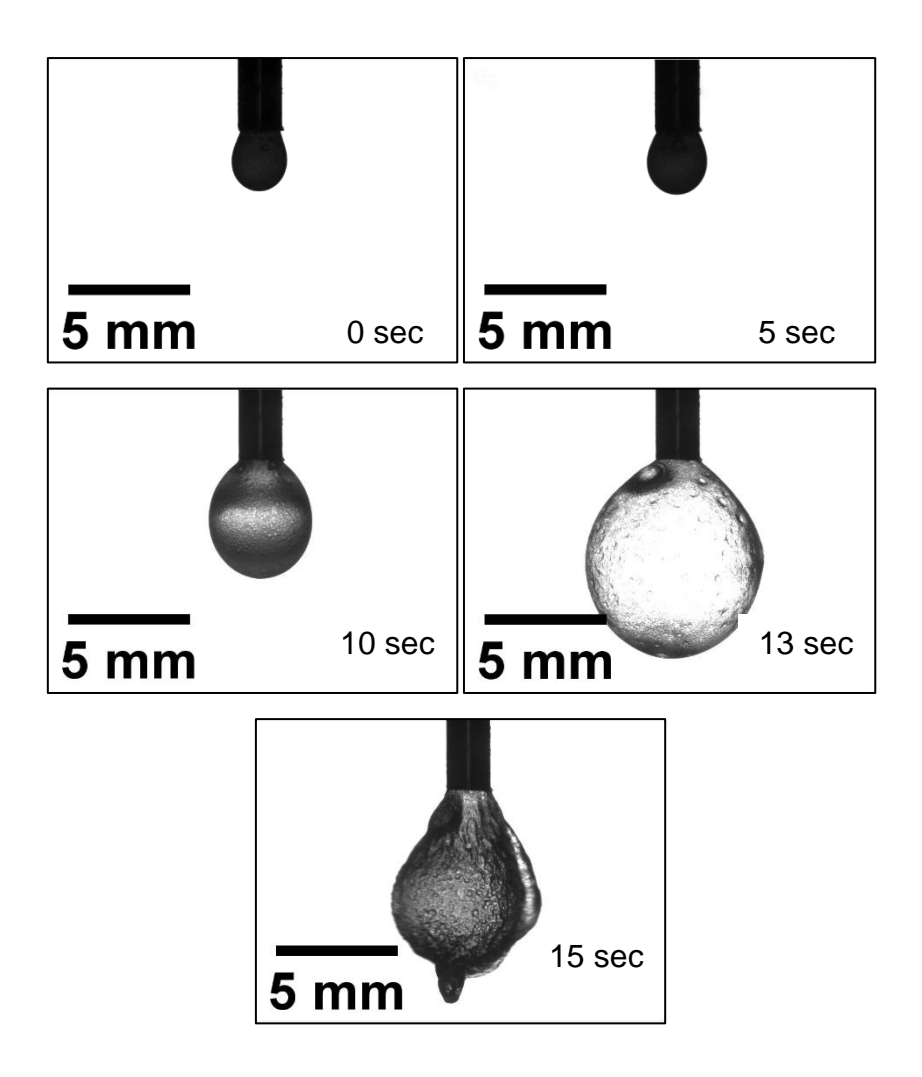


Figure 4.30. Photos taken by the KRUSS DSA 100 instrument showing the W/O emulsion (organic phase: 100 g/L BR in hexane, aqueous phase: 0 g/L CaSt<sub>2</sub>) drop changing through time until the final collapse at 130 °C.

In every experiment, the hexane located at the outside of the drop was evaporated first, resulting in a dry BR layer. As the heat was transferred towards the inside of the drop, more hexane was evaporated. The combination of the vapours generated in the drop and the impermeability of the outer BR layer, resulted in an expansion of the drop (Figure 4.30 at the 13<sup>th</sup> second) until a certain point, when it collapsed (Figure 4.30 at the 15<sup>th</sup> second). The stretching of the drop outer layer reduced its thickness and, eventually it ruptured resulting in release of hexane/water vapour and collapse of the drop. The same behaviour was observed at every temperature that was tested, although events occurred at different time frames, as discussed below. Figure 4.31 shows the normalised volume change, which was obtained by the KRUSS DSA 100 instrument, of the emulsion drops exposed to various temperatures (70, 80, 100 and

130 °C) with and without the presence of CaSt<sub>2</sub> through time until their collapse, as described in Section 3.7.1.

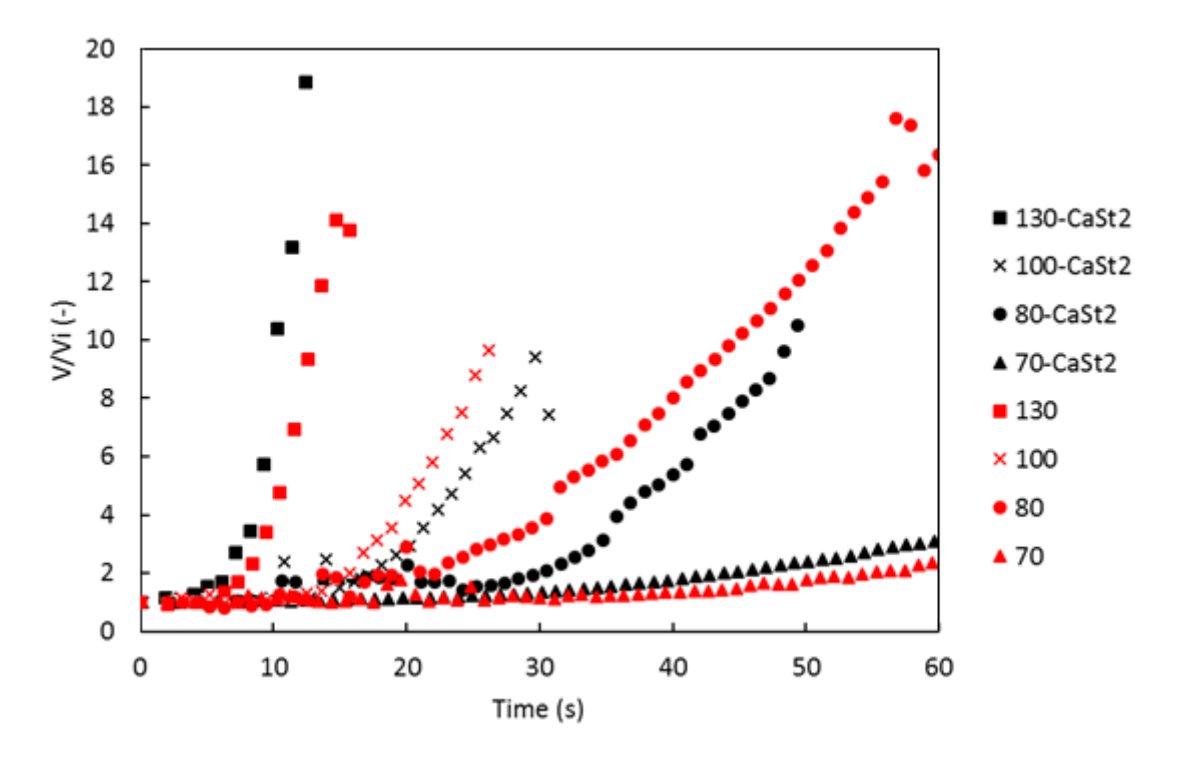


Figure 4.31. Emulsion drop evaporation at various temperature with (black) and without (red) CaSt<sub>2</sub>.

As shown from Figure 4.31, a higher temperature resulted in higher heat transfer rates to the pendant drop, and as a result the evaporation occurred more rapidly. In all temperatures tested, there is an initial time where there is no significant volume change. During this time evaporation of the outer surface was taking place. The organic solvent (hexane) formed the continuous phase and as a result after its evaporation a thin outer layer of BR was formed, as shown in Figure 4.30. At later times, the internal temperature of the drop exceeds the boiling point of the hexane (68 °C) and a vapour is generated internally within the pendant drop, which made the drop expand and then eventually collapse, as the outer skin ruptured. At higher temperatures of 100 and 130 °C, the vapours generated inside the drop would contain higher mole fractions of water, as well as hexane and as a result more rapid evaporation took place compared to the lower temperatures. The evaporation of the emulsion at 130 °C took place in approximately 10 seconds. At 70 °C (lowest temperature) the volume change showed the slowest increase compared to the other temperatures, as the heat transfer rate was lower, given that the boiling point of pure

hexane is 68 °C. In comparison, at 80 °C the heat transfer rate increased resulting in higher evaporation rate and larger rates of volume change.

In Figure 4.31, the black points represent the experiments conducted with 15 g/L CaSt<sub>2</sub> in the aqueous phase. There is no consistent effect shown in results, and it was not clear if the presence of CaSt<sub>2</sub> in the emulsion drop had any effect on the evaporation mechanism. The presence of the solids could promote the nucleation of vapour bubbles inside the emulsion droplet and hence could provide earlier expansion of the droplet. After nucleation of vapour bubbles had occurred, there could be no further effect on the evaporation rate with and without CaSt<sub>2</sub> particles.

From the emulsion pendant drop experiments it could be concluded, the highest the exposed temperature for the emulsion the faster the evaporation rate, and that the 15 g/L CaSt<sub>2</sub> have no effect on the evaporation mechanism.

### 4.6.2. W/O emulsion flash drum evaporation

This section shows the stages of the experimental configuration development for the formation of rubber particles, as achieved in the industrial process flash drum, described in Section 2.1.6. As described in Section 3.7.2, initially, a peristaltic pump was used to transfer the W/O emulsion from the emulsification vessel into the "flash drum" and form the rubber particles. Due to the high viscosity of the emulsion, the highest speed was set on the pump in order to reduce the pulsing effect and have a more constant flow rate at the inlet to the "flash drum". Figure 4.32 shows the "flash drum" with the partially dried rubber particles on the free surface, after the first attempt using the experimental configuration.

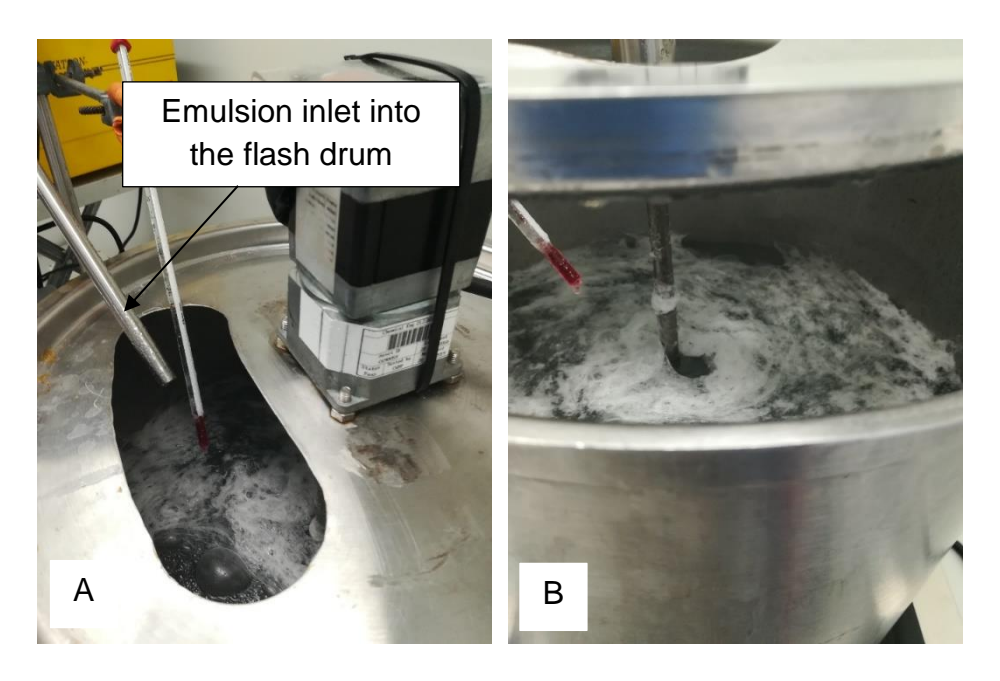


Figure 4.32. (A) Emulsion inlet pipe in the "flash drum", (B) Partially dried BR in the "flash drum" (W/O emulsion: organic phase: 50 g/L BR, aqueous phase: 0.1 M NaOH and 15 g/L CaSt<sub>2</sub>).

It is believed that the time from the emulsion inlet into the "flash drum" (Figure 4.32 A) until hitting the water level and the amount of the heat transfer from the "flash drum" to the emulsion stream were not sufficient for the emulsion to totally evaporate. The emulsion stream was only partially evaporated before hitting the water. The weak agitation in the "flash drum" allowed it to float to the surface of the water, where slow evaporation took place resulting in the formation of sheets of agglomerated particles. The rubber particles agglomerated creating a BR layer (Figure 4.32 B) at the free surface of the water due to the weak agitation in the "flash drum", unlike the industrial process, where individual rubber particles are formed, as shown in 2.1.6.

In order to improve the hexane evaporation, there were two options. The first option was to increase the distance between the emulsion inlet pipe and the water surface, allowing more time for the evaporation to take place. However, by increasing that distance significantly in this experimental rig, the inlet pipe would be above the vessel's lid. This could lead to lower temperature at the area of the emulsion inlet pipe, as well as the emulsion stream would encounter wider range of temperatures during its discharge. This could possibly cause an initial evaporation of the outside of the emulsion stream, similar to the pendant drop experiment, resulting in external BR layer. This BR layer would not allow the correct formation of the rubber particles before

the emulsion stream hit the surface water, as it could act as a shield. In addition to that, there were safety concerns due to the exposed emulsion stream at high temperature outside the "flash drum" lid.

Alternatively, it was chosen to use the volume phase ratio of the emulsion to 1:1 (O:W), as shown in Table 3.15, in order to reduce the amount of organic compound it the mixture. That way, with the same amount of heat it was achieved full evaporation of the hexane, as the water is not required to be evaporated because the BR is insoluble in it. This resulted in separated rubber particles, as more of hexane evaporated before the feed stream hit the water, as shown in Figure 4.33. In this case, the particles were less agglomerated compared to the previous experiment having irregular shapes, similar to the industrial process (Figure 2.5).



Figure 4.33. BR particles after their formation in the "flash drum" (W/O emulsion: organic phase: 50 g/L BR, aqueous phase: 0.1 M NaOH and 15 g/L CaSt<sub>2</sub>).

The emulsion stream in a larger scale industrial process has lower surface area to volume ratio, due to the large diameter of the inlet pipe. Therefore, it may be concluded that solvent evaporation from the emulsion, before hitting the water surface, would be more difficult to achieve, as a very high heat transfer rate would be required. In addition the use 2-3 atm of pressure inside the industrial flash drum (McDonald et al., 2000), means that the boiling point of hexane would be higher, approximately 68-90 °C, which may decrease the driving force for heat transfer. It could be suggested for the emulsion stream to be dispersed with the use of a nozzle to increase the surface area to volume ratio, which would allow better heat transfer and faster evaporation.

The particles created during the experiment with low hexane content had a flat shape, as shown in the Figure 4.34, due to the low intensity mixing in the flash drum. The single stirrer created a vortex at the surface of the water which did not allow the particles to circulate under the water level due to the vortex flow force. As the particles remained on the surface, they were spread resulting in 2D shape.



Figure 4.34. Dried BR particles formulated in the lab.

In order to avoid these flat agglomerated 2D shapes, two stirrers could be introduced to keep the formulated particles under the water level and away from the surface, where they tend to accumulate as they contain a small amount of hexane (less dense). In addition, the presence of two separate stirrers will eliminate the vortex and achieve better mixing.

Finally, the development of a new way to discharge the emulsion into the "flash drum" by using a high pressure transfer, achieved by pressurised nitrogen supply, was designed in the lab as described in Section 3.7.2 and shown in Figure 3.9. The pressurised emulsification vessel was designed to improve control of the discharge flow rate of the emulsion into the "flash drum", as well as to reduce the pulsing effect of the previously used peristaltic pump. These modifications would contribute to improved formation of the desired rubber particles in the laboratory scale equipment. This experimental configuration could then be used to examine the effect of various parameters, such as emulsion stream speed and angle, on the size and shape of the rubber particles, aiming at for a narrower size distribution.

#### Chapter 5

#### 5. Conclusions and future work

This research project was to provide process understanding of the manufacturing halobutyl rubber production, focussing on two aspects. The first aspect was the neutralisation of the by-products of the halogenation with the use of an alkaline aqueous phase and the second was the formation of the rubber particles by emulsion evaporation in the flash drum. The first aim was to study the parameters affecting the interfacial mass transfer of the acids (by-products) from the organic to the aqueous phase in order to be neutralised. Parameters examined were the organic phase viscosity and the calcium stearate concentration, as well as their effect on the size and stability of the W/O Pickering emulsion. In addition, a second aim was to understand the fundamentals on the formation of the rubber particles in the flash drum and how a W/O emulsion evaporates under high temperature. Finally, it was important to develop an experimental configuration that could be used to examine the effect of various parameters on the size and shape of the particles, also aiming to understand where inside the flash drum these particles were formed.

In order to investigate the interfacial mass transfer, a Lewis-cell apparatus was developed in the lab to study the mass transfer rate. Initially, metals (copper and chromium) were used as solutes. However, both metals were proved to be inappropriate. To extract the copper from an organic to an aqueous phase, low pH was needed. The required pH was achieved by the addition of sulfuric acid which resulted in an unwanted reaction with the calcium stearate, producing stearic acid, a fatty acid. The chromium extraction from the aqueous to organic phase could be achieved in alkaline environment, according to the literature. In this study, it was achieved to transfer the chromium back to the aqueous phase, by mixing the organic phase containing the chromium-Aliquat 366 complex with a new aqueous phase. This aqueous phase contained high amount of sodium hydroxide and a small amount of sodium chloride. This could allow us to investigate the interfacial mass transfer in the Lewis-cell. By mixing the two phases, the extraction efficiency from the organic to aqueous phase was 100% without the formation of any solids, even in the case where the calcium stearate was present. However, during the Lewis-cell experiment, the

calcium stearate reacted with the chromium due to the long exposure time, creating calcium stearate-chromium solids that could not be measured in the FAAS. Under these circumstances, it was not be possible to make reliable mass transfer measurements. It was concluded that metal solvent extraction was not an appropriate way to address the problems affecting the interfacial mass transfer of the acid in W/O emulsion in the halobutyl rubber industrial production process.

The alternative way to overcome the above problems was to use a weak acid, acetic acid, for the investigation of the industrial interfacial mass transfer, where an acid (hydrogen chloride or hydrogen bromine) is the solute. Hydrogen bromine could not be used in the lab due to the its harmful properties and the hydrogen chloride had low solubility in the organic solvents.

Acetic acid was used as solute in the Lewis-cell experiments to investigate the effect of organic phase viscosity and calcium stearate concentration, with and without the presence of sodium hydroxide, on the interfacial mass transfer. The viscosity of the organic phase was modified by changing the concentration of the butyl rubber from 0 to 100 g/L. As it was concluded from the Lewis-cell experiments, a slight increase of the butyl rubber content, from 0 to 50 g/L, decreased the mass transfer coefficient sharply. Further increase of the viscosity (50 to 100 g/L) resulted in very low deduction on the overall mass transfer coefficient. As the industrial production process is working at 200 g/L of butyl rubber, a slight decrease on the butyl rubber concentration is not expected to have a large effect on the neutralisation step, as the overall mass transfer coefficient would not change significantly. For future work, the effect of high temperatures on the overall mass transfer coefficient in the Lewis-cell could be examined by the addition of a heating jacket in the cell. This would allow to understand how the temperature affects the interfacial mass transfer.

On the Lewis-cell, several concentrations of calcium stearate were tested without the presence of sodium hydroxide in the aqueous phase. It was found that low concentration of calcium stearate (<5 g/L) promotes the interfacial mass transfer rate. It is believed that the calcium stearate reacts with the acid in the aqueous phase, resulting in high concentration difference of acetic acid between the two phases causing the higher rate. However, this comes in contrast to the fact that the extraction rate could not be increased further in case of distribution coefficient equal to zero, as

happens in this case. Further addition of calcium stearate in the Lewis-cell (concentrations higher than 10 g/L) reduced the mass transfer rate. This happened because the stearic acid, formed by the reaction of calcium stearate with the acetic acid, accumulated on the interface acting as barrier not allowing the transfer of the acetic acid. Following the above observations and in order to mimic better the industrial process, sodium hydroxide was used to achieve alkaline environment in the aqueous phase and reduce the reaction between acetic acid and calcium stearate. It was observed that the addition of sodium hydroxide increased the mass transfer, while resulting in very low formation of stearic acid, as the acid was neutralised by the sodium hydroxide. For future work, several concentrations of sodium hydroxide could be used in the aqueous phase without the presence of calcium stearate on the Lewiscell experiment. This would allow to understand if the chemical reaction promotes the interfacial mass transfer rate even if the distribution coefficient is zero.

In addition to the above, the effect of acidic and alkaline environment, as well as the high temperature, on the calcium stearate were investigated. The reaction between the industrial calcium stearate and acids, acetic acid or hydrogen chloride, was investigated in the lab. It was concluded that the use of excess acid did not increase the amount of reacted calcium stearate above a certain value, at it is believed that the produced stearic acid acts as a barrier to the calcium stearate not allowing to react further. On the other hand, the alkaline environment, up to approximately 14, and the high temperatures, up to 70 °C, have negligible effect of the calcium stearate. In addition, the morphology of the calcium stearate particles was tested using SEM and their shape was plate-like. Finally, the decrease of pH value, increases slightly their size, due to the stearic acid that agglomerates around them, compared to the neutral pH.

As the size and stability of the emulsion during the halobutyl rubber production process is important, the effect of butyl rubber in the organic phase and the addition of calcium stearate were examined. Calcium stearate is used as a stabiliser of the product in a later stage and in this research was investigated as a solid emulsifier in the earlier emulsification stage. Several concentrations of butyl rubber were examined (50 to 150 g/L) with only 5 g/L of calcium stearate and it was concluded that, at low viscosity of the organic phase (50 g/L), the W/O emulsion was not stable after 10 minutes. On the contrary, at concentrations higher than 100 g/L, the emulsion showed very good

stability under gentle stirring. Here, it should be mentioned that, in the industrial process, the concentration of the rubber is above 200 g/L, which seems likely to lead to a highly stable emulsion, particularly when CaSt<sub>2</sub> is added. This stable emulsion would result in sufficient interfacial contact area between the two phases to achieve the neutralisation of the acids.

Furthermore, the emulsification stability of the calcium stearate, the solid emulsifier, was tested. The absence of calcium stearate in the W/O emulsion with 100 g/L butyl rubber resulted in an unstable emulsion after the first 10 minutes with gentle stirring. Concentrations higher than 5 g/L of calcium stearate resulted in a very stable Pickering emulsion through time, with a mean size equal to  $\sim$ 20  $\mu$ m.

The last step of this study was to investigate the emulsion evaporation and the rubber particles formation mechanisms. A preliminary experiment was conducted, where a single W/O emulsion drop exposed at various high temperatures to understand from where the evaporation starts. It was concluded that the higher temperature, the higher heat transfer, resulting in faster evaporation rate. As the continuous phase of the emulsion contained the butyl rubber, it was observed that, at the start of the experiment, the hexane at the outside of the drop was evaporated resulting in a thin layer of BR, which formed an impermeable skin. This layer trapped the vapours inside, and the drop expanded with time until it collapsed. It is possible that, in the single drop emulsion evaporation experiment, the heat transfer rate was low, and it is suggested that higher temperatures should be used. In addition, it was expected the calcium stearate to affect the evaporation mechanism of the emulsion drop, because the solids could act as nucleation points for the evaporation. However, the experimental results showed that the calcium stearate had no obvious effect on the emulsion evaporation mechanism.

Finally, the experimental configuration to mimic the industrial flash drum was built in the lab. During the experiments conducted in this apparatus, incomplete evaporation of the hexane from the emulsion stream took place before it hit the water surface. This, in combination with poor mixing conditions inside the "flash drum", resulted in the formation of agglomerated particles on the surface of the water, as well as presence of unevaporated hexane. Therefore, higher amount of heat transfer was required in laboratory scale to evaporate the emulsion, before hitting the water, and further

modification was necessary in order to achieve it. It was concluded that, in the industrial process, where the diameter of the emulsion stream is larger (lower surface area to volume ratio compared to laboratory one), the total evaporation of the emulsion is more challenging as very high heat rate would be required to achieve total evaporation at the area above the water. This leaves the possibility, that a small amount of hexane is evaporated inside the water. The wide size distribution of the rubber particles in the industry could be the result of the low heat transfer rate and a dispersion of the emulsion entering the flash drum would be required. It was suggested that dispersion of the emulsion stream would achieve higher surface area to volume ratio, and this could result in better heat transfer in the emulsion and more uniform evaporation.

To conclude, the emulsion evaporation and rubber particles formation are a complex mechanism which requires further investigation. The experimental configuration built in the lab could be potentially used for the testing of various parameters, such as heat transfer, emulsion stream inlet angle and diameter, that could affect the emulsion evaporation and the morphology of the rubber particles. For that purpose, improvements to the operation and design of the "flash drum" experimental configuration were proposed and would be implemented in order to be available for future work. The controlled discharge speed of the emulsion through a pressure vessel and the two stirrers in the "flash drum" could help the formation of the desired rubber particles in the lab. Finally, a modification on the existing experimental configuration is proposed, where boiling water could be sprayed above the emulsion, aiming to increase the heat transfer rate and to better mimic the industrial process, as the heat transfer rate plays important role. All the above improvements and suggestions will contribute to achieving the desired rubber particles in laboratory scale and this will allow further investigation of parameters that affect their final size.

#### 6. References

- Adebayo, S.A., Adeyemi, B.J., 2018. Science and Technology Behind Nanoemulsions, 1st ed, Science and Technology Behind Nanoemulsions. InTech, Instabul. https://doi.org/10.5772/intechopen.71147
- Aguilar, M., Cortina, J.L., 2008. Solvent Extraction and Liquid Membranes: Fundamentals and Applications in the New Materials, 1st ed. CRC Press, Boca Raton.
- Albert, C., Beladjine, M., Tsapis, N., Fattal, E., Agnely, F., Huang, N., 2019. Pickering emulsions: Preparation processes, key parameters governing their properties and potential for pharmaceutical applications. J. Control. Release 309, 302–332. https://doi.org/10.1016/j.jconrel.2019.07.003
- Alliod, O., Valour, J.P., Urbaniak, S., Fessi, H., Dupin, D., Charcosset, C., 2018. Preparation of oil-in-water nanoemulsions at large-scale using premix membrane emulsification and Shirasu Porous Glass (SPG) membranes. Colloids Surfaces A Physicochem. Eng. Asp. 557, 76–84. https://doi.org/10.1016/j.colsurfa.2018.04.045
- Alvarado, V., Wang, X., Moradi, M., 2011. Stability proxies for water-in-oil emulsions and implications in aqueous-based enhanced oil recovery. Energies 4, 1058–1086. https://doi.org/10.3390/en407105
- Antonov, D. V, Piskunov, M. V, Strizhak, P.A., 2019. International Journal of Thermal Sciences Breakup and explosion of droplets of two immiscible fluids and emulsions. Int. J. Therm. Sci. 142, 30–41. https://doi.org/10.1016/j.ijthermalsci.2019.04.011
- Arlanxeo, 2017. Tire & Specialty Rubbers Supplying Butyl Rubber Globally for Growing Industries [WWW Document]. Perform. Elastomers. URL http://tsr.arlanxeo.com/fileadmin/user\_upload/ARLANXEO\_X\_Butyl\_R\_\_Rubber \_Brochure.pdf (accessed 5.20.20).
- Arnaut, L., Formosinho, S., Burrows, H., 2006. Chemical Kinetics From Molecular Structure to Chemical Reactivity, 1st ed. Elsevier Science, Coimbra. https://doi.org/10.1016/B978-0-444-52186-6.X5000-7
- Aryal, S., 2018. High Performance Liquid Chromatography (HPLC) [WWW Document]. Online Microbiol. Notes. URL https://microbenotes.com/high-performance-liquid-chromatography-hplc/ (accessed 12.3.19).
- Aveyard, R., Binks, B.P., Clint, J.H., 2003. Emulsions stabilised solely by colloidal particles. Adv. Colloid Interface Sci. 100, 503–546. https://doi.org/10.1016/S0001-8686(02)00069-6
- Bagalkot, N., Hamouda, A.A., Isdahl, O.M., 2018. Dynamic interfacial tension measurement method using axisymmetric drop shape analysis. MethodsX 5, 676–683. https://doi.org/10.1016/j.mex.2018.06.012
- Bai, L., Huan, S., Gu, J., McClements, D.J., 2016. Fabrication of oil-in-water

- nanoemulsions by dual-channel microfluidization using natural emulsifiers: Saponins, phospholipids, proteins, and polysaccharides. Food Hydrocoll. 61, 703–711. https://doi.org/10.1016/j.foodhyd.2016.06.035
- Bandyopadhyay, M., Datta, S., Sanya, S.K., 1996. Correlation of mass transfer coefficients for tellurium(IV) extraction with instantaneous reaction in a modified Lewis cell. Hydrometallurgy 42, 115–123. https://doi.org/10.1016/0304-386X(95)00070-W
- Barker, G., Lawn, F., Barabash, M.J., 1977. Water-oil emulsions and method of preparing same. US4104403A.
- BASF SE, 2015. BASF History We create chemistry 1865 2015 [WWW Document]. BASF Gr. URL https://www.basf.com/global/images/about-us/history/BASF\_Chronik\_Gesamt\_en.pdf (accessed 12.2.19).
- Behrend, O., Ax, K., Schubert, H., 2000. Influence of continuous phase viscosity on emulsification by ultrasound. Ultrason. Sonochem. 7, 77–85. https://doi.org/10.1016/S1350-4177(99)00029-2
- Belkhouche, N.-E., Didi, M.A., Villemin, D., 2005. Separation of Nickel and Copper by Solvent Extraction Using Di-2 Ethylhexylphosphoric Acid-Based Synergistic Mixture . Solvent Extr. Ion Exch. 23, 677–693. https://doi.org/10.1081/SEI-200066290
- Berton-Carabin, C., Schroën, K., 2019. Towards new food emulsions: designing the interface and beyond. Curr. Opin. Food Sci. 27, 74–81. https://doi.org/10.1016/j.cofs.2019.06.006
- Berton-Carabin, C.C., Schroën, K., 2015. Pickering Emulsions for Food Applications: Background, Trends, and Challenges. Annu. Rev. Food Sci. Technol. 6, 263–297. https://doi.org/10.1146/annurev-food-081114-110822
- Binks, B.P., 1998. Modern Aspects of Emulsion Science, 1st ed. The Royal Society of Chemistry, Cambridge. https://doi.org/0-85404-439-6
- Binks, B.P., Fletcher, P.D.I., Holt, B.L., Beaussoubre, P., Wong, K., 2010. Selective retardation of perfume oil evaporation from oil-in-water emulsions stabilized by either surfactant or nanoparticles. Langmuir 26, 18024–18030. https://doi.org/10.1021/la103700g
- Binks, B.P., Horozov, T.S., 2006. Colloidal particles at liquid interfaces. An Introduction, 1st ed, Cambridge University Press. Cambridge. https://doi.org/10.1017/CBO9780511536670.007
- Cao, Y., Chen, Y., Liu, N., Lin, X., Feng, L., Wei, Y., 2014. Mussel-inspired chemistry and Stöber method for highly stabilized water-in-oil emulsions separation. J. Mater. Chem. A 2, 20439–20443. https://doi.org/10.1039/c4ta05075d
- Cha, Y., Shi, X., Wu, F., Zou, H., Chang, C., Guo, Y., Yuan, M., Yu, C., 2019. Improving the stability of oil-in-water emulsions by using mussel myofibrillar proteins and lecithin as emulsifiers and high-pressure homogenization. J. Food Eng. 258, 1–8. https://doi.org/10.1016/j.jfoodeng.2019.04.009

- Chang, S.H., 2016. Types of bulk liquid membrane and its membrane resistance in heavy metal removal and recovery from wastewater. Desalin. Water Treat. 57, 19785–19793. https://doi.org/10.1080/19443994.2015.1102772
- Cheremisinoff, N.P., 2000. Handbook of Chemical Processing Equipment, 1st ed. Butterworth-Heinemann, Woburn. https://doi.org/https://doi.org/10.1016/B978-0-7506-7126-2.X5000-2
- Chevalier, Y., Bolzinger, M.A., 2013. Emulsions stabilized with solid nanoparticles: Pickering emulsions. Colloids Surfaces A Physicochem. Eng. Asp. 439, 23–34. https://doi.org/10.1016/j.colsurfa.2013.02.054
- Coneac, G., Vlaia, V., Olariu, I., Muţ, A.M., Anghel, D.F., Ilie, C., Popoiu, C., Lupuleasa, D., Vlaia, L., 2015. Development and Evaluation of New Microemulsion-Based Hydrogel Formulations for Topical Delivery of Fluconazole. AAPS PharmSciTech 16, 889–904. https://doi.org/10.1208/s12249-014-0275-8
- De Folter, J.W.J., Hutter, E.M., Castillo, S.I.R., Klop, K.E., Philipse, A.P., Kegel, W.K., 2014. Particle shape anisotropy in pickering emulsions: Cubes and peanuts. Langmuir 30, 955–964. https://doi.org/10.1021/la402427q
- Deferm, C., Voord, V. de, E, M., Luyten, J., Oosterhof, H., Fransaer, J., Binnemans, K., 2016. Purification of indium by solvent extraction with undiluted ionic liquids. Green Chem. 18, 4116–4127. https://doi.org/10.1039/C6GC00586A
- Devi, N., 2016. Solvent extraction and separation of copper from base metals using bifunctional ionic liquid from sulfate medium 26, 874–881. https://doi.org/10.1016/S1003-6326(16)64179-1
- Dickinson, E., 2010. Food emulsions and foams: Stabilization by particles. Curr. Opin. Colloid Interface Sci. 15, 40–49. https://doi.org/10.1016/j.cocis.2009.11.001
- Dickinson, E., Pawlowsky, K., 1996. Effect of High-Pressure Treatment of Protein on the Rheology of Flocculated Emulsions Containing Protein and Polysaccharide. J. Agric. Food Chem. 44, 2992–3000. https://doi.org/10.1021/jf960188z
- dos Santos, A.B., Kohlmeier, K.A., Rocha, M.E., Barreto, G.E., Barreto, J.A., de Souza, A.C.A., Bezerra, M.A., 2018. Hair in Parkinson's disease patients exhibits differences in Calcium, Iron and Zinc concentrations measured by flame atomic absorption spectrometry FAAS. J. Trace Elem. Med. Biol. 47, 134–139. https://doi.org/10.1016/j.jtemb.2018.02.003
- Dragosavac, M.M., Holdich, R.G., Vladisavljević, G.T., Sovilj, M.N., 2012. Stirred cell membrane emulsification for multiple emulsions containing unrefined pumpkin seed oil with uniform droplet size. J. Memb. Sci. 392–393, 122–129. https://doi.org/10.1016/j.memsci.2011.12.009
- Dymond, J.H., O/ye, H.A., 1994. Viscosity of Selected Liquid n-Alkanes. J. Phys. Chem. Ref. Data 23, 41–53. https://doi.org/10.1063/1.555943
- El-Nadi, Y.A., 2017. Solvent Extraction and Its Applications on Ore Processing and

- Recovery of Metals: Classical Approach. Sep. Purif. Rev. 46, 195–215. https://doi.org/10.1080/15422119.2016.1240085
- Evans, M.S., 2001. Tyre Compounding for Improved Performance, 1st ed. Smithers Rapra Press, Hessian.
- ExxonMobil, 2017. Exxon TM chlorobutyl rubber compounding and applications manual [WWW Document]. URL https://www.exxonmobilchemical.com/~/media/chemicals/kl-media-assets/2017/12/13/00/01/chlorobutyl\_rubber\_compounding\_and\_applications\_m anual\_enpdf.pdf (accessed 2.5.20).
- Ferreira, A., Ferreira, C., Teixeira, J.A., Rocha, F., 2010. Temperature and solid properties effects on gas-liquid mass transfer. Chem. Eng. J. 162, 743–752. https://doi.org/10.1016/j.cej.2010.05.064
- Fontàs, C., Salvadó, V., Hidalgo, M., 1999. Solvent extraction of Pt(IV) by Aliquat 336 and its application to a solid supported liquid membrane system. Solvent Extr. Ion Exch. 17, 149–162. https://doi.org/10.1080/07360299908934605
- Foog, P.G.T., Gerrard, W., Clever, H.L., 1990. Hydrogen Halides in Non-Aqueous Solvents, International Union of Pure and Applied Chemistry. Pergamon Press, Ontario.
- Frelichowska, J., Bolzinger, M.A., Pelletier, J., Valour, J.P., Chevalier, Y., 2009. Topical delivery of lipophilic drugs from o/w Pickering emulsions. Int. J. Pharm. 371, 56–63. https://doi.org/10.1016/j.ijpharm.2008.12.017
- French, D.J., Brown, A.T., Schofield, A.B., Fowler, J., Taylor, P., Clegg, P.S., 2016. The secret life of Pickering emulsions: particle exchange revealed using two colours of particle. Sci. Rep. 6, 31401. https://doi.org/10.1038/srep31401
- French, D.J., Taylor, P., Fowler, J., Clegg, P.S., 2015. Making and breaking bridges in a Pickering emulsion. J. Colloid Interface Sci. 441, 30–38. https://doi.org/10.1016/j.jcis.2014.11.032
- Fusco, J.V., Gardner, I.J., Hous, P., 1990. Improved halogenated butyl rubber. Eur. Pat. Appl. 89310227.7.
- Garti, N., Katz, M., 1985. Adsorption and Interfacial Tension in Emulsion. J. Dispers. Sci. Technol. 6, 149–158. https://doi.org/10.1080/01932698508943940
- Gupta, A., Eral, H.B., Hatton, T.A., Doyle, P.S., 2016. Nanoemulsions: formation, properties and applications. Soft Matter 12, 2826–2841. https://doi.org/10.1039/C5SM02958A
- Hanna, G.J., Noble, R.D., 1985. Measurement of liquid-liquid interfacial kinetics. Chem. Rev. 85, 583–598. https://doi.org/10.1021/cr00070a004
- Happ, M., Duffy, J., Wilson, G., Pask, S.D., Buding, H., Ostrowicki, A., 2012. Rubber, 8. Synthesis by Polymer Modification, in: Ullmann's Encyclopedia of Industrial Chemistry. WILEY-VCH Verlag GmbH & Co. KGaA. https://doi.org/10.1002/14356007.o23\_o05

- Harmsen, J., 2019. Industrial Process Scale-up: A Practical Innovation Guide from Idea to Commercial Implementation, 2nd ed. Elsevier, Amsterdam.
- Horozov, T.S., Aveyard, R., Clint, J.H., Binks, B.P., 2003. Order-disorder transition in monolayers of modified monodisperse silica particles at the octane-water interface. Langmuir 19, 2822–2829. https://doi.org/10.1021/la020858x
- Hsu, C.S., Robinson, P.R., 2019. Petroleum Science and Technology, 1st ed. Springer International Publishing. https://doi.org/10.1007/978-3-030-16275-7
- Huang, Z., Ye, C., Li, L., Zhang, X., Qiu, T., 2016. Measurement and Correlation of the Mass Transfer Coefficient for a Liquid-Liquid System With High. Brazilian J. Chem. Eng. 33, 897–906.
- Hunter, T.N., Pugh, R.J., Franks, G. V., Jameson, G.J., 2008. The role of particles in stabilising foams and emulsions. Adv. Colloid Interface Sci. 137, 57–81. https://doi.org/10.1016/j.cis.2007.07.007
- Hussein, M.A., Mohammed, A.A., Atiya, M.A., 2019. Application of emulsion and Pickering emulsion liquid membrane technique for wastewater treatment: an overview. Environ. Sci. Pollut. Res. 26, 36184–36204. https://doi.org/10.1007/s11356-019-06652-3
- Hwisa, N.T., Katakam, P., Chandu, B.R., Adiki, S.K., 2013. Solvent Evaporation Techniques as Promising Advancement in Microencapsulation. https://doi.org/10.14259/bmc.v1i1.29
- Instruments Malvern Ltd, 2007. Mastersizer 2000 User Manual.
- Jain, S.K., Soni, V., 2011. Bentley's Textbook of Pharmaceutics, 1st ed, Journal of Chemical Information and Modeling. Elsevier Health Sciences, New York.
- Javanshir, S., Abdollahy, M., Abolghasemi, H., Khodadadi Darban, A., 2012. The effect of kinetics parameters on gold extraction by lewis cell: Comparison between synthetic and leach solution. Iran. J. Chem. Chem. Eng. 31, 59–67.
- Jirgensons, B., Straumanis, M.E., 1962. A Short Textbook of Colloid Chemistry, 2nd ed. Elsevier Ltd, New York. https://doi.org/10.1016/C2013-0-05285-1
- Jorin, 2006. Core Technology [WWW Document]. Jorin Ltd. URL http://www.jorin.co.uk/technology/flow-cell/ (accessed 1.25.20).
- Joshi, D.R., Adhikari, N., 2019. An Overview on Common Organic Solvents and Their Toxicity. J. Pharm. Res. Int. 1–18. https://doi.org/10.9734/jpri/2019/v28i330203
- Kaplanow, I., Goerzgen, F., Merz, J., Schembecker, G., 2019. Mass Transfer of Proteins in Aqueous Two-Phase Systems. Sci. Rep. 9, 1–6. https://doi.org/10.1038/s41598-019-39797-9
- Kargar, M., Fayazmanesh, K., Alavi, M., Spyropoulos, F., Norton, I.T., 2012. Investigation into the potential ability of Pickering emulsions (food-grade particles) to enhance the oxidative stability of oil-in-water emulsions. J. Colloid Interface Sci. 366, 209–215. https://doi.org/10.1016/j.jcis.2011.09.073

- Kasaie, M., Bahmanyar, H., Moosavian, M.A., 2017. A kinetic study on solvent extraction of copper from sulfate solution with Cupromex-3302 using Lewis cell. J. Environ. Chem. Eng. 5, 3044–3050. https://doi.org/10.1016/j.jece.2017.06.013
- Knowlton, J., Pearce, S., 1993. Handbook of Cosmetics Science & Technology, 1st ed. Elsevier Advanced Technology, Oxford.
- Kowalski, R.C., Davis, W.M., Newman, N.F., Foroulis, Z.A., Baldwin, F.P., 1987. Process For The Manufacture of Haloganated Polymers. US465083 2A.
- Kowalski, R.C., Davis, W.M., Newman, N.F., Foroulis, Z.A., Baldwin, F.P., 1986. Extruction process for preparing improved brominated butyl rubber. US4563506.
- Krasodomska, O., Jungnickel, C., 2015. Viability of fruit seed oil O/W emulsions in personal care products. Colloids Surfaces A Physicochem. Eng. Asp. 481, 468–475. https://doi.org/10.1016/j.colsurfa.2015.06.022
- Kresge, E., Wang, H.-C., 2000. Butyl Rubber, in: Kirk-Othmer Encyclopedia of Chemical Technology. John Wiley & Sons, Inc. https://doi.org/10.1002/0471238961.0221202511180519.a01
- Kumar, R., Shah, D.J., Tiwari, K.K., 2013. Separation of Copper and Nickel by Solvent Extraction Using LIX 664N 2013, 315–318.
- Lewis, W.K., Whitman, W.G., 1924. Principles of Gas Absorption. Ind. Eng. Chem. 16, 1215–1220. https://doi.org/10.1021/ie50180a002
- Low, L.E., Siva, S.P., Ho, Y.K., Chan, E.S., Tey, B.T., 2020. Recent advances of characterization techniques for the formation, physical properties and stability of Pickering emulsion. Adv. Colloid Interface Sci. 277, 102117. https://doi.org/10.1016/j.cis.2020.102117
- Lozano-Sánchez, J., Borrás-Linares, I., Sass-Kiss, A., Segura-Carretero, A., 2018. Chromatographic Technique: High-Performance Liquid Chromatography (HPLC), in: Modern Techniques for Food Authentication. Academic Press, Granada, pp. 459–526. https://doi.org/10.1016/B978-0-12-814264-6.00013-X
- Lucassen-Reynders, E.H., Kuijpers, K.A., 1992. The role of interfacial properties in emulsification. Colloids and Surfaces 65, 175–184. https://doi.org/10.1016/0166-6622(92)80272-4
- Maestro, A., Rio, E., Drenckhan, W., Langevin, D., Salonen, A., 2014. Foams stabilised by mixtures of nanoparticles and oppositely charged surfactants: Relationship between bubble shrinkage and foam coarsening. Soft Matter 10, 6975–6983. https://doi.org/10.1039/c4sm00047a
- Mark, J.E., Erman, B., Roland, C.M., 2013. The Science and Technology of Rubber, 4th ed, Journal of Chemical Information and Modeling. Elsevier Ltd, Waltham. https://doi.org/10.1017/CBO9781107415324.004
- McDonald, M.F., Lond, R.L., Thomas, C.J., 2000. On-line control of a chemical process plant. US6072576. https://doi.org/10.1074/JBC.274.42.30033.(51)

- McMullen, R.L., Gorcea, M., Chen, S., 2014. Emulsions and their Characterization by Texture Profile Analysis, in: Dayan, N. (Ed.), Apply Topically: A Practical Guide to Formulating Topical Applications. Allured Publishing, pp. 131–154.
- Melgarejo-Torres, R., Torres-Martínez, D., Castillo-Araiza, C.O., Arriaga-Juárez, C., Gutiérrez-Rojas, M., Esponda-Aguilar, P., Aroca, G., Lye, G.J., Huerta-Ochoa, S., 2012. Mass transfer coefficient determination in three biphasic systems (water-ionic liquid) using a modified Lewis cell. Chem. Eng. J. 181–182, 702–707. https://doi.org/10.1016/j.cej.2011.12.060
- Mhaske, A., Dhadke, P., 2002. Extraction of tin(II) with Cyanex 925 in toluene-interaction coefficient between SnCl3- and H+. Solvent Extr. Ion Exch. 20, 127–137. https://doi.org/10.1081/SEI-100108829
- Miyabe, K., Isogai, R., 2011. Estimation of molecular diffusivity in liquid phase systems by the Wilke-Chang equation. J. Chromatogr. A 1218, 6639–6645. https://doi.org/10.1016/j.chroma.2011.07.018
- Monakov, Y.B., Zaikov, G.E., 2006. Molecular and High Molecular: Theory and Practise, 1st ed. Nova Science Publishers, Inc., New York.
- Nayl, A.A., Aly, H.F., 2015. Solvent extraction of V(V) and Cr(III) from acidic leach liquors of ilmenite using Aliquat 336. Trans. Nonferrous Met. Soc. China (English Ed. 25, 4183–4191. https://doi.org/10.1016/S1003-6326(15)64021-3
- NIIR Board of Consultants and Engineers, 2016. The Complete Book on Rubber Processing and Compounding Technology (with Machinery Details), 2nd ed. Asia Pacific Business Press Inc., Delhi.
- Niskanen, I., Suopajärvi, T., Liimatainen, H., Fabritius, T., Heikkilä, R., Thungström, G., 2019. Determining the complex refractive index of cellulose nanocrystals by combination of Beer-Lambert and immersion matching methods. J. Quant. Spectrosc. Radiat. Transf. 235, 1–6. https://doi.org/10.1016/j.jqsrt.2019.06.023
- Pandolfe, W.D., 1981. Effect of dispersed and continuous phase viscosity on droplet size of emulsions generated by homogenization. J. Dispers. Sci. Technol. 2, 459–474. https://doi.org/10.1080/01932698108943924
- Parent, J.S., Thom, D.J., White, G.D.F., Whitney, R.A., Hopkins, W.D., 2001. Thermal stability of brominated poly(isobutylene-co-isoprene). J. Polym. Sci. Part A Polym. Chem. 39, 2019–2026. https://doi.org/10.1002/pola.1177
- Paulo, F., Santos, L., 2018. Industrial Crops & Products Double emulsion solvent evaporation approach as a novel eugenol delivery system Optimization by response surface methodology. Ind. Crop. Prod. 126, 287–301. https://doi.org/10.1016/j.indcrop.2018.10.027
- Pickering, S.U., 1907. Emulsions. J. Chem. Soc. 91, 2001–2021.
- Potts, P.J., 1987. Atomic absorption spectrometry, in: A Handbook of Silicate Rock Analysis. Springer US, Boston, MA, pp. 106–152. https://doi.org/10.1007/978-1-4615-3270-5 4
- Qi, F., Wu, J., Sun, G., Nan, F., Ngai, T., Ma, G., 2014. Systematic studies of

- Pickering emulsions stabilized by uniform-sized PLGA particles: preparation and stabilization mechanism. J. Mater. Chem. B 2, 7605–7611. https://doi.org/10.1039/C4TB01165A
- Rai, D., Sass, B.M., Moore, D.A., 1987. Chromium(III) hydrolysis constants and solubility of chromium(III) hydroxide. Inorg. Chem. 26, 345–349. https://doi.org/10.1021/ic00250a002
- Rayner, M., Dejmek, P., 2015. Engineering Aspecs of Food Emulsification and Homogenizations, First. ed. CRC Press Taylor & Francis Group.
- Rayner, M., Marku, D., Eriksson, M., Sjöö, M., Dejmek, P., Wahlgren, M., 2014. Biomass-based particles for the formulation of Pickering type emulsions in food and topical applications. Colloids Surfaces A Physicochem. Eng. Asp. 458, 48–62. https://doi.org/10.1016/j.colsurfa.2014.03.053
- Rayner, M., Timgren, A., Sjöö, M., Dejmek, P., 2012. Quinoa starch granules: A candidate for stabilising food-grade Pickering emulsions. J. Sci. Food Agric. 92, 1841–1847. https://doi.org/10.1002/jsfa.5610
- Reed, K.M., 2011. Wettability of Particles in Realation to Particle Stabilised Foams and Emulsions. University of Hull.
- Reese, K.M., 1988. Butyl rubber enters 51st year since invention. Chem. Eng. News 66, 70. https://doi.org/10.1021/cen-v066n007.p070
- Reffas, H., Benabdallah, T., Hadi Youcef, M., Ilikti, H., 2009. Extraction of Copper (II) from Sulphate Aqueous Medium with N, N'-bis (2-hydroxy-Polydentate Schiff Base in Aqueous Two-phase Micellar of Non-Ionic Surfactant. Tenside Surfactants Deterg. 46, 361–367.
- Research Adroit Market, 2019. Global Butyl Rubber Market Size 2018, By Type (Regular Butyl rubber, Halobutyl Rubber) By Application (Hoses, Tire & Tire Products, Seal, O-rings & Gaskets, Adhesives & Sealants, others), By End-User (Industrial, Automotive & Transportation, Healthcare & [WWW Document]. Adroit Mark. Res. URL https://www.adroitmarketresearch.com/industry-reports/butyl-rubber-market (accessed 3.2.20).
- Ritcey, G.M., 2006. Solvent extraction in hydrometallurgy: Present and future. Tsinghua Sci. Technol. 11, 137–152. https://doi.org/10.1016/S1007-0214(06)70168-7
- Roberts, E.A., 1952. The Rubber Industry: A History of American Achievement. Anal. J. 8, 77–81.
- Rodgers, B., 2015. Rubber compounding: Chemistry and applications, 2nd ed. CRC Press, New York. https://doi.org/https://doi.org/10.1201/b18931
- Rydberg, J., Musikas, C., Cox, M., Choppin, G.R., 2004. Solvent Extraction Principles and Practice, Revised and Expanded, 2nd ed. CRC Press, Boca Raton, USA. https://doi.org/10.1201/9780203021460
- Safari, H., Adili, R., Holinstat, M., Eniola-adefeso, O., 2018. Modified two-step emulsion solvent evaporation technique for fabricating biodegradable rod-

- shaped particles in the submicron size range. J. Colloid Interface Sci. 518, 174–183. https://doi.org/10.1016/j.jcis.2018.02.030
- Saien, J., Daliri, S., 2012. Mass Transfer from Single Drops and the Influence of Temperature. Ind. Eng. Chem. Res. 51, 7364–7372. https://doi.org/10.1021/ie300649d
- Sakamoto, K., Lochhead, R.Y., Maibach, H.I., Yamashita, Y., 2017. Cosmetic Science and Technology. Theoritical Principles and Applications, 1st ed. Elsevier Science Publishing Co Inc, New York. https://doi.org/10.1016/B978-1-85617-943-0.10041-3
- San-Miguel, A., Behrens, S.H., 2012. Influence of nanoscale particle roughness on the stability of pickering emulsions. Langmuir 28, 12038–12043. https://doi.org/10.1021/la302224v
- Schlesinger, M.E., Sole, K.C., Davenport, W.G., 2011. Extractive Metallurgy of Copper, 5th ed. Elsevier, Oxford. https://doi.org/10.1016/C2010-0-64841-3
- Schramm, L.L., 2005. Emulsions, Foams, and Suspensions, 1st ed. Wiley, Weinheim. https://doi.org/10.1002/3527606750
- Shan, Y., Yu, C., Yang, J., Dong, Q., Fan, X., Qiu, J., 2015. Thermodynamically Stable Pickering Emulsion Configured with Carbon-Nanotube-Bridged Nanosheet-Shaped Layered Double Hydroxide for Selective Oxidation of Benzyl Alcohol. ACS Appl. Mater. Interfaces 7, 12203–12209. https://doi.org/10.1021/acsami.5b02595
- Sharifzadeh, E., Salami-Kalajahi, M., Salami Hosseini, M., Razavi Aghjeh, M.K., Najafi, S., Jannati, R., Hatef, Z., 2017. Defining the characteristics of spherical Janus particles by investigating the behavior of their corresponding particles at the oil/water interface in a Pickering emulsion. J. Dispers. Sci. Technol. 38, 985–991. https://doi.org/10.1080/01932691.2016.1216861
- Sharma, B.K., 1991. Industrial Chemistry Including Chemical Engineering, 16st ed. GOEL Publishing House, Meerut.
- Shirani, M., Salari, F., Habibollahi, S., Akbari, A., 2020. Needle hub in-syringe solid phase extraction based a novel functionalized biopolyamide for simultaneous green separation/preconcentration and determination of cobalt, nickel, and chromium (III) in food and environmental samples with micro sampling flame a. Microchem. J. 152, 104340. https://doi.org/10.1016/j.microc.2019.104340
- Sikora, E., 2019. Cosmetic emulsions, 1st ed, Journal of the Japan Society of Colour Material. Politechnika Krakowska, Krakow.
- Simovic, S., Prestidge, C.A., 2007. Nanoparticle layers controlling drug release from emulsions. Eur. J. Pharm. Biopharm. 67, 39–47. https://doi.org/10.1016/j.ejpb.2007.01.011
- Stavert, D.M., Archuleta, D.C., Behr, M.J., Lehnert, B.E., 1991. Relative acute toxicities of hydrogen fluoride, hydrogen chloride, and hydrogen bromide in nose- and pseudo-mouth-breathing rats. Fundam. Appl. Toxic. 16, 636–655.

- https://doi.org/10.1016/0272-0590(91)90152-T
- Stevens, G.W., Perera, J.M., 1997. Kinetics of solvent extraction processes. Miner. Process. Extr. Metall. Rev. 17, 205–226. https://doi.org/10.1080/08827509708914148
- Strizhak, P.A., Piskunov, M. V, Volkov, R.S., Legros, J.C., 2017. Evaporation, boiling and explosive breakup of oil water emulsion drops under intense radiant heating. Chem. Eng. Res. Des. 127, 72–80. https://doi.org/10.1016/j.cherd.2017.09.008
- Tadros, T.F., 2013. Emulsion Formation and Stability, 1st ed. John Wiley & Sons, London.
- Taherpour, A., Hashemi, A., 2018. A novel formulation of the pickering emulsion stabilized with silica nanoparticles and its thermal resistance at high temperatures. J. Dispers. Sci. Technol. 39, 1710–1720. https://doi.org/10.1080/01932691.2018.1461645
- Tesch, S., Schubert, H., 2002. Influence of increasing viscosity of the aqueous phase on the short-term stability of protein stabilized emulsions. J. Food Eng. 52, 305–312. https://doi.org/10.1016/S0260-8774(01)00120-0
- Timgren, A., Rayner, M., Dejmek, P., Marku, D., Sjöö, M., 2013. Emulsion stabilizing capacity of intact starch granules modified by heat treatment or octenyl succinic anhydride. Food Sci. Nutr. 1, 157–71. https://doi.org/10.1002/fsn3.17
- Vitiello, R., Tesser, R., Turco, R., Santacesaria, E., Compagnone, G., Di Serio, M., 2017. A critical review on analytical methods and characterization of butyl and bromobutyl rubber. Int. J. Polym. Anal. Charact. 22, 348–360. https://doi.org/10.1080/1023666X.2017.1297887
- Volkon, A.G., 2001. Liquid interfaces in chemical, biological, and pharmaceutical applications, 1st ed. Marcel Dekker, INC, New York Basel.
- Wellens, S., Binnemans, K., 2012. Green Chemistry An environmentally friendlier approach to hydrometallurgy: highly selective separation of cobalt from nickel by solvent extraction with undiluted phosphonium ionic liquids. Green Chem. 14, 1657–1665. https://doi.org/10.1039/c2gc35246j
- Wilke, C.R., Chang, P., 1955. Correlation of diffusion coefficients in dilute solutions. AIChE J. 1, 264–270. https://doi.org/10.1002/aic.690010222
- Wionczyk, B., Apostoluk, W., 2005. Equilibria of extraction of chromium (III) from alkaline solutions with trioctylmethylammonium chloride (Aliquat 336). Hydrometallurgy 78, 116–128. https://doi.org/10.1016/j.hydromet.2005.03.007
- Wionczyk, B., Apostoluk, W., 2004. Solvent extraction of Cr(III) from alkaline media with quaternary ammonium compounds. Part II. Hydrometallurgy 72, 195–203. https://doi.org/10.1016/S0304-386X(03)00139-7
- Wionczyk, B., Cierpiszewski, R., Mól, A., Prochaska, K., 2011. Studies on the kinetics and equilibrium of the solvent extraction of chromium (III) from alkaline aqueous solutions of different composition in the system with Aliquat 336. J.

- Hazard. Mater. 198, 257–268. https://doi.org/10.1016/j.jhazmat.2011.10.038
- Wong, S.F., Lim, J.S., Dol, S.S., 2015. Crude oil emulsion: A review on formation, classification and stability of water-in-oil emulsions. J. Pet. Sci. Eng. 135, 498–504. https://doi.org/10.1016/j.petrol.2015.10.006
- Wu, J., Ma, G.H., 2016. Recent Studies of Pickering Emulsions: Particles Make the Difference. Small J. 12, 4633–4648. https://doi.org/10.1002/smll.201600877
- Wu, L., Liao, Z., Liu, M., Yin, X., Li, X., Wang, M., Lu, X., Lv, N., Singh, V., He, Z., Li, H., Zhang, J., 2016. Fabrication of non-spherical Pickering emulsion droplets by cyclodextrins mediated molecular self-assembly. Colloids Surfaces A Physicochem. Eng. Asp. 490, 163–172. https://doi.org/10.1016/j.colsurfa.2015.11.036
- Xie, P., Wang, K., Luo, G., 2018. Calcium Stearate as an Acid Scavenger for Synthesizing High Concentrations of Bromobutyl Rubber in a Microreactor System. Ind. Eng. Chem. Res. 57, 3898–3907. https://doi.org/10.1021/acs.iecr.8b00285
- Xu, Q.Y., Nakajima, M., Binks, B.P., 2005. Preparation of particle-stabilized oil-in-water emulsions with the microchannel emulsification method. Colloids Surfaces A Physicochem. Eng. Asp. 262, 94–100. https://doi.org/10.1016/j.colsurfa.2005.04.019
- Zhang, G., Chen, D., Zhao, W., Zhao, H., Wang, L., Wang, W., 2016. A novel D2EHPA-based synergistic extraction system for the recovery of chromium (III ). Chem. Eng. J. 302, 233–238. https://doi.org/10.1016/j.cej.2016.05.063
- Zhang, J., Xu, S., Li, W., 2012. High shear mixers: A review of typical applications and studies on power draw, flow pattern, energy dissipation and transfer properties. Chem. Eng. Process. Process Intensif. 57–58, 25–41. https://doi.org/10.1016/j.cep.2012.04.004
- Zhao, Y., Zhang, X., Sanjeevi, J., Yang, Q., 2016. Hydroformylation of 1-octene in Pickering emulsion constructed by amphiphilic mesoporous silica nanoparticles. J. Catal. 334, 52–59. https://doi.org/10.1016/j.jcat.2015.11.011
- Zheng, Y., Zheng, M., Ma, Z., Xin, B., Ruihua, G., Xu, X., 2015. Sugar Fatty Acid Esters, in: Ahmad, M.U., Xu, X. (Eds.), Polar Lipids Biology, Chemistry and Technology. Academic Press and AOCS Pres, Urbana, p. 568.
- Zhongqi, R., Weidong, Z., Huilin, M., YiMing, L., Yuan, D., 2007. Extraction equilibria of copper(II) with D2EHPA in kerosene from aqueous solutions in acetate buffer media. J. Chem. Eng. Data 52, 438–441. https://doi.org/10.1021/je0603700

### **Appendices**

In this section, the analytical techniques, alongside with fundamental theory, that used in the research are presented, as well as their calibration method, which took place prior to every analysis of the experimental samples. In addition, the equations used for the error between the experimental repeats are presented. Finally, the measurements of viscosity, interfacial tension and particle size are discussed.

## A 1. UV-Vis spectrophotometer

The UV-Vis spectrophotometer was used for the determination of the concertation of copper in water. This analytical technique is based on the absorption of specific wavelengths of UV or visible light by groups within a molecule, which are known as chromophores. The relationship between the absorbance and the concentration of these chemical species if given by the Beer-Lambert law as shown in Equation A.1 (Niskanen et al., 2019). The instrument used was the Spectrophotometer PerkinElmer Lambda 35.

$$Abs = log_{10} {l_0/I} = (\lambda)CL$$
 (A.1)

Where: *Abs* is the absorbance.

 $I_0$  and I are the intensities of the light before and after the sample.

 $\in$  is the molar absorption coefficient at wavelength  $\lambda$ .

C is the solute molar concentration.

*L* is the optical beam length in the spectrophotometer.

# A 1.1. Calibration of UV-Vis spectrophotometer for copper

A copper standard metal solution (copper (II) nitrate 1000 ppm, HNO<sub>3</sub> 1M), supplied by Sigma Aldrich, was used to prepare the 6 calibration solutions. The concentrations of copper, distilled water and ammonia that used to prepare the 6 calibration solutions are shown in Table A.1. The concentration of the ammonia solution (NH<sub>4</sub>OH) was

7.5 M and was added to the copper solution to convert the [Cu(H<sub>2</sub>O)<sub>6</sub>]<sup>2+</sup> ions into ammonium complexes, as is shown in the Chemical Reaction A.2. The addition of the ammonia changes the colour of the solutions from pale blue to deep blue and is used to enhance the reading. Table A.2 shows the absorbance measured, on every of the three repeats by the instrument, are presented, as well as the average absorbance. The spectrophotometric analysis of copper took place at 610 nm as suggested from manufacturer of the spectrophotometer in the manual and plastic cuvettes were used. Figure A.1 shows the calibration curve of copper for the UV-Vis spectrophotometer with error bars.

$$\begin{bmatrix} OH_2 & OH_2$$

Table A.1. Copper calibration solution' preparation.

	Volume Cu	Distilled	Ammonia	Cu
#	Standard	water	solution	(g/L)
	(mL)	(mL)	(mL)	
1	9	0	1	0.9
2	7	1	1	0.7
3	5	3	1	0.5
4	3	5	1	0.3
5	1	7	1	0.1
6	0	9	1	0.0

Table A.2. Absorbances measured for every calibration solution by the UV-Vis spectrophotometer.

#	Cu (g/L)	Absorb. 1 (-)	Absorb. 2 (-)	Absorb. 3 (-)	Average Absorb.
					(-)
1	0.9	0.565	0.568	0.565	0.566
2	0.7	0.458	0.459	0.459	0.459
3	0.5	0.356	0.346	0.349	0.350
4	0.3	0.177	0.177	0.177	0.177
5	0.1	0.065	0.071	0.071	0.069
6	0.0	0.000	0.000	0.000	0.000

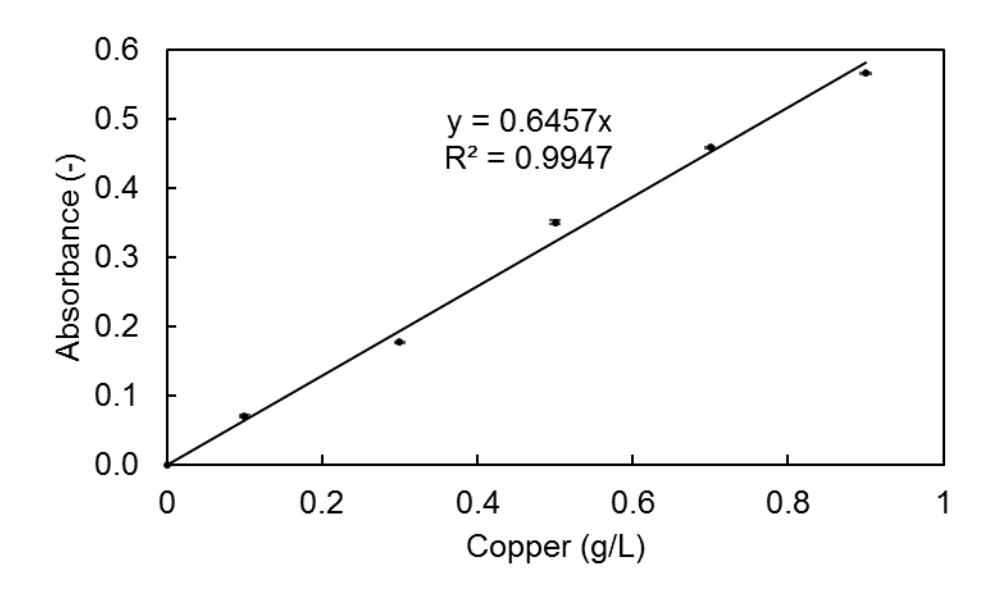


Figure A.1. Calibration curve of UV-Vis spectrophotometer for copper.

As shown in Figure A.1 the correlation coefficient (R<sup>2</sup>) is close to unity which indicates a good fit to the straight line and it comes in agreement with the Beer-Lambert law. In addition, the Root Mean Square Error (RMSE) was calculated by using the Equation A.3. The RMSE was calculated equal to 1.14%, which indicate that a negligible error was added by the calibration curve on the experimental samples.

$$RMSE = \left[\frac{1}{N} \sum_{i=1}^{N} (x_{pred} - x_{act})^{2}\right]^{1/2}$$
 (A.3)

Where: *N* is the number of different values.

 $x_{pred}$  is the predicted value.

 $x_{act}$  is the actual value.

# A 2. Flame Atomic Absorption Spectroscopy (FAAS)

FAAS is analytical technique for determining the concentration of metals elements in samples. The analysis and determination of the elements is based on the different wavelengths of light that are absorbed by a sample and on the Lambert-Beer law (Equation A.1). The instrument consists of three main parts, as shown in Figure A.2: (1) A light source with a wavelength which is specific to the element being detected.

(2) A nebulizer to create an aerosol of the sample solution and a flame which evaporates any solvent and ionises the analyte. (3) A detector which measures the amount of light absorbed.

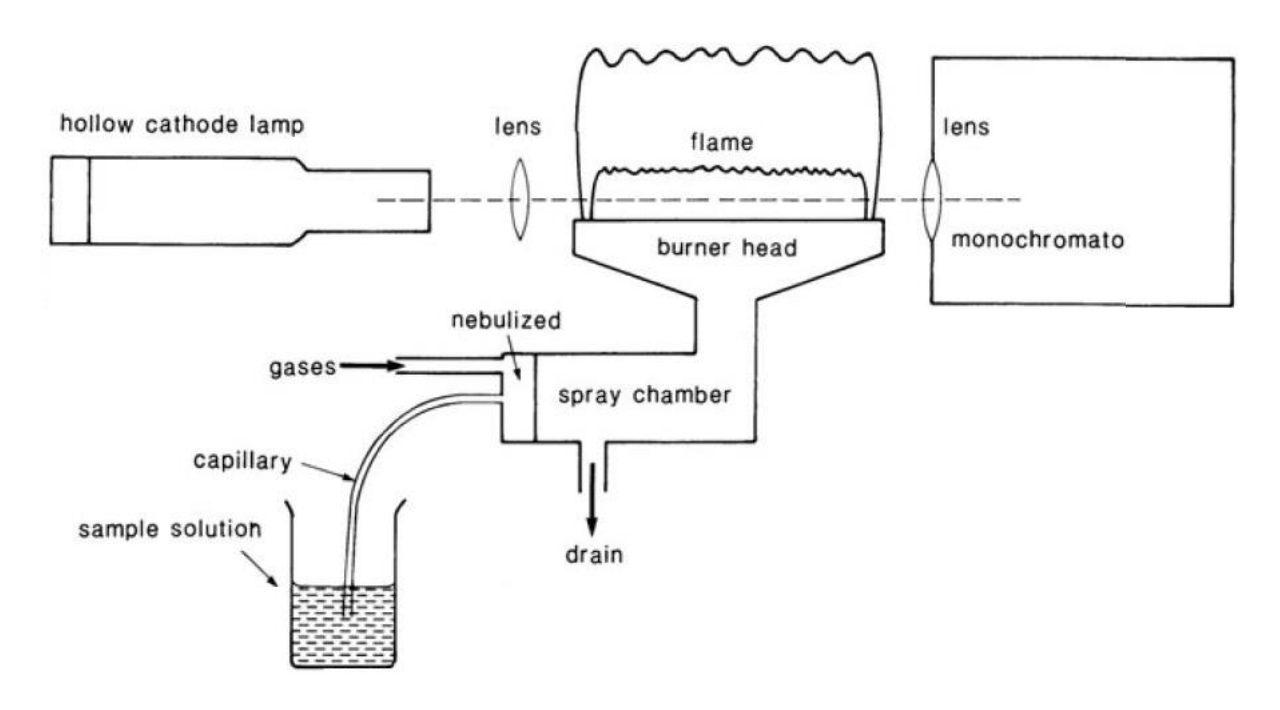


Figure A.2. Main parts of the FAAS. (Potts, 1987)

The instrument that used was the Agilent 55B AA Spectrometer by Agilent Technologies. Two ions were measured in the FAAS, chromium on the interfacial mass transfer experiments (Section 4.2) and calcium on the effect of acids on the CaSt<sub>2</sub> (Section 4.3.1). For chromium, the Chromium Coded HC Lamp at 429.0 nm wavelength was used. The calcium lamp that was used was the Hollow Cathode Lamp 1-element Calcium 37 mm at 422.7 nm wavelength (dos Santos et al., 2018; Shirani et al., 2020).

#### A 2.1. Calibration of FAAS for chromium

By using the chromium standard metal solution (1000 ppm chromium trioxide, HNO<sub>3</sub> 1 M) 6 calibration solutions were prepared and the concentrations of chromium and distilled water are shown in the

Table A.3. Table A.4 shows the measured absorbance of the three repeats and their average value. Figure A.3 shows the calibration curve of the FAAS for chromium.

Table A.3. Chromium calibration solutions' preparation.

щ	Volume Cr	Distilled	Cr
#	Standard (mL)	water (mL)	(g/L)
1	0	50	0
2	0.25	49.75	0.005
3	0.5	49.5	0.01
4	1	49	0.02
5	2.5	47.5	0.05
6	5	45	0.1

Table A.4. Absorbances measured for every calibration solution of Cr by the FAAS.

#	Cr	Absorb. 1	Absorb. 2	Absorb.	Average
#	(g/L)	(-)	(-)	3 (-)	Absorb. (-)
1	0	0.000	0.000	0.000	0.000
2	0.005	0.011	0.014	0.010	0.012
3	0.01	0.021	0.030	0.021	0.024
4	0.02	0.043	0.055	0.041	0.046
5	0.05	0.104	0.127	0.101	0.111
6	0.1	0.200	0.257	0.235	0.231

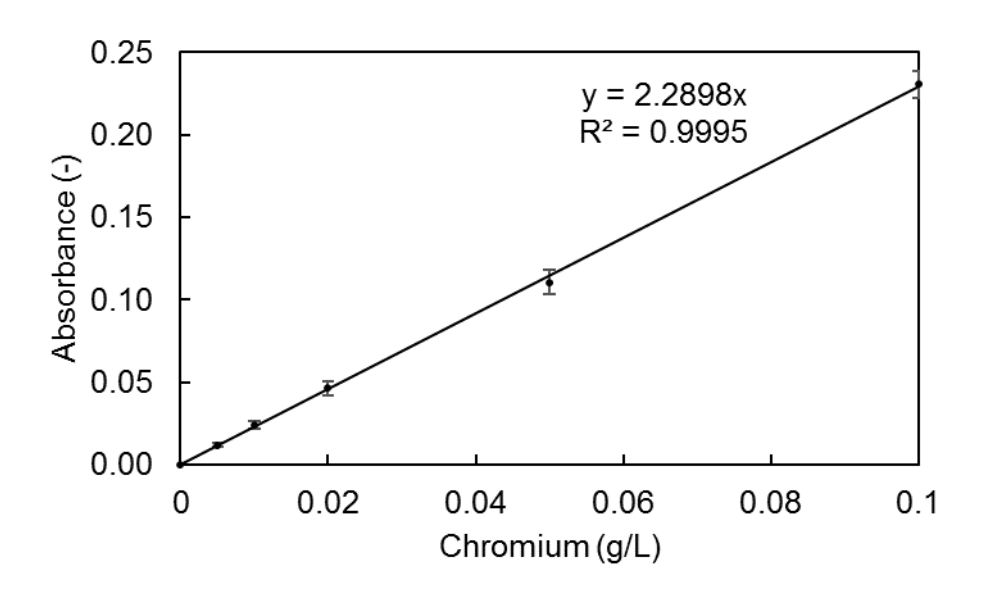


Figure A.3. Calibration curve of FAAS for chromium.

The correlation coefficient (R<sup>2</sup>), shown in Figure A.3, is equal to 0.9995 which is close to unity which indicates a perfect fit with the trend line. Like in the Cu calibration curve, the RMSE was calculated by using the Equation A.3, and calculated equal to 0.18%, which indicate that a negligible error was added by the calibration curve on the experimental samples.

#### A 2.2. Calibration of FAAS for calcium

Calcium standard metal solution in the form of calcium carbonate (1000 ppm, HNO<sub>3</sub> 1 M) used for the preparation of the calibration solutions as shown in Table A.5. Table A.6 shows the measured absorbance of the calibration solutions on the three repeats as well as their average values. On Figure A.4 shows the calibration curve of FAAS for calcium with the error bars.

Table A.5. Calcium calibration solutions' preparation.

#	Volume Ca	Distilled	Ca (M*10 <sup>5</sup> )
	Standard (mL)	water (mL)	
1	0	50	0.00
2	0.25	49.75	1.25
3	0.5	49.5	2.50
4	1	49	4.99
5	2.5	47.5	7.49
6	5	45	12.48

Table A.6. Absorbances measured for every calibration solution of Ca by the FAAS.

#	Ca	Absorb.	Absorb.	Absorb.	Average
	$(M*10^5)$	1 (-)	2 (-)	3 (-)	Absorb. (-)
1	0.00	0.000	0.000	0.000	0.000
2	1.25	0.011	0.014	0.010	0.012
3	2.50	0.021	0.030	0.021	0.024
4	4.99	0.043	0.055	0.041	0.046
5	7.49	0.104	0.127	0.101	0.111
6	12.48	0.200	0.257	0.235	0.231

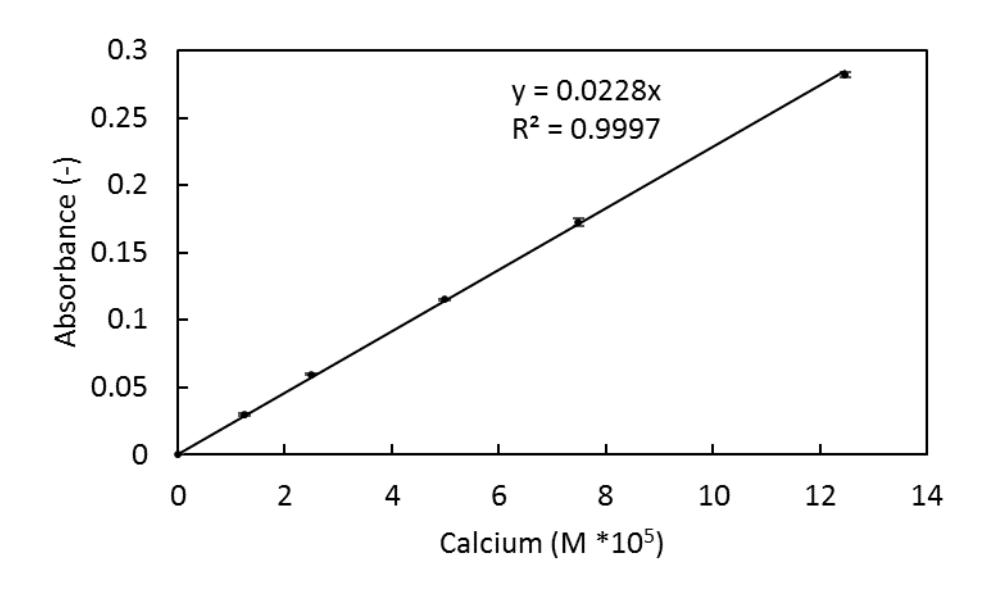


Figure A.4. Calibration curve of FAAS for calcium.

The correlation coefficient  $(R^2)$  of the trendline is equal to 0.9997 as shown in Figure A.4.  $R^2$  is equal to unity indicates a very good correlation. Like in the previous calibrations, the RMSE was calculated by using the Equation A.3. The calculated was equal to 4.55%, which indicate that a very small error was added from the calibration curve on the experimental samples.

# A 3. High Performance Liquid Chromatography (HPLC)

HPLC is an analytical technique which was used to determine the AcOH concentration in water. In the HPLC, a solvent (medium) is forced through a column filled with adsorbent material (stationary phase) under high pressure. A small amount of sample is injected to the solvent in order to pass through the column. Each component of the sample interacts different with the adsorbent material and a result they exit the column at different times. A detector is used to measure each component (Lozano-Sánchez et al., 2018). Figure A.5 shows the main parts of the HPLC.

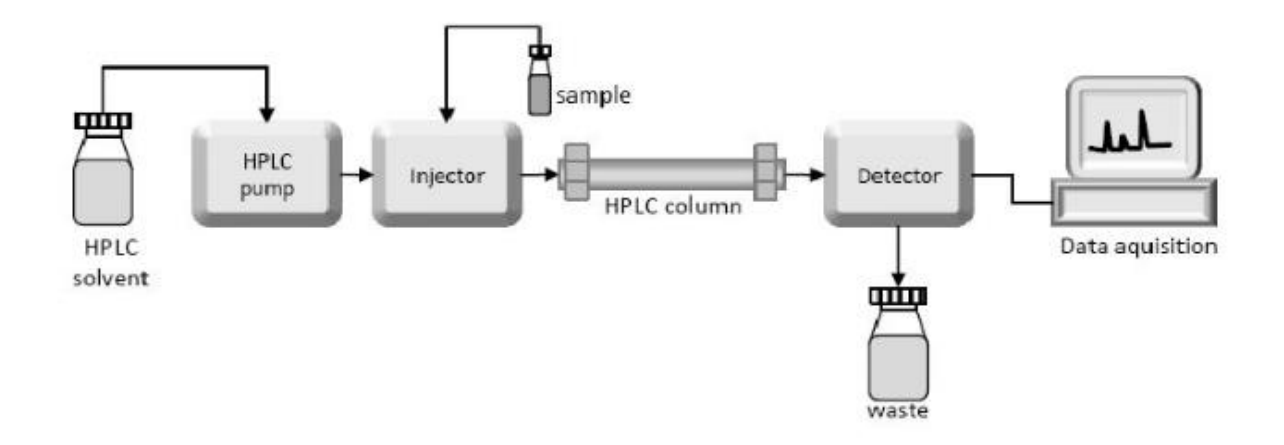


Figure A.5. Main parts of the HPLC. (Aryal, 2018)

#### A 3.1. Calibration of HPLC for AcOH in water

AcOH (99.7% purity) was used in order to prepare the calibration solutions in distilled water. Table A.7 shows the concentrations of AcOH and distilled water that were used to prepare the calibration solutions. Table A.8 shows the HPLC measurements for each calibration solution and their average value. HPLC Hewlett Packard Series 1100 and Ultra AQ C18 5μm column were the HPLC instrument and the column that were used. As medium, 0.05% v/v phosphoric acid in water was used. The flow rate that was between 1 and 5 mL/min depending on the dilution of the samples. Figure A.6 shows the calibration curve of AcOH for the HPLC.

Table A.7. AcOH calibration solutions' preparation for HPLC.

#	Volume	Distilled	AcOH
#	AcOH (mL)	water (mL)	(M)
1	0	50	0.00
2	0.005	49.995	0.002
3	0.05	49.95	0.02
4	0.1	49.9	0.03
5	0.3	49.7	0.10
6	0.5	49.5	0.17

Table A.8. Area measured for every calibration solution of AcOH by the HPLC.

#	AcOH	Area 1	Area 2	Area 3	Average area
#	(M)	(mAU.s)	(mAU.s)	(mAU.s)	(mAU.s)
1	0.00	0	0	0	0
2	0.00	37.3	38.5	36.8	37.5
3	0.02	383.5	400.5	395.5	393.2
4	0.03	762.1	785.1	749.9	765.7
5	0.10	2211.1	2251.2	2200.1	2220.8
6	0.17	3678.5	3700.5	3689	3689.3

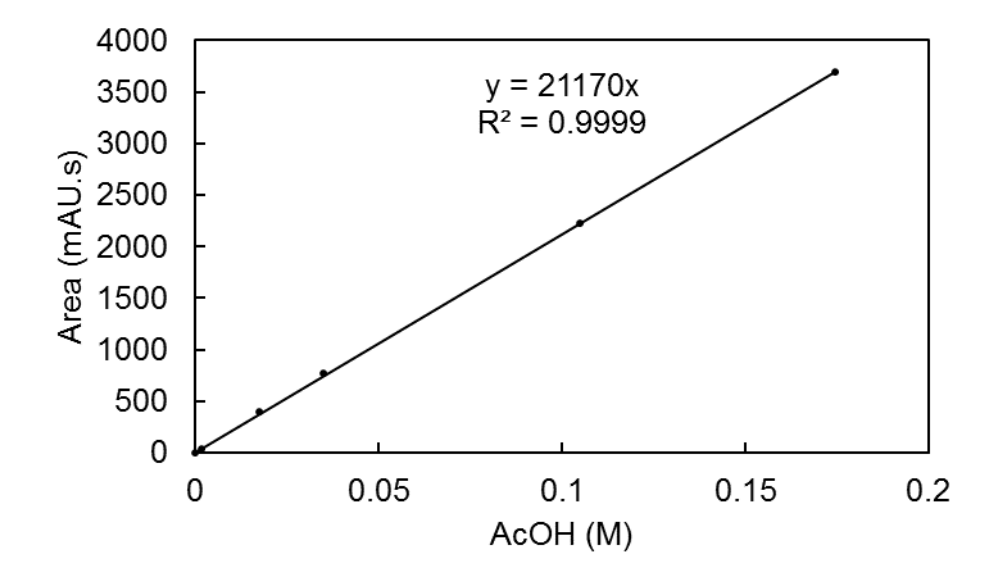


Figure A.6. Calibration curve of HPLC for AcOH.

The correlation coefficient (R<sup>2</sup>) of the trendline was equal to 0.9999, which indicates perfect fit, as shown in Figure A.6. Like in the previous calibrations RMSE was calculated by using the Equation A.3. The calculated RMSE was equal to 7.85%, which indicate that a very small error was added from the calibration curve on the experimental samples.

# A 4. Mathematical equations for calculating the error

Every experimental and calibration was conducted 3 times in order to calculate the error and check the repeatability of the experiment. First the average value was calculated and then the standard deviation (s) by the Equation A.4.

$$s = \sqrt{\frac{\sum_{i=1}^{N} (x_i - \bar{x})^2}{X - 1}}$$
 (A.4)

Where: X is the number of values.

x<sub>i</sub> is the value of every measurement.

 $\bar{x}$  is the average value of the measurements.

The standard error was calculated by using the Equation A.5 and is presented in the form of error bars for every experimental point on the graphs presenting on the results section.

$$Error = \frac{s}{\sqrt{N}} \tag{A.5}$$

#### A 5. Viscosity measurement

The viscosity of the organic phase containing butyl rubber was measured in the lab by using the HAAKE Viscotester IQ rheometer. The viscosity measured at two different temperatures, at room temperature (20 °C), where the experiments took place, and at 50 °C which is a possible industrial process temperature. In every viscosity measurement, the appropriate amount of liquid was placed in the coaxial cylinder of the viscometer until it reaches the desired temperature. An increasing shear rate was applied to the liquid and the shear stress was measured by the viscometer. Different range of shear rate applied in every liquid due to different viscosities.

Three different solutions of various concentrations of BR (50, 100 and 200 g/L) in n-heptane were prepared in order to measure their viscosity. The Figures A.7, A.8 and A.9 shows the relationship between the shear rate and the shear stress at the two temperatures for the tested solutions, of various BR concentrations.

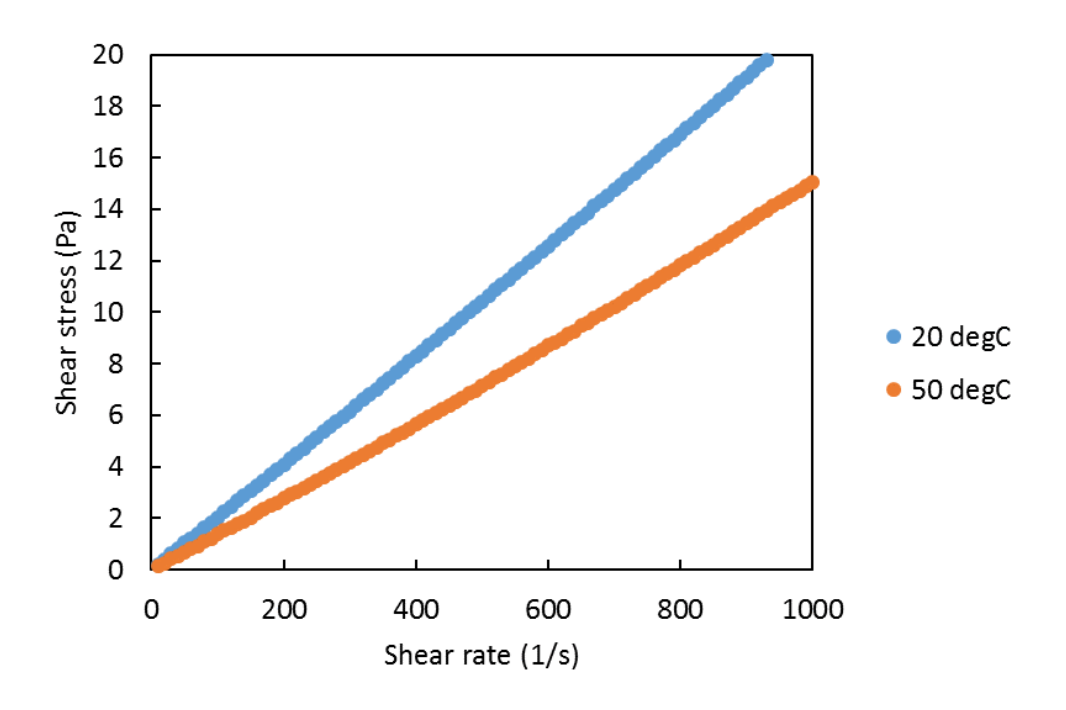


Figure A.7. Shear stress as a function of shear rate for 50 g/L BR in heptane.

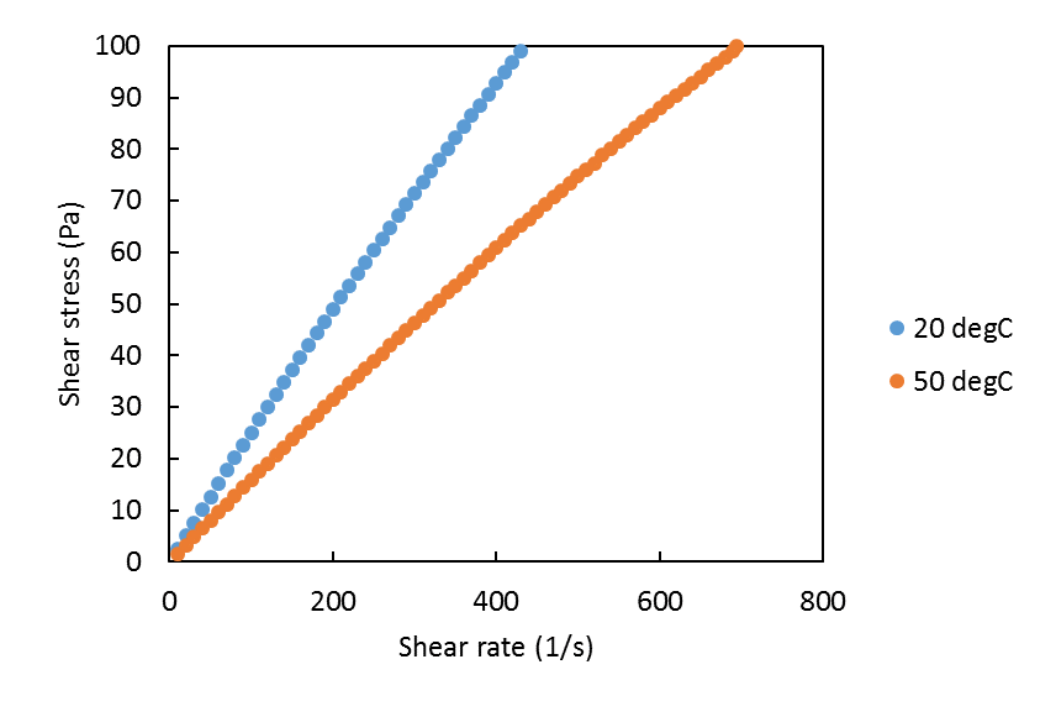


Figure A.8. Shear stress as a function of shear rate for 100 g/L BR in heptane.

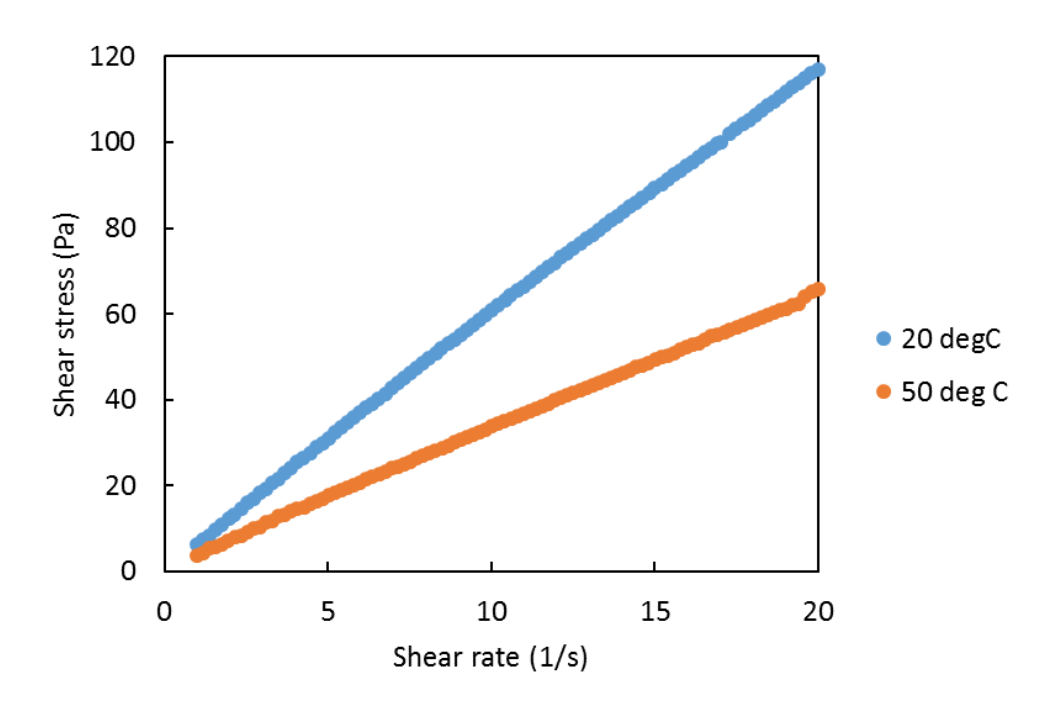


Figure A.9. Shear stress as a function of shear rate for 200 g/L BR in heptane.

All solutions had Newtonian behaviour on the tested shear rate range, as there is linear relationship between the shear rate and shear stress. The slope on every line represents the viscosity of each solution and is presented in Table A.9. The viscosity of heptane (0 g/L BR) at 20 °C was found in the literature (Dymond and O/ye, 1994). The viscosity of n-heptane at 50 °C was not measured and it was assumed to be lower than the one on 20 °C.

Table A.9. Solutions' viscosities, containing various BR concentrations, at 20 and 50 °C.

BR (g/L)	Viscosity (cP)	
	20 °C	50 °C
0	0.389	-
50	21.5	15.0
100	229.0	144.1
150	5872.1	3182.3

#### A 6. Interfacial tension measurement

The interfacial tension measurement was measured in the Drop Shape Analyser KRUSS (DSA 100) by using the technique of the pendant. Prior to the measurements, the surface tension of distilled water was measured in order to ensure the correct

calibration of the instrument. The calibration of the instrument achieved by setting the outside diameter of the needle in the instrument. For the measurement of the interfacial tensions, a pendant drop, containing the one phase, was created with the use of a syringe inside the second phase, as shown in Figure A.10, which shows the configuration of the KRUSS DSA 100 instrument. The second phase was in a quartz cuvette dimension of 2 cm (H) x 2 cm (D) x 2 cm (W).

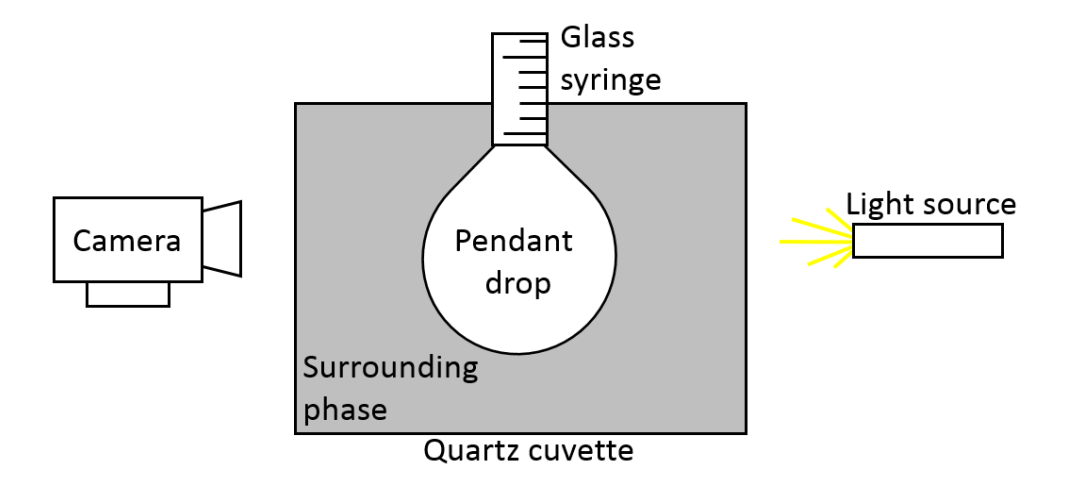


Figure A.10. Instrumental configuration for the measurement of the interfacial tension with the technique of the pendant drop in the KRUSS DSA 100 instrument.

The instrument was measuring the interfacial tension with time until the equilibrium (steady interfacial tension). The analysis of the drop and the calculation of the interfacial tension is based on the Young-Laplace equation (Equation A.6) (Bagalkot et al., 2018).

$$\Delta P = \sigma \left( \frac{1}{r_1} + \frac{1}{r_2} \right) \tag{A.6}$$

Where:  $\Delta P$  is the pressure difference across the interface.

 $\sigma$  is the interfacial tension.

 $r_1$  and  $r_2$  are the principal radii of the curvature.

The instrument uses the Equation A.7 to calculate the interfacial tension ( $\sigma$ ), where the density difference  $\Delta \rho$  is equal to the  $\Delta P$ . The density of the pendant drop and the surrounding liquid was set by the operator.

$$\sigma = \frac{\Delta \rho g d^2}{B} \tag{A.7}$$

Where: g is the acceleration of gravity.

*d* is the maximum horizontal diameter of the pendant drop.

*B* is the shape parameter, that is adjusted by the operator to be above 0.5.

## A 7. Image analysis

Microscope analysis was used to measure the diameter of the aqueous drops of the W/O emulsions that were formulated in the lab. The microscope used was the GX Microscope GXML3201. The photos of the W/O emulsion taken from the microscope analysed with the ImageJ software. Prior to the analysis, every photo was calibrated in the software by using a photo with a scale taken with the same lens from the microscope. Figure A.11 shows the initial example photo taken from the microscope, which was converted in black and white automatically from the software, as shown in Figure A.12. Any black mark smaller than 100 pixel<sup>2</sup> was manually removed as they did not represent dispersed phase drop. By using edge detection, as shown in Figure A.13, the software measured the diameter of each drop in the photo. The same procedure was followed for every photo until 250 drops were measured. The stability of the emulsion on the microscope slide was good as there was no visible coalescence.

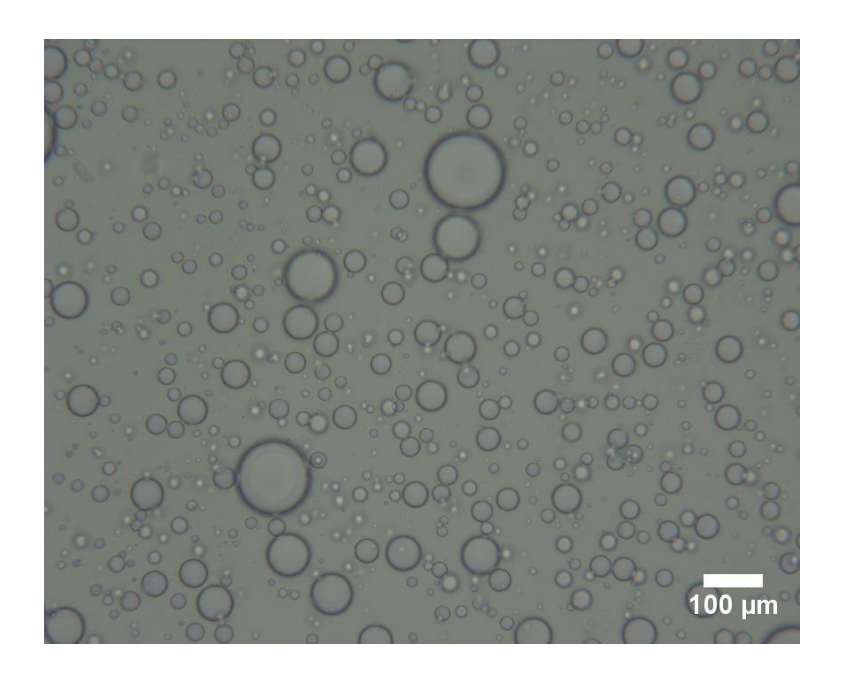


Figure A.11. W/O emulsion (100 g/L BR, 5 g/L CaSt<sub>2</sub>, volume phase ratio 4:1 O:W).

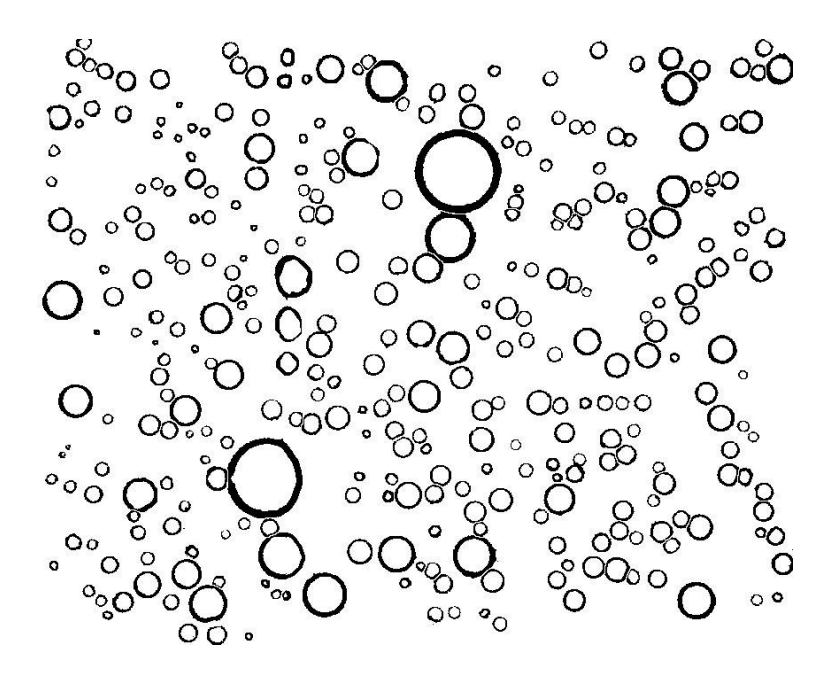


Figure A.12. Conversion to black and white of the W/O emulsion photo (100 g/L BR, 5 g/L CaSt<sub>2</sub>, volume phase ratio 4:1 O:W).

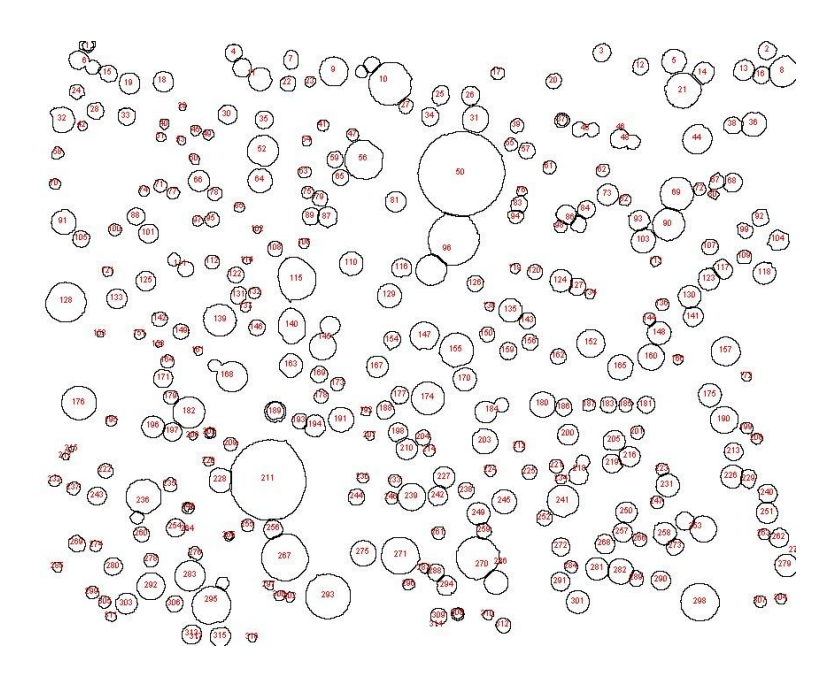


Figure A.13. Detection of aqueous drops from the software (100 g/L BR, 5 g/L CaSt<sub>2</sub>, volume phase ratio 4:1 O:W).

## A 8. Particle size distribution analysis

The Malvern Mastersizer 2000 is a particle size analyser which is based on principle of static light scattering is used by the instrument to measure the particles' size. The size of the particles makes the light to scatter at a specific angle and by using the Mie scattering theory the size particle distribution can be calculated. For example, small particles result in large scatter angle of the light (Instruments Malvern Ltd, 2007). Figure A.14 shows the basic parts of the Malvern Mastersizer 2000.

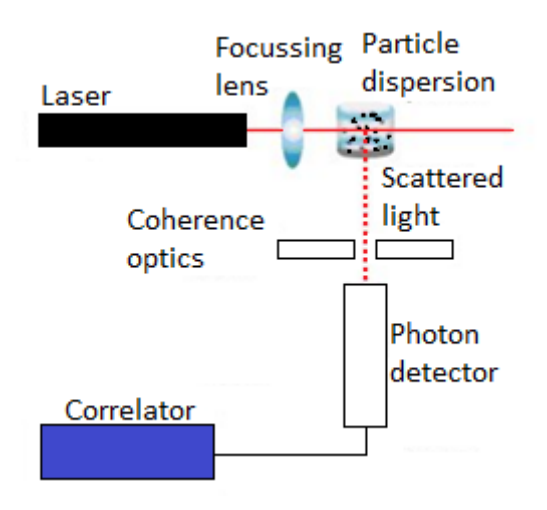


Figure A.14. Schematic diagram of the Malvern Mastersizer 2000

Prior to the analysis the CaSt<sub>2</sub> suspension was sonicated for 10 minutes to break any agglomerations. First part of the analysis was the instrument to measure the background electrical noise that could be from dust and eliminate it from the results. Next step was to add a small amount of sample in a circulating particle dispersion of water, the Hydro 2000SM dispersion unit. At the appropriate sample concentration, the laser intensity was above 50%. The sample concentration could be change by draining part of the suspension the water and replace it with clean one. After the correct sample concentration was achieved the instrument could measure the scatter angles with a detector and calculate the particle size distribution.